HYDROGEOLOGIC INVESTIGATION OF THE BOULDER VALLEY, JEFFERSON COUNTY, MONTANA GROUNDWATER MODELING REPORT

Julie A. Butler[1] and Andrew L. Bobst

Montana Bureau of Mines and Geology

Ground Water Investigations Program

[1]Currently employed by the Massachusetts Department of Environmental Protection, Boston, MA

MBMG

Montana Bureau of Mines and Geology

Cover photo by Andrew L. Bobst, 2011

HYDROGEOLOGIC INVESTIGATION OF THE BOULDER VALLEY, JEFFERSON COUNTY, MONTANA GROUNDWATER MODELING REPORT

March 2017

Julie A. Butler[1] and Andrew L. Bobst

Montana Bureau of Mines and Geology

Ground Water Investigations Program

[1]Currently employed by the Massachusetts Department of Environmental Protection, Boston, MA

Montana Bureau of Mines and Geology Open-File Report 688

TABLE OF CONTENTS

FIGURES

TABLES

PREFACE

The Ground Water Investigations Program (GWIP) at the Montana Bureau of Mines and Geology (MBMG) investigates areas prioritized by the Ground-Water Assessment Steering Committee (2-15-1523 MCA) based on current and anticipated growth of industry, housing and commercial activity, or changing irrigation practices. Additional program information and project-ranking details are available at: http://www.mbmg.mtech.edu/gwip/gwip.asp.

The final products of the Boulder Valley investigation are:

An Interpretive Report (Bobst and others, 2016) that presents data, addresses questions, offers interpretations, and summarizes project results. For the Boulder Valley groundwater investigation, questions included: what are the potential impacts to surface-water availability from increased groundwater development, and what is the feasibility of using managed recharge to enhance late-summer flows?

An area-wide Groundwater Modeling Report (this report) that describes the construction, the assumptions used, and the results from groundwater models. Groundwater modelers should be able to evaluate and use the models as a starting point for testing additional scenarios and for site-specific analyses. The GWIP website (http://www.mbmg.mtech.edu/gwip/gwip.asp) provides access to the files needed to run the models.

A Montana Tech Master's Thesis (Carlson, 2013) that focused on the potential to use managed recharge to enhance late-summer flow was also prepared in support of this investigation.

MBMG's Groundwater Information Center (GWIC) online database (http://mbmggwic.mtech.edu/) provides a permanent archive for the data collected during this study.

ABSTRACT

Portions of the Lower Boulder River often dry up in the late summer; the Montana Department of Fish Wildlife and Parks has identified the reach from the town of Boulder to Cold Spring as "chronically dewatered." The MBMG prepared an area-wide groundwater flow model to better understand the impacts to surface-water availability from increased residential groundwater development in this area.

The Area-Wide Model covered 377 mi^2 of the Boulder River drainage basin between the towns of Boulder and Cardwell. This model had one layer and was developed using the MODFLOW-NWT code. The numerical model design was based on the conceptual model, which was derived from analysis of groundwater and surface-water monitoring; aquifer tests; well logs; interviews with local landowners and NCRS staff; and GIS analysis of soil, climate, vegetation, land use, and water-rights data. Specified-flux boundary conditions bordered the model grid, while head-dependent and specified-flux boundaries represented stream flow, irrigation diversions, canal leakage, upland recharge, irrigation recharge, pumping wells, and riparian evapotranspiration.

In the steady-state simulation, observed groundwater elevations, stream flows, and the conceptual groundwater budget were used with automated parameter estimation and manual trial-and-error to estimate hydraulic conductivity, recharge, streambed vertical hydraulic conductivity, and alluvial groundwater inflow/outflow. The resulting parameter estimates were consistent with the conceptual model and the numerical model's simulated water levels were similar to observations. The resulting array of head values had an RMS error of 2.4 ft, representing about 0.1 percent of the modeled groundwater elevation range (2,172 ft). Stream flow and stream flux results were also similar to observed values.

The transient version of the model simulated time-dependent stresses, such as seasonal irrigation activities and changes in precipitation. It was calibrated to the 22 months of recently collected data (2011–2013), as well as 15 months prior to the study period in order to capture large changes in precipitation-derived recharge. Calibration was conducted by adjusting specific yield (Sy) and specific storage values (Ss) until observed water-level and stream-flow fluctuations were reasonably replicated by the model. Upland recharge was also included

in the transient calibration using an approach based on its seasonal variation as well as inter-annual variation between relatively wet and dry years (2010–2011 and 2012–2013, respectively).

Four hypothetical predictive scenarios were simulated to evaluate changes in groundwater levels and stream baseflow from increased residential development. Domestic well withdrawals associated with subdivisions (10 or 20 acres per lot) were simulated over 20-yr periods. Results showed that groundwater drawdown and stream depletion were linearly proportional to well withdrawal rates. Depletion was also proportional to the proximity of streams, when viewed both from the well's perspective (i.e., the percent of its water supply) and from the stream's perspective (i.e., decrease in its baseflow). The timing of maximum drawdown was consistently in late summer, when water demands were the highest. The rate of change for both drawdown and depletion decreased over time but did not stabilize in any of the scenarios.

The simulated depletion rates (13 to 26 gallons per minute, gpm) were small in comparison to effects from irrigation diversions. To ensure that unanticipated impacts do not occur, it is recommended that wells and streams in areas of concern are monitored to establish baseline conditions, and that impact thresholds for groundwater levels and stream flow are established. Water conservation measures are recommended to alleviate the late summer supply shortages that irrigators often face. A detailed record of irrigation practices, most notably diversion rates and durations, would help to refine conceptual and numerical models, which in turn would assist in developing the most sensible water conservation measures.

INTRODUCTION

Background

The Boulder Valley study area covers 377 mi^2, and is located between the towns of Boulder and Cardwell, Montana (fig. 1). The study area boundaries follow the USGS watershed for the Lower Boulder River (hydrologic unit code 1002000605). Approximately 60% of the study area is composed of private land, with the remaining 40% being public (Forest Service, BLM, and State; Montana State Library, 2013). Most wells are completed on private land in the unconsolidated aquifers along the valley bottoms (fig. 2).

Portions of the Boulder River typically run dry in the late summer, when appropriations exceed physical flow. The State of Montana adheres to the Prior Appropriation Doctrine, so a water user can divert within the parameters of their right until the point that water in the source is exhausted. Therefore these diversions by senior water-rights holders may eliminate the ability to irrigate for junior water-rights holders, and impact the river's utility for aquatic life and recreation. This has been a long-standing issue (Buck and Bille, 1956). There are concerns that additional groundwater development in the watershed will further reduce water availability.

There have been several attempts to supplement late summer flows in the Boulder River. A study in the 1960s investigated the feasibility of constructing a surface reservoir on the Boulder River just upstream of its confluence with Basin Creek (13 mi upstream from the town of Boulder; Montana Water Resources Board, 1968). Another 1960s study evaluated the feasibility of supplementing the irrigation system with groundwater from the alluvial aquifer near Boulder (Botz, 1968). In the 1970s, plans were developed to build a surface reservoir near the mouth of the Little Boulder River (SCS, 1975; Darr, 1975); however, construction never began due to issues regarding foundation stability, water rights, and a low cost/benefit ratio (W.A. Jolly, Project Development and Maintenance—Boulder River Watershed, unpublished manuscript, 1982).

Purpose and Scope

The Boulder Valley groundwater investigation addresses concerns about the potential impacts from increased groundwater withdrawals, and evaluates the potential for using managed aquifer recharge to supplement late summer flows in the Boulder River. As such, the study focused on the unconsolidated valley-fill deposits. Limited monitoring and modeling of the bedrock uplands provided an estimate of flux into the valley-fill; therefore, any model results from the bedrock areas should be treated as a first-order estimate. The study results are intended to provide a basis for future groundwater management in the area by focusing on the large-scale behavior of the hydrogeologic system, and provide a framework within which site-specific issues can be considered.

Model Objectives

Two groundwater flow models were developed for the Boulder Valley groundwater investigation to address concerns over groundwater and surface-water availability. The first model, known as the Managed Recharge Model, included a central portion of the Boulder Valley floodplain and pediment. The primary objective was to predict impacts of managed recharge scenarios. The Managed Recharge Model is documented in a Montana Tech thesis by Carlson (2013), and a summary is provided in the Interpretive Report (Bobst and others, 2016). The interpretive report also summarizes overall project results.

The second model, known as the Area-Wide Model, encompasses the entire study area, and the primary modeling objective was to predict impacts to surface-water flow from potential future groundwater development. Various scenarios were simulated to examine the effects of pumping from domestic wells on groundwater levels and stream baseflow.

This report focuses on the design, calibration, and predictive scenarios of the Area-Wide Model. Details of the procedures and assumptions inherent in the model and model results are presented in this report. The files needed to operate the groundwater model are posted on the project website (http://www.mbmg.mtech.edu/gwip/gwip.asp), and file details are provided in appendix A.

Previous Investigations

A review of previous work is included in the interpretive report for this project (Bobst and others, 2016). The geologic framework for the study area is primarily based on composite geologic maps prepared by Vuke and others (2004, 2014) and Reynolds and Brandt (2006).

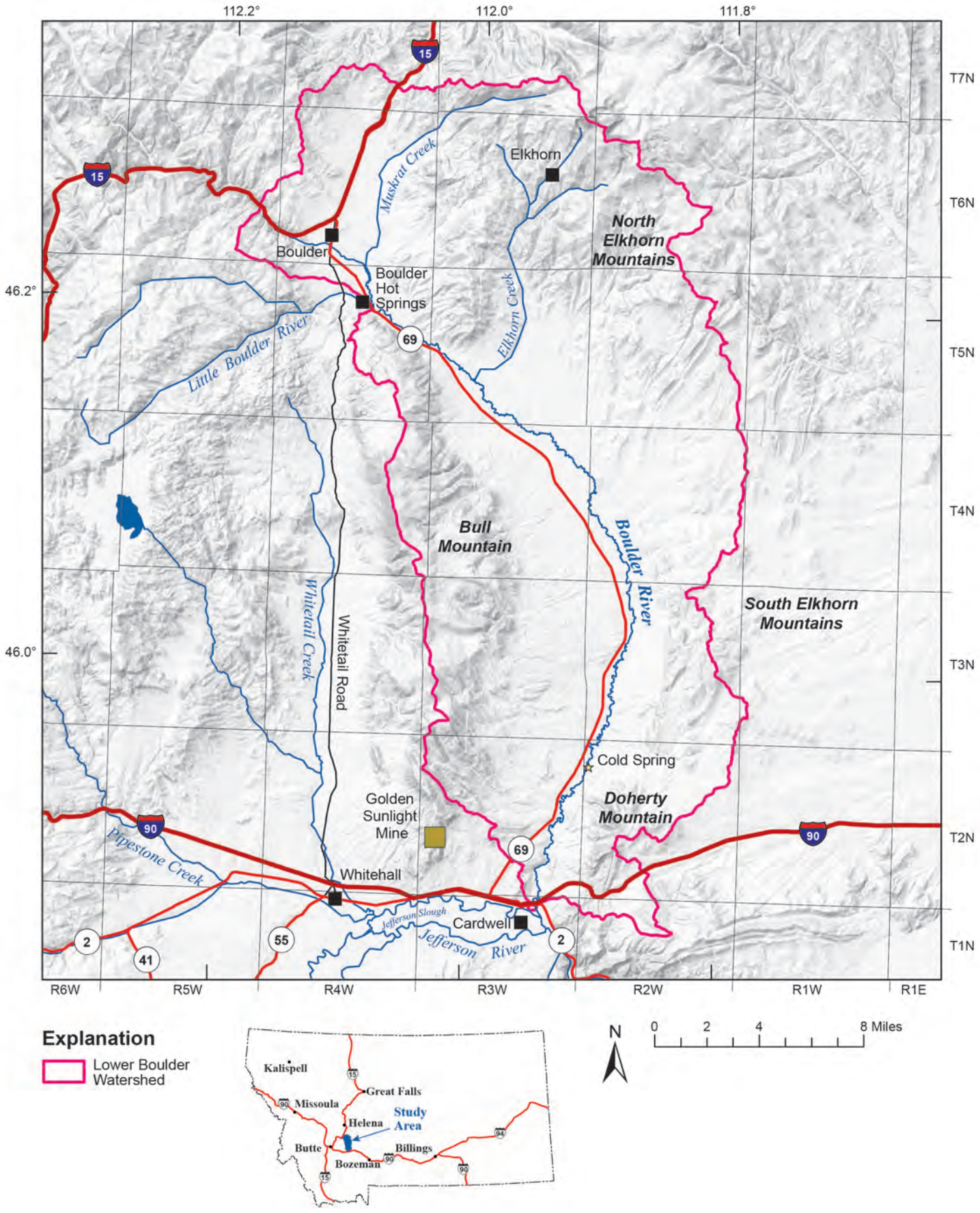

Figure 1. The Boulder Valley groundwater investigation evaluated the Lower Boulder River Watershed (USGS HUC 1002000605) between Boulder and Cardwell. The study area covers 377 mi^2.

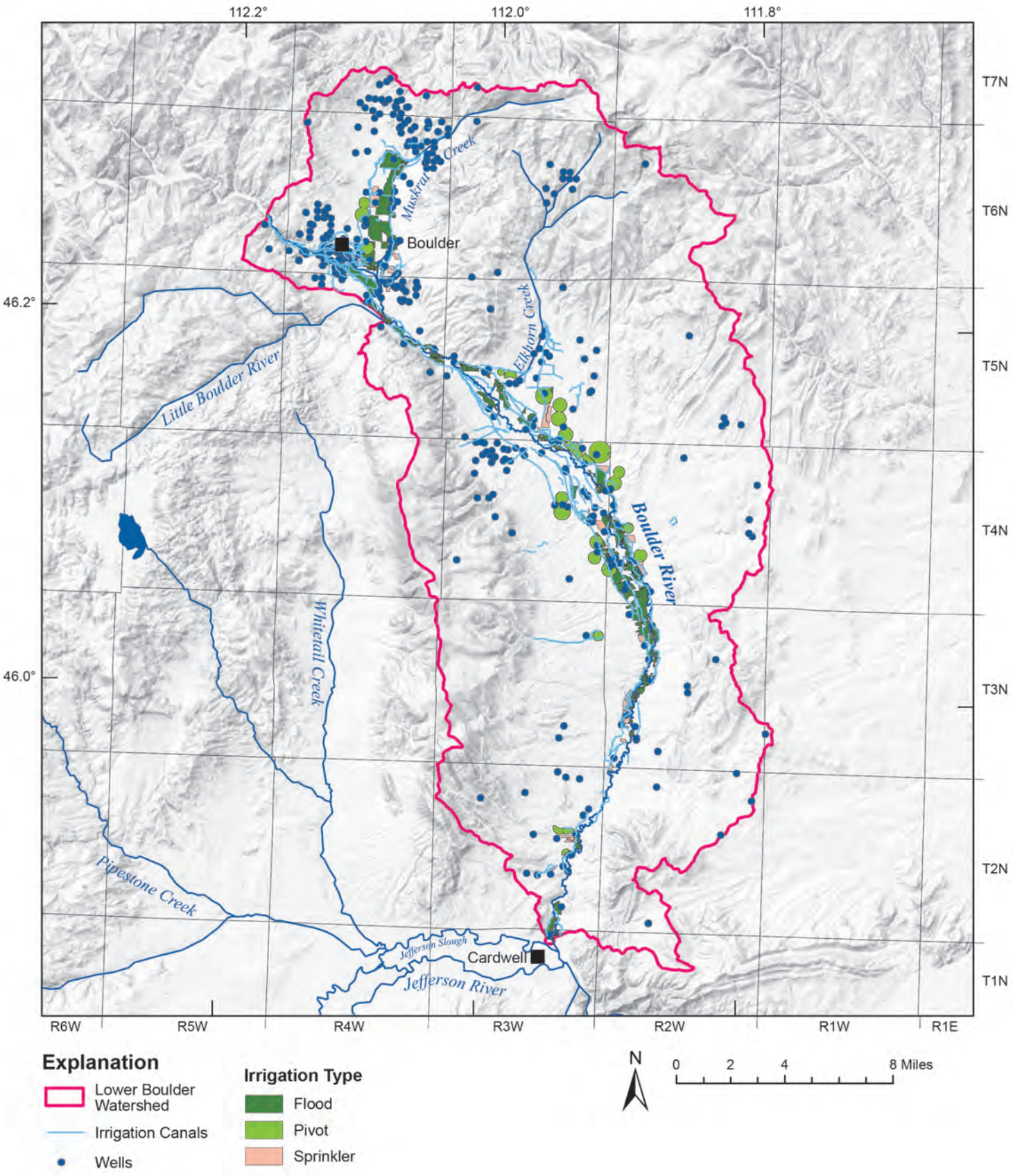

Figure 2. Wells in the study area are used to supply domestic, stock, and irrigation water. Irrigation infrastructure includes canals and fields.

Previous hydrogeologic work in the Boulder Valley has been limited. Botz (1968) evaluated the feasibility of supplementing surface-water supplies with groundwater withdrawals to meet the needs of late summer agricultural irrigation. The assessment included well log analysis, groundwater levels, aquifer recharge and discharge sources, and two aquifer tests in the Quaternary alluvium. In 1991, groundwater levels were measured in 35 wells by the United States Geological Survey (USGS; Dutton and others, 1995). The Montana Bureau of Mines and Geology (MBMG) Groundwater Monitoring Program (GWAAMON) has conducted quarterly water-level monitoring of nine wells in or near the valley as part of their Statewide monitoring network (http://mbmggwic.mtech.edu).

Physiography

The Boulder Valley is an intermontane basin within the Northern Rocky Mountains physiographic province. The valley trends north–northwest. Bull Mountain is on the west and the Elkhorn Mountains are on the east (fig. 1). The Boulder River meanders within a well-defined floodplain that is about 0.5 to 1 mi wide. To the east and west of the floodplain are broad pediments and alluvial fans at the bases of the mountains. There is an abrupt change in slope where the alluvial fans meet the mountains. Elevations within the study area range from 4,270 ft above mean sea level (ft-amsl) where the Boulder River flows into the Jefferson Slough, to 9,414 ft-amsl in the Elkhorn Mountains.

The bedrock notch below the confluence of the Boulder and Little Boulder Rivers divides the study area into two basins. All surface water flows through this notch, and due to the high permeability of the unconsolidated materials relative to the bedrock, it is likely that groundwater flows through this notch as well. At the southern end of the valley, the Boulder River flows through another narrow bedrock gorge near Doherty Mountain that also likely restricts groundwater and surface-water flow (Kendy and Tresch, 1996).

Climate

The Boulder Valley generally has cold winters and mild summers. Precipitation is low in the valley bottom, and increases with elevation in the mountains (fig. 3). Based on the 1981–2010 climate normal data for Boulder (NOAA, 2011), the coldest month is December, with a mean monthly temperature of 21.7°F, and the warmest month is July, with a mean monthly temperature of 65.2°F. Precipitation is the greatest in June, when Boulder receives an average of 2.2 in, and February is the driest, with an average of 0.3 in (fig. 4; NOAA, 2011). Boulder receives an average of 10.86 in of precipitation per year; however, year-to-year variability is significant (fig. 4). Data from the Parameter-elevation Regressions on Independent Slopes Model (PRISM) Climate Group at Oregon State University (800 m data; Oregon State University, 2013) indicate that from 1981 to 2010 average annual precipitation within the study area ranged from 11.4 in. in the valley to 38.2 in. in the upper elevations of the Elkhorn Mountains (fig. 3). This matches well with data developed by the Montana Department of Environmental Quality (Farnes and others, 2011), which shows precipitation in the study area varying from 11.3 to 37.0 in.

Vegetation

Vegetation within the study area varies with elevation, precipitation, and depth to groundwater. Where groundwater is shallow, there are plants that obtain a significant portion of their water from groundwater (i.e., the phreatic zone). These plants are known as phreatophytes, and they include plants such as Cottonwood, Willow, Aspen, and wetland grasses. These phreatophytes occur within the alluvial floodplain of the Boulder River and along some tributaries. Upland vegetation includes grasses, sagebrush, Ponderosa Pine, Douglas Fir, Lodgepole Pine, Engleman Spruce, and Whitebark Pine. Agricultural areas are dominated by alfalfa and grass hay.

Information from the LANDFIRE Existing Vegetation Type database (USGS, 2010), the National Land Cover database (USGS, 2011a), the GAP land cover database (USGS, 2011b), air photographs, and field visits were evaluated and used to reclassify the LANDFIRE raster into a simplified vegetation coverage for the study area (fig. 5).

Water-Development Infrastructure

Water-development infrastructure within the Boulder Valley study area includes irrigation canals, irrigated fields, irrigation wells, domestic and stock wells (fig. 2), and septic systems. The main sources of irrigation water are the Boulder River, Elkhorn Creek, and Muskrat Creek. The primary irrigated

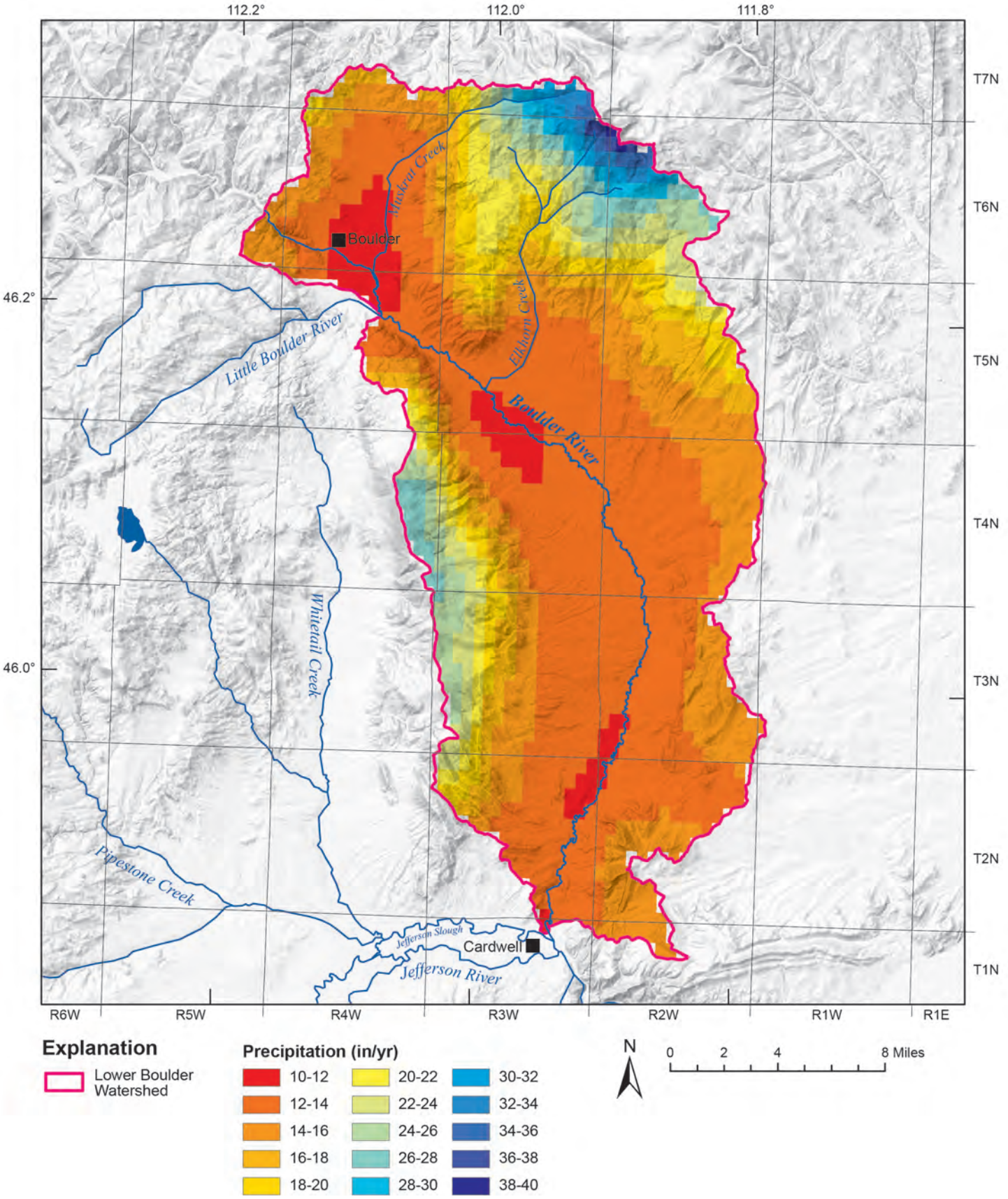

Figure 3. Precipitation within the study area varies with elevation. Central areas in the valley may receive less than 12 in/yr, but the highest peaks receive more than 38 in/yr (data from PRISM, 2012; 800 m resolution; 1981–2010 normal).

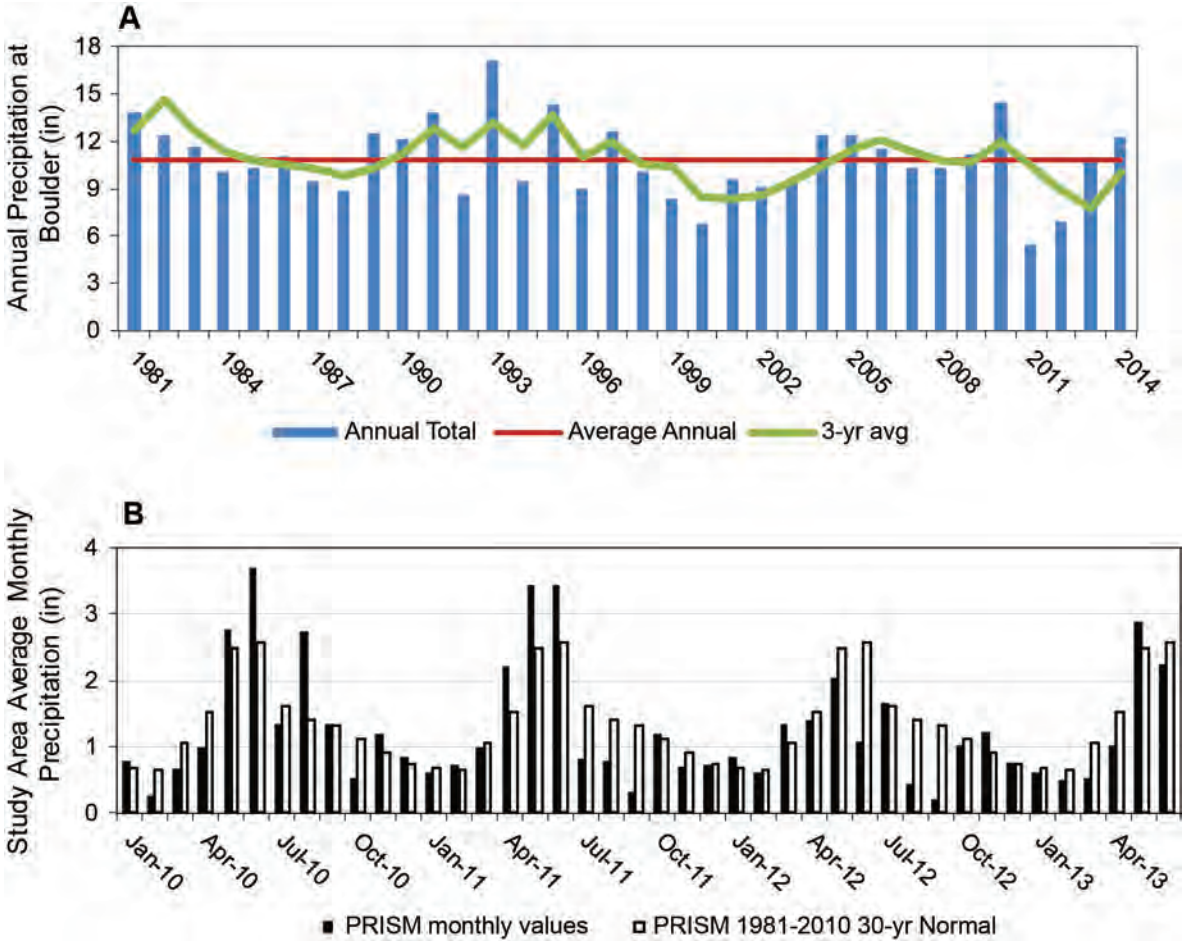

Figure 4. Precipitation at Boulder from 1981 to 2014 averaged 10.86 in/yr (NOAA, 2016), varying annually from 50% to 158% of average (A). Monthly precipitation values from 2010 to mid-2013 varied from 0.19 to 3.70 in. During 2010 and the first half of 2011 it was wetter than average. The second half of 2011 and 2012 were relatively dry. The first half of 2013 was near average.

crops are alfalfa and grass hay (L. Ovitt, NRCS-Whitehall, oral commun., September–December, 2012).

Canals affect groundwater by recharging underlying aquifers through leakage; similarly, irrigated fields provide infiltration recharge when water is applied in excess of crop demand. Wells extract water and septic systems return a portion of that water to the groundwater system.

CONCEPTUAL MODEL

A conceptual model is an interpretation of the characteristics and dynamics of the physical groundwater flow system. It is based on the analysis of all available hydrogeologic data for the study area. The conceptual model includes the system's geologic framework, aquifer properties, groundwater flow directions, locations and rates of recharge and discharge, and locations and hydraulic characteristics of natural boundaries (ASTM, 1995). The conceptual model provides the hydrogeologic framework to be used for the numerical model.

Geologic Framework

The Boulder Valley is down-dropped relative to the adjacent mountains due to faulting at the mountain fronts. The valley has been filled with unconsolidated to poorly consolidated Tertiary and Quaternary deposits (fig. 6; Ts, QTs, QTg, Qg, and Qal). Tertiary deposits include the Climbing Arrow member of the Renova formation and the Sixmile Creek formation (Ts). Tertiary and Quaternary pediment gravels (QTg) occur at the bases of the mountains. Quaternary alluvium (Qal) underlies the modern floodplain (Noble and others, 1982; Lewis, 1998; Vuke and others, 2004, 2014; Reynolds and Brandt, 2006). Depth to bedrock is greatest in the central valley, west of the Boulder River, where gravity data suggest that the basin-fill is more than 4,000 ft thick (Parker, 1961; Nelson, 1962; Wilson, 1962; Burfeind, 1967).

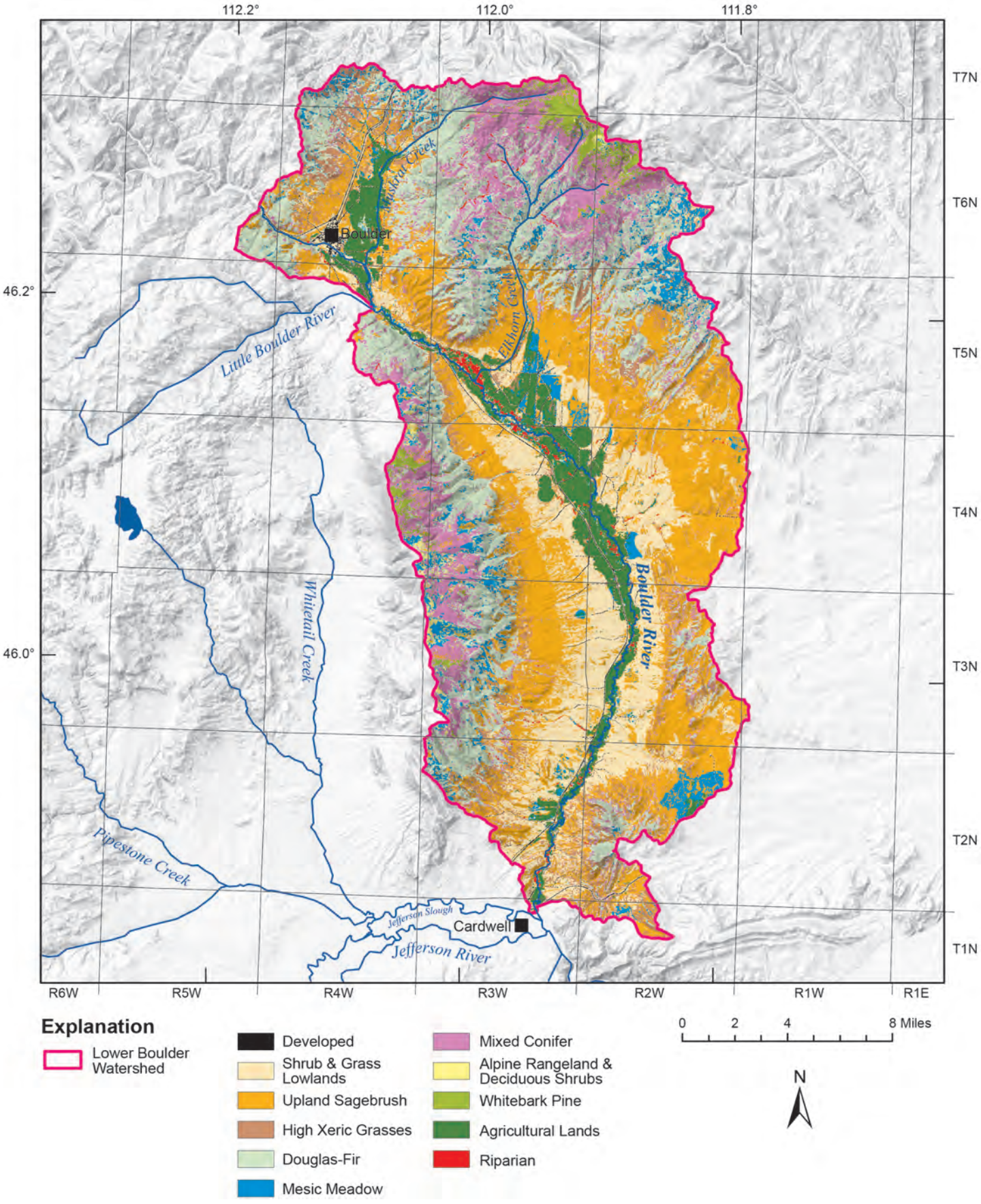

Figure 5. Vegetation within the study area varies with elevation and precipitation. Shrubs and grasses dominate at lower elevations; conifers dominate at higher elevations.

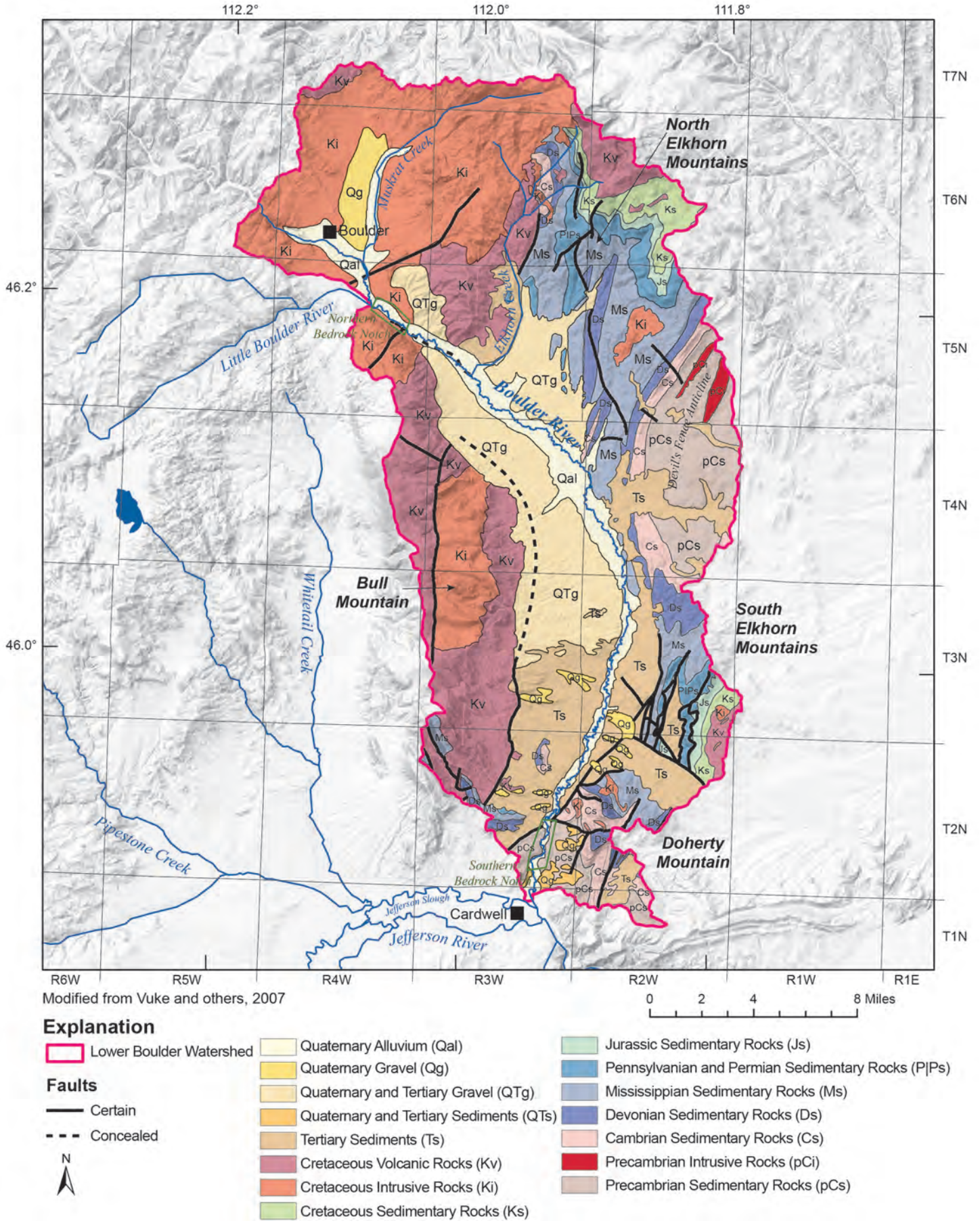

Figure 6. The northern and western parts of the study area are underlain by intrusive and extrusive igneous rocks of the Boulder Batholith and Elkhorn Mountain volcanics. The eastern and southeastern parts of the study area are underlain by fractured, faulted, and folded sedimentary rocks. In the central fault-bounded valley bedrock is overlain by unconsolidated Tertiary and Quaternary deposits.

The southern Elkhorn Mountains are composed of fractured, faulted, and folded sedimentary and metasedimentary rocks that are Precambrian to Cretaceous in age. Doherty Mountain is located at the south end of the Elkhorn Mountains, and is composed of highly deformed Precambrian to Cretaceous sedimentary and igneous rocks. The northern part of the Elkhorn Mountains and Bull Mountain are composed of Cretaceous intrusive and extrusive igneous rocks of the Boulder Batholith and the Elkhorn Mountains Volcanics (figs. 1 and 6; Lewis, 1998; Kendy and Tresch, 1996; Vuke and others, 2004, 2014; Reynolds and Brandt, 2006; Mahoney and others, 2008).

Hydrogeologic Setting

Water well completion logs were reevaluated along with geologic maps and existing literature to understand the distribution of hydrogeologic units in the study area. Logs from the MBMG's Ground Water Information Center (GWIC; MBMG, 2011) database (http://mbmggwic.mtech.edu/) were reviewed for such attributes as total depth, depth to bedrock, depth to water, and lithology. Well locations were verified to the extent possible through comparison to the Cadastral land ownership database (Montana State Library, 2013). We used 363 logs that could be located with confidence to develop a hydrogeologic model of the area.

Lithologic descriptions were compared with surrounding well logs and geologic maps to determine the distribution of the different rock/sediment types. The logs were also plotted as 3D boreholes in GMS (Aquaveo, 2012), and these were used to create cross sections to refine the spatial distribution of the hydrogeologic units (HGUs). Though they revealed little information on the maximum depth of the geologic units, the geographic distribution of lithologic groups was in close agreement with geologic maps.

Based on the analysis of geologic maps, well logs, and existing literature, the geologic units within the Boulder River study area were initially grouped into eight geologic groups: Belt rocks, carbonate rocks, siliciclastic rocks, intrusive rocks ("granite"), volcanic rocks, fine unconsolidated deposits, unconsolidated gravel, and alluvium. For modeling, these eight groups were further simplified into three hydrogeologic units (HGUs; fig. 7): alluvium, bench sediments (fine unconsolidated deposits and unconsolidated gravel), and bedrock (Belt, carbonate rocks, siliciclastic, intrusive, and volcanic rocks).

The hydrogeologic units within the study area readily exchange water with each other and are viewed as one aquifer system, with each unit having different aquifer properties. The consolidated bedrock units have little primary permeability, and groundwater moves through and is extracted from the secondary permeability of fractures and solution voids. At the study-area scale, the bedrock units have sufficient secondary permeability to be treated as equivalent porous media. At local scales, the geometry of fractures and solution voids may strongly affect groundwater flow and aquifer properties. The productivity of any individual well completed in bedrock is closely tied to the number of saturated fractures and voids the borehole encountered, the aperture of those openings, and how well the openings are interconnected. Unlike bedrock, the unconsolidated deposits have significant intergranular primary permeability and are typically more productive than the bedrock aquifers.

The carbonate rocks differ from the rest of the bedrock in that they are more susceptible to dissolution and re-precipitation of carbonate minerals (e.g., calcite). This may increase or decrease the unit's secondary permeability. Where dissolution occurs, fracture apertures widen and improve secondary permeability. Where re-precipitation occurs, permeability is decreased.

Within the Boulder Valley study area, faults have been reported or are presumed at the mountain front on both sides of the valley (fig. 6; Jerde, 1984; Reynolds and Brandt, 2006; Vuke and others, 2014). Zones of high secondary permeability can be created within a fault zone due to shear (i.e., highly fractured rocks); however, at the fault plane where the units slip past each other, the rock can be finely ground and form clay-sized particles (fault gouge) that plug pore spaces and act as a barrier to flow (Freeze and Cherry, 1979). Water-level and spring data suggest that many faults within the study area act as flow barriers (Bobst and others, 2016).

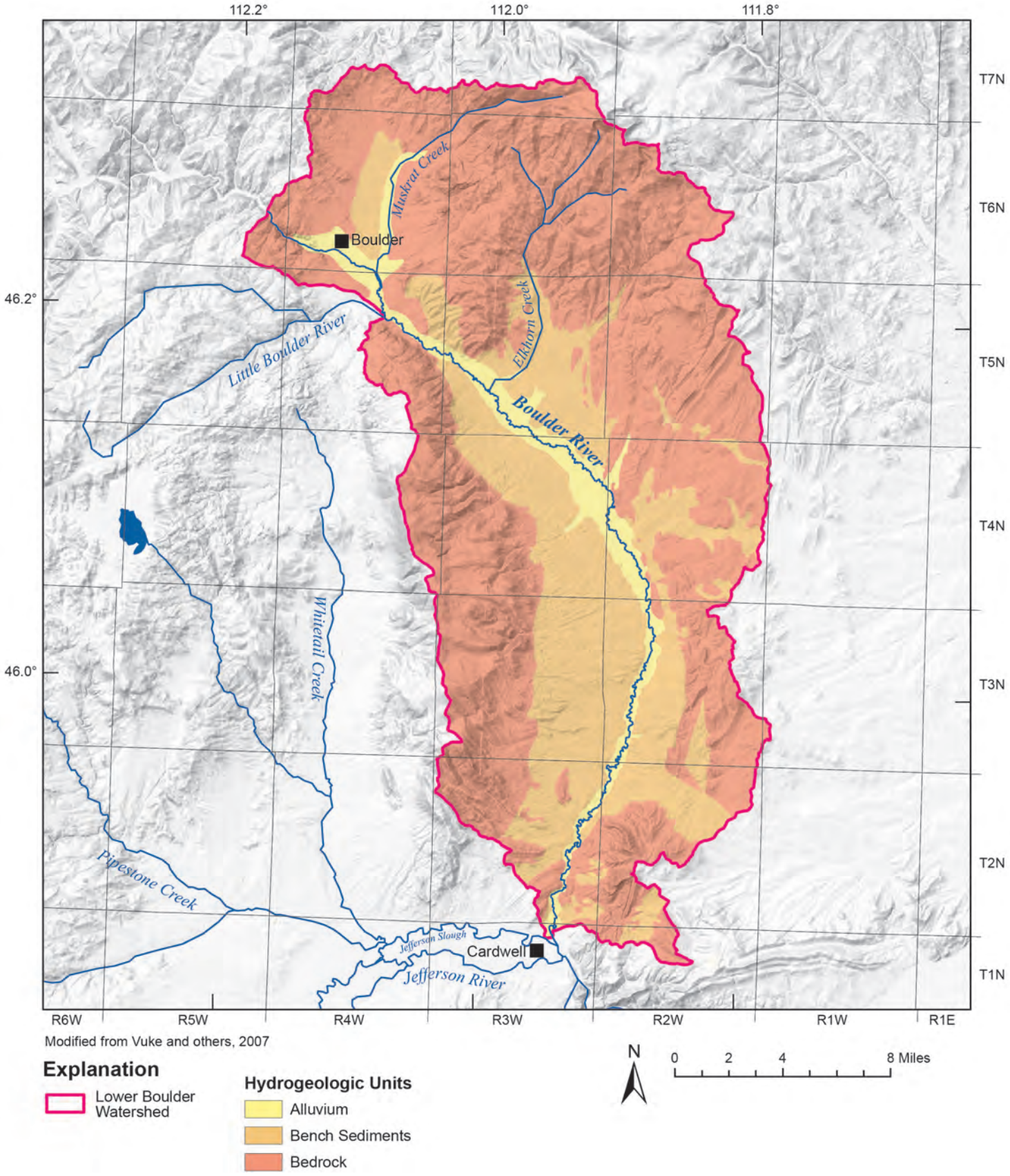

Figure 7. The geologic formations were grouped into three hydrogeologic units: alluvium, bench sediments, and bedrock. While these units have different hydrogeologic characteristics, they exchange water with each other, and can be viewed as an integrated aquifer system at the study area scale.

Groundwater Flow System

Groundwater and surface-water levels were monitored throughout the study area, and were used to analyze the groundwater flow system (figs. 8 and 9). Groundwater flow is from the topographic highs, where there is relatively high groundwater recharge, and flows towards the center of the valley (fig. 10). When groundwater reaches the center of the valley, it either discharges into the Boulder River, if that reach of the river is gaining, or it flows parallel to the river within the alluvium. Large decreases in aquifer transmissivity (T) can force groundwater flow into the river, such as in the narrow bedrock canyons below the confluence of the Boulder River and the Little Boulder River, and in the southern portion of the study area.

This overall groundwater flow pattern holds throughout the study area; however, local flow patterns are apparent in certain areas. In particular, fractures, faults, preferential flow paths along bedding planes, and differences in permeability affect the direction of groundwater flow. Additionally, water levels in and near the floodplain vary cyclically in response to stream stage and irrigation practices. In upland bedrock areas water levels show varying degrees of seasonal fluctuation depending on the local influence of mountain block recharge and inter-annual variations in precipitation.

Hydrologic Boundaries

Most of the Boulder Valley study area boundary follows the watershed divide (fig. 1). The watershed divide is presumed to be near the groundwater divide, so it is assumed that no groundwater flows across this portion of the boundary. Groundwater enters and leaves the study area through alluvium along the Boulder and Little Boulder Rivers.

Significant hydrologic features within the study area include streams and irrigation canals. The canals serve to recharge underlying aquifers through leakage, while streams both recharge and discharge water to/from the aquifer depending on local head conditions.

Aquifer Properties

Aquifer property data sources included aquifer tests conducted as part of this study (fig. 8) and a previous hydrogeologic study (Botz, 1968). The aquifer test data and analysis for this study are included in aquifer test reports (available from the GWIC sites page for the pumping wells). A summary of aquifer properties is provided in table 1.

Sources and Sinks

Sources of recharge in the conceptual model include upland recharge, irrigation recharge, canal leakage, stream infiltration, and groundwater inflow through the floodplain alluvium. Sinks, or points of discharge, include pumping wells, riparian phreatophytes and sub-irrigated grass evapotranspiration, stream baseflow, and groundwater outflow through the floodplain alluvium. These sources and sinks are further discussed in the Groundwater Budget and Boundary Conditions sections.

Groundwater Budget

A groundwater budget quantitatively summarizes the processes within the conceptual model. While some uncertainty is inherent with the calculations, a groundwater budget is useful for determining the relative importance of different processes affecting the groundwater flow system, and for evaluating the numerical model during calibration to ensure that it is realistic.

A groundwater budget accounts for water entering and leaving the study area from boundaries, sources, and sinks. The idea of a water budget is the same as the more general law of mass balance. That is, matter

Table 1. Aquifer properties estimated in the study area.

	Aquifer Properties						
	K (ft/day)			S		T (ft^2/day)	
Hydrogeologic Unit	Min	Max	Geometric Mean	Min	Max	Min	Max
Bedrock	1.2	75	9.5	0.0001		2	3,000
Bench Sediments	22	750	159	$3.2x10^{-4}$	$3.0x10^{-3}$	550	2,300
Alluvium	6	850	85	---	---	60	20,736

Note. K, Hydrologic Conductivity; S, Storativity; T, Transmissivity .

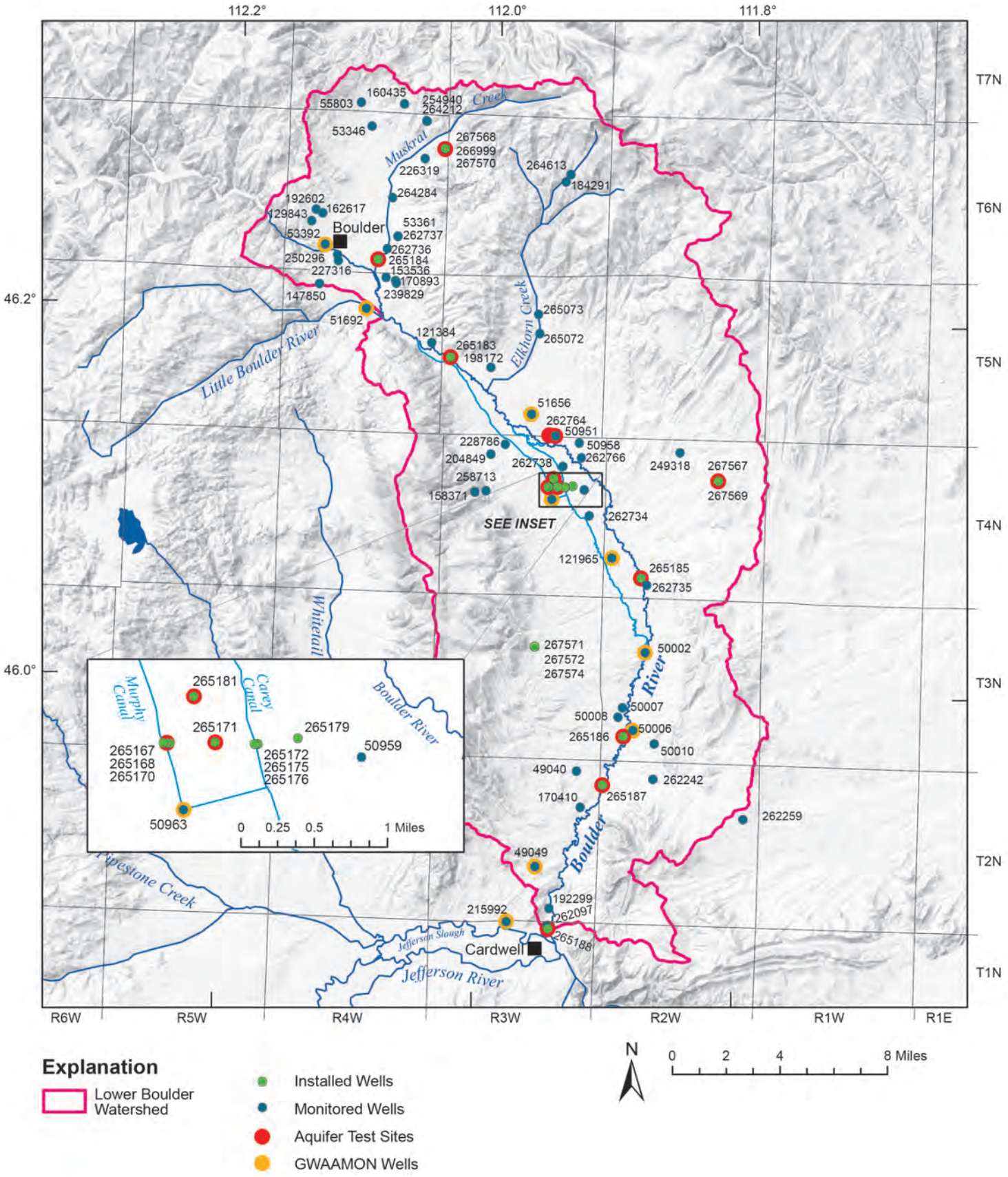

Figure 8. Seventy–eight wells were monitored monthly, with data collection occurring from July 2011 to June 2013. Twenty-three wells were installed at 10 sites for this study, and 13 aquifer tests were conducted. There are 9 long-term monitoring wells from the GWAAMON network within or near the project area. See appendix A of Bobst and others (2016) and GWIC for site details.

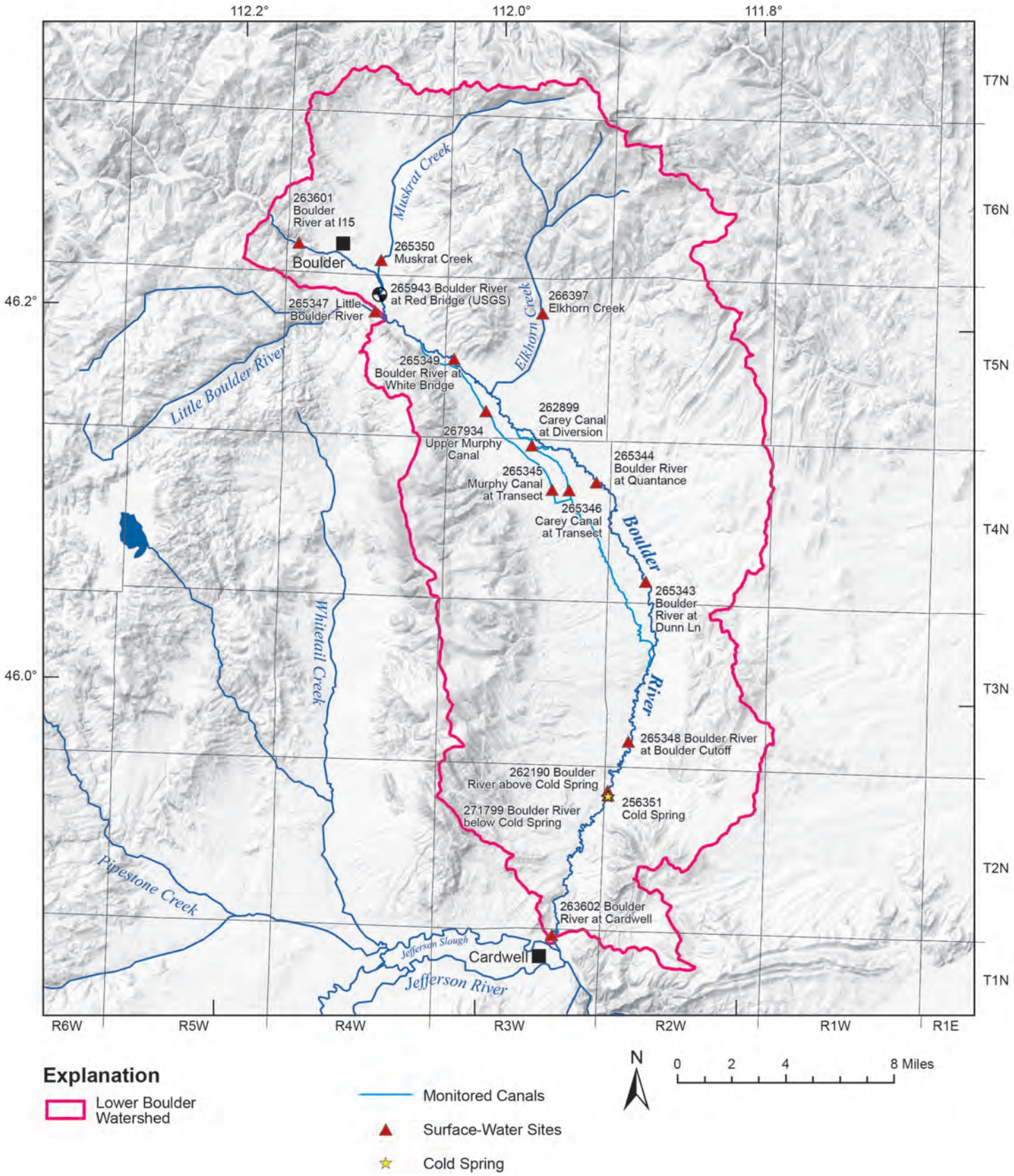

Figure 9. Surface-water monitoring was conducted at 16 sites. One spring was also monitored. See appendix A of Bobst and others (2016) and GWIC for site details.

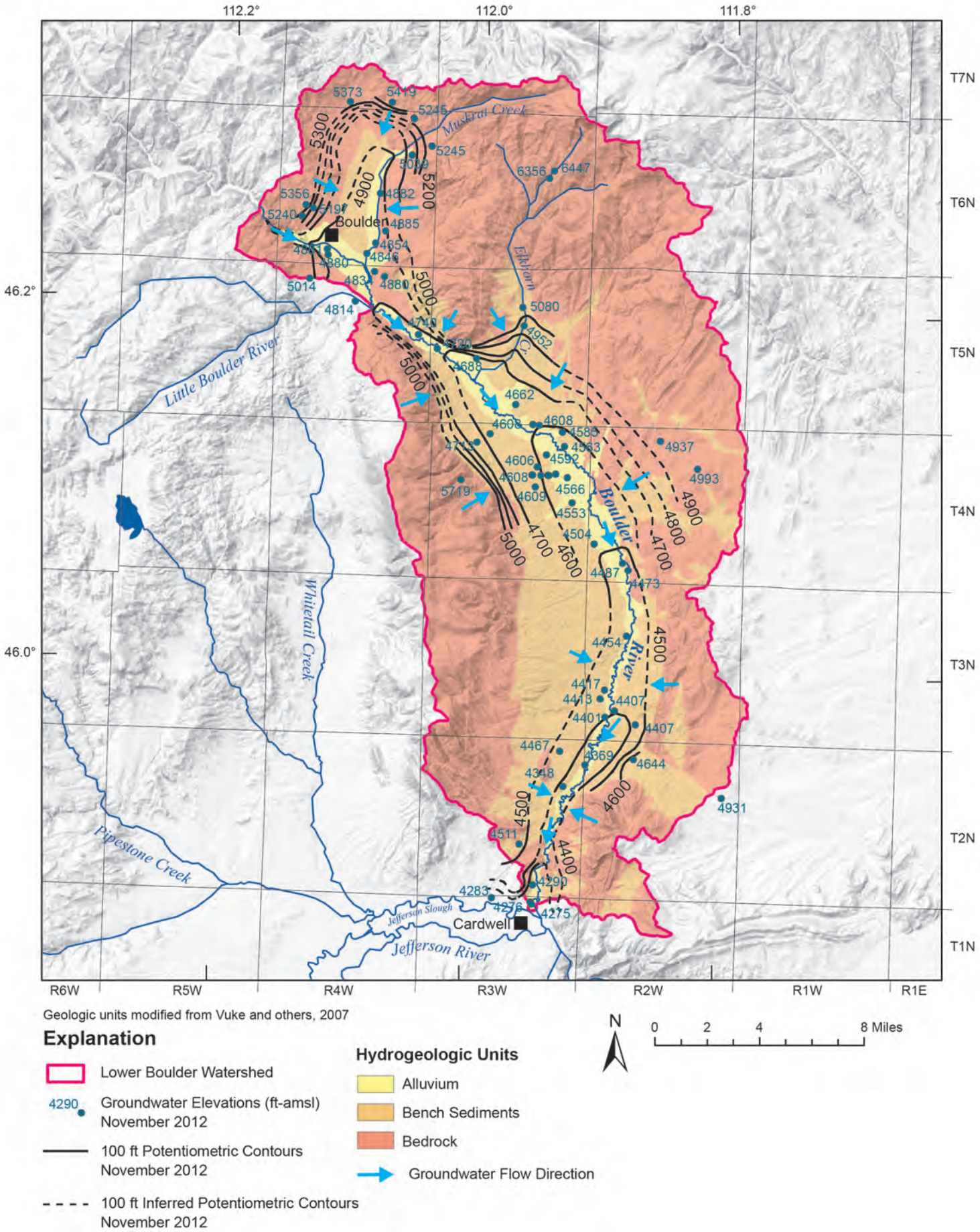

Figure 10. The November 2012 potentiometric surface is generally a subdued representation of the land surface. Hydraulic gradients are steeper in bedrock areas and flatter in the valley center.

cannot disappear or be created spontaneously. Thus, the amount of water that enters over a period of time must be equal to the amount of water that leaves over that same time period, plus or minus any water that is removed from or put into storage. In a groundwater system, changes in storage are directly related to changes in groundwater levels. The general form of the mass balance equation is:

Inputs = Outputs ± Changes in storage

The mass balance equation can be expanded for the Boulder Valley study area to:

$$IR + UR + CL + AGI = AGD + PW + ET_r + RIV \pm \Delta S,$$

where:

IR is irrigation recharge;

UR is upland recharge;

CL is irrigation canal leakage;

AGI is alluvial groundwater inflow;

AGD is alluvial groundwater discharge;

PW is pumping-well withdrawals;

ET_r is evapotranspiration by riparian vegetation;

RIV is net discharge to rivers and creeks; and

ΔS is change in storage.

The groundwater budget components are summarized below, and further details are provided in appendices B–E.

Irrigation Recharge (IR)

When the amount of water applied to an area is in excess of plant demand and evaporation (evapotranspiration, ET), the excess must either run off or infiltrate. The water applied to an irrigated field is from flood, pivot, or sprinkler irrigation, and from precipitation. Infiltrated water that passes through the crop's root zone will recharge the underlying aquifer, and is termed irrigation recharge (IR). For this study IR was estimated based on the Natural Resources Conservation Service's (NRCS's) Irrigation Water Requirements program (IWR) (NRCS, 2012a), techniques employed by the Idaho Department of Water Resources (IDWR, 2013), interviews with local NRCS staff, and groundwater water-level and flow observations in the study area.

The IWR program computes monthly crop ET rates. A monthly net irrigation water requirement (NIR) is also calculated, which is equal to the ET rate minus the effective precipitation received by the crop and any carryover moisture at the beginning and end of each season (Dalton, 2003). The Blaney–Criddle method (Blaney and Criddle, 1962) is typically used by the NRCS in western Montana (L. Ovitz and R. Pierce, NRCS Bozeman, oral commun., 2012) and was used in IWR calculations for this study.

The following equation was used to calculate irrigation recharge:

$$IR = [(NIR/IME + P_{eff} - ET) \times DP_{ex}],$$

where inputs are in length units and:

NIR is net irrigation requirement (an IWR output);

IME is irrigation method application efficiency;

P_{eff} is effective precipitation (an IWR output);

ET is evapotranspiration (an IWR output); and

DP_{ex} is portion of applied water in excess of ET that results in deep percolation (i.e., groundwater recharge) rather than runoff.

Irrigation recharge was calculated for the three irrigation methods used in the study area (pivot, flood, and sprinkler) and each of the dominant crop types (alfalfa and pasture grass/grass hay). Recharge values were then multiplied by the total acreage per irrigation method based on land-use data [Montana Department of Revenue (MDOR), 2012], and were summed to obtain a volumetric irrigation recharge estimate for the study area (appendix C, table C1). For this calculation the DP_{ex} value was set to 0.5 for flood parcels and 1.0 for pivot and sprinkler parcels (IDWR, 2013 and L. Ovitz, oral commun., 2012). These values reflect the assumption that there is no runoff from pivot and sprinkler irrigated parcels, and that half of the excess water infiltrates on flood irrigated parcels.

Approximately 90% of irrigated land in the study area is irrigated using surface water (L. Ovitz, oral commun., 2012). Surface-water availability is much greater in the early season (e.g., April–June) when spring runoff is highest. Consequently, irrigation water is often applied in excess of crop demand during this period, whereas water applied in the late season often

falls short of crop demand (P. Carey, oral commun., 2013). The theoretical crop needs calculated in IWR do not take this seasonal water availability into account. In order to more realistically represent the timing of irrigation recharge, the recharge was temporally distributed to follow water availability rather than the theoretical crop needs (appendix C, table C2). Monthly recharge rates were distributed to be consistent with the timing of irrigation canal diversions. Canal diversion rates are detailed in appendix D and were based on field observations, water-level and discharge hydrographs, and landowner interviews (P. Carey, oral commun., 2013). Irrigation season duration was divided into three periods: April–October (full season), April–September, and April–July. Multipliers were developed based on the duration of irrigation water availability and applied to monthly recharge values to distribute recharge within these periods (appendix C, table C2). Each irrigation parcel was assigned to one of the three periods based on the canal from which it derived its water. Groundwater-irrigated parcels were assigned to the full season period (April–October). Irrigation recharge volumes for the shorter, partial service irrigation seasons of April–September and April–July were reduced to 93 and 74 percent, respectively (table 2). These values resulted from increasing the application rates for the April to September parcels to 5% greater than the parcels that get irrigation water for the full season, and increasing the application rates for the April to July parcels to 10% greater than the full season parcels. These increases were to account for the observed heavier water application in the spring on fields that normally do not have irrigation water for the whole season. The final irrigation recharge values are shown in table 2. The average annual irrigation recharge was calculated to be 6,805 acre-ft/yr.

Upland Recharge (UR)

Similar to irrigation recharge, upland recharge (UR) occurs when the amount of water applied to an area (precipitation) exceeds runoff, and actual evapotranspiration (ET) (Lerner and others, 1990; DeVries and Simmers, 2002; Ng and others, 2009). Upland recharge was evaluated for the parts of the study area that are not irrigated.

Area wide and distributed water budget methods were used to estimate actual ET. Using and comparing the results of multiple methods increases the level of certainty in the estimates (Healy, 2010). The ET results were used to estimate upland recharge. The full details of each approach are provided in appendix B.

The first method assumes that the sum of precipitation (PCP), stream inflow (SW_{in}), and groundwater inflow (GW_{in}) to a given area is equal to the sum of ET, stream outflow (SW_{out}), and groundwater outflow (GW_{out}) from the area. Because long-term average values are used, it is assumed that changes in storage are negligible. Therefore, ET is equal to precipitation minus the net change in surface-water flow, minus the net change in groundwater flow. That is:

$$ET = PCP - [(SW_{out} - SW_{in}) + (GW_{out} - GW_{in})].$$

Mean annual precipitation was calculated for the study area by using the 30-yr (1981–2010) normal 800-m PRISM precipitation dataset; these data showed that the area receives an average of 325,485 acre-ft/yr. The long-term average stream flow for the surface-water stations was calculated based on extrapolation from the period of record from the USGS station [USGS 06033000 (GWIC 265943); intermittent record from 1929 to 2013] and monitoring conducted during this study (2011–2013). The average stream inflow and outflow to and from the study area was calculated to be about 97,909 acre-ft/yr and 80,049 acre-ft/yr, respectively, for a net loss of 17,860 acre-ft/yr. The average groundwater flows to and from the study area were estimated to be 148 acre-ft/yr and 150 acre-ft/yr, respectively, for a net gain of 2 acre-ft/yr (see the Groundwater Inflow/Outflow section below). Adding these two values (17,860 acre-ft/yr and 2 acre-ft/yr) to the study-area annual precipitation results in an ET estimate of 343,343 acre-ft/yr. The fact that total ET is greater than precipitation is not surprising given the extent to which surface water from outside the study area is used for irrigation.

The second ET approach estimated distributed ET values based on vegetation types (fig. 5). Over 40 vegetative classes provided in the LANDFIRE database (USGS, 2010) were grouped into 11 plant types based on their altitude and geographic distribution in the study area. Literature values were used to estimate actual ET rates of the different plant types, which ranged from 12 in/yr for lowland grass and sagebrush to 28 in/yr for riparian phreatophytes (appendix B, table B1). The estimates resulted in an area-wide ET rate of 326,002 acre-ft/yr. This value is 95% of the first approach, a good match given the uncertainties

Table 2. Irrigation recharge estimates for the full irrigation season (April to October), and for those areas irrigated for part of the irrigation season (April to September and April to July).

Irrigation Method:	April–October			April–September			April–July		
	Flood	Sprinkler	Pivot	Flood	Sprinkler	Pivot	Flood	Sprinkler	Pivot
Application efficiency: Month	35% (in)	65% (in)	80% (in)	35% (in)	65% (in)	80% (in)	35% (in)	65% (in)	80% (in)
January	0	0	0	0	0	0	0	0	0
February	0	0	0	0	0	0	0	0	0
March	0	0	0	0	0	0	0	0	0
April	0.81	0.5	0.24	0.84	0.51	0.24	0.83	0.51	0.24
May	3.51	2.16	1.03	3.68	2.27	1.07	3.80	2.35	1.11
June	3.45	2.13	1.01	3.62	2.23	1.06	3.74	2.31	1.09
July	2.35	1.45	0.69	2.46	1.52	0.72	2.55	1.57	0.75
Aug	1.54	0.95	0.45	1.62	1.00	0.47	0	0	0
Sept	1.45	0.89	0.42	1.51	0.93	0.44	0	0	0
October	1.63	1.00	0.48	0	0	0	0	0	0
November	0	0	0	0	0	0	0	0	0
December	0	0	0	0	0	0	0	0	0
Annual	*14.75*	*9.09*	*4.31*	*13.72*	*8.45*	*4.01*	*10.92*	*6.74*	*3.2*
Percent of originally calculated recharge:	100%	100%	100%	93%	93%	93%	74%	74%	74%

Assumptions:
1. The predominant soil type in the study area is silt loam.
2. Only grass is grown in flooded parcels.
3. Sprinkler and pivot parcels are an even mix of alfalfa and grass.
4. Study-area weather conditions reflect an average of the Boulder and Trident weather station conditions.
5. 50% of excess applied flood irrigation goes to run off.

inherent in each method. An advantage of the vegetation method is that it provides geographically distributed ET values, rather than a single value for the entire study area.

An upper-bound estimate for geographically distributed upland recharge on an annual basis was calculated by subtracting the distributed ET values from precipitation values (PCP-ET), both of which were averaged over 1-in precipitation zones (based on PRISM). The results were used as an initial upper-bound estimate of upland recharge where they were positive (fig. 11). The greatest excesses occurred in the Elkhorn Mountains and on Bull Mountain. There is no excess on the pediment (grass and sagebrush), and strongly negative values occur in the floodplain that is irrigated, or contains phreatophytic vegetation (fig. 5). Using this approach, the average annual excess for the study area is 30,050 acre-ft/yr. This result provided an upper bound of potential recharge because the approach does not account for other pathways, such as runoff. If the fate of excess water in the uplands is similar to that of excess water on flood-irrigated lands, about half the excess water should be runoff (DPex = 0.5), leaving about 15,025 acre-ft/yr for upland recharge.

Upland recharge does not occur at a constant rate. Most recharge occurs during snowmelt in the spring and early summer, and very little recharge occurs during the fall and winter. Also, more recharge occurs during wet periods than during dry periods. Intra-annual and inter-annual variations in upland recharge are discussed in appendix B (section B5) and are summarized in figure 12.

Canal Leakage (CL)

Canals in the study area are not lined, and most of them are above the water table, so canal leakage to the underlying groundwater occurs. Canal leakage was estimated using channel length (DNRC, 2007) combined with field observations and inspection of 2011 aerial photographs from the National Agriculture Imagery Program (NAIP). Leakage was measured for portions of the Carey and Murphy canals for this study. The leakage rates for other canal reaches were estimated by classifying the canals based on size as being similar to the Carey Canal (large; 1.61 cfs/mi), similar to the Murphy Canal (small; 0.26 cfs/mi), or between these (moderate; 0.94 cfs/mi). The leakage values were combined with canal length to determine the volumetric leakage rate.

The duration of flow in each canal was estimated based on field observations, water-level and discharge hydrographs, and landowner interviews (P. Carey, oral commun., 2013). As with the irrigation recharge approach, the canals were assigned as having water for the full season (April–October), or for a shortened season (April–September or April–July). The resulting average annual canal leakage within the study area was 16,568 acre-ft/yr. Appendix D provides further detail on this approach.

Groundwater Inflow/Outflow (AGI and AGD)

Groundwater flow into the study area occurs in the alluvium underlying the Boulder and Little Boulder Rivers entering the study area. Similarly, groundwater outflow is through the alluvium of the Boulder River near Cardwell (fig. 6). Darcy's Law was used to estimate the groundwater flux into and out of the study area. Darcy flux is defined by:

$$Q = -KA\frac{dh}{dl},$$

where:

Q is volumetric flux (ft^3/d);

K is horizontal hydraulic conductivity (ft/d);

A is cross-sectional area (ft^2); and,

$\frac{dh}{dl}$ is hydraulic gradient (ft/ft, or unitless).

Based on aquifer test results (Aquifer Properties section), the alluvial K was estimated to range from 6 to 850 ft/d, and bulk K is likely in the range of 30 to 70 ft/d. Cross-sectional area was estimated using geologic and topographic maps for alluvial width and well logs for alluvial thickness. Saturated thicknesses ranged from 10 to 30 ft. The hydraulic gradients in the alluvium at the Boulder River and Little Boulder River were based on the valley slope due to a lack of water-level data and were 0.012 and 0.003, respectively. The gradient near Cardwell was estimated to be 0.0039, which was based on both water levels and the valley slope.

The resulting groundwater inflow ranged from 44 to 443 acre-ft/yr, and the estimate using mid-range values was 148 acre-ft/yr. Calculation of groundwater outflow yielded a range of 45 to 451 acre-ft/yr, and the estimate using mid-range values was 150 acre-ft/yr (table 3).

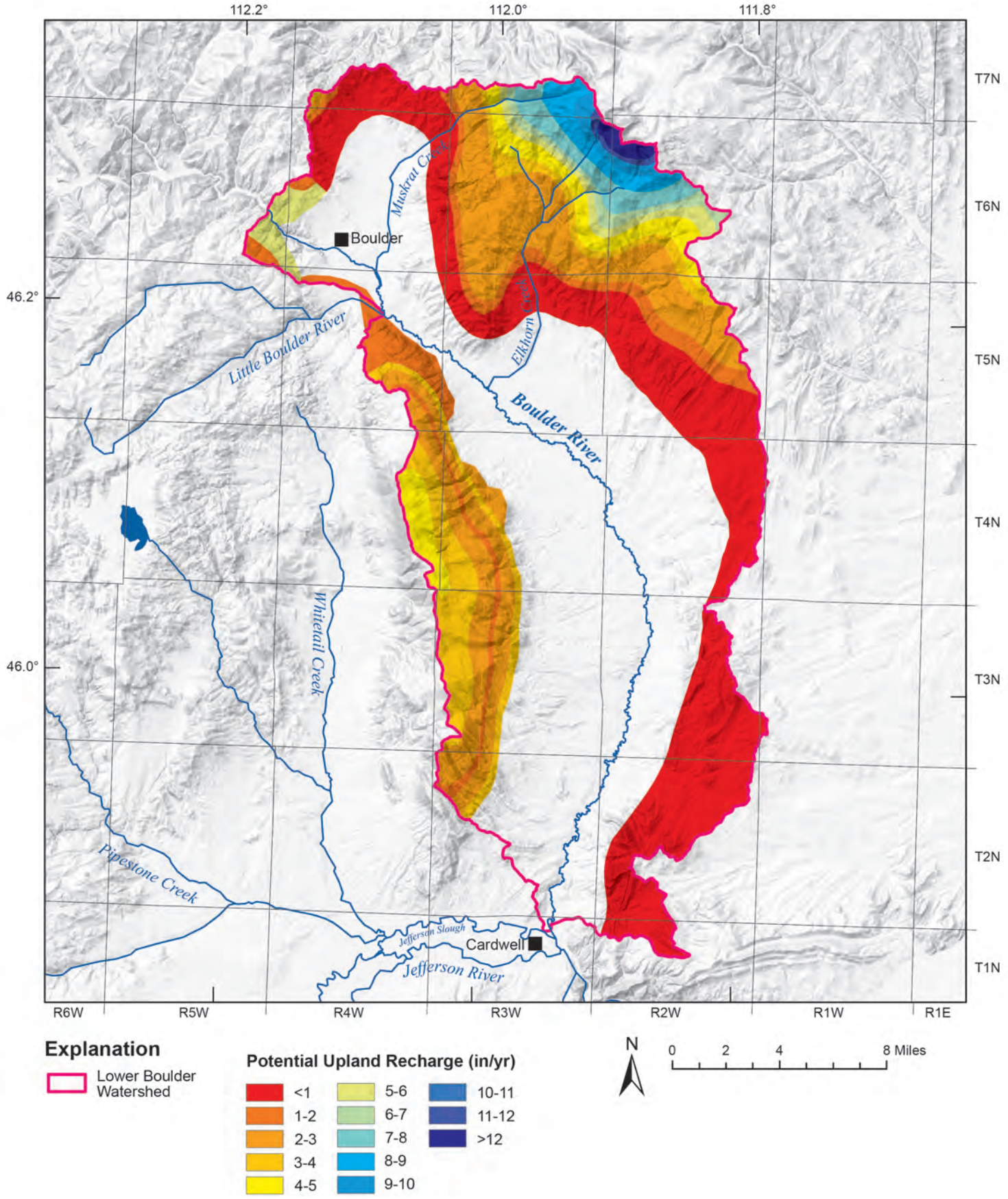

Figure 11. The upper bound estimate of the potential upland recharge is highest at the highest elevations, and declines with elevation. Because processes other than infiltration and ET are not accounted for by this approach, actual upland recharge is less.

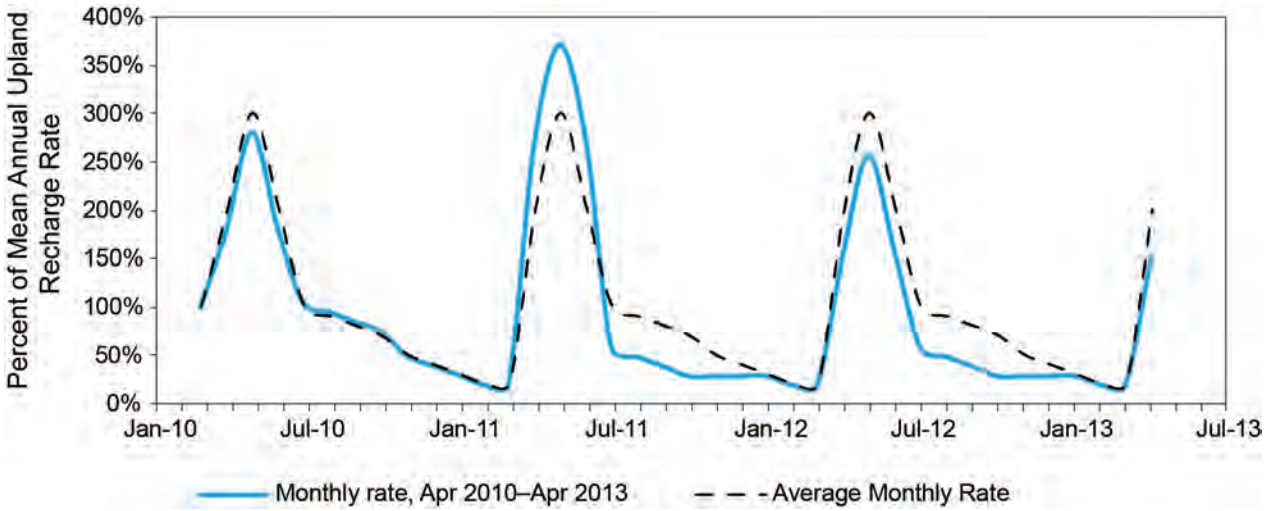

Figure 12. Seasonal distribution of upland recharge in the transient simulation involved most of the annual recharge being applied in the spring; fall and winter rates were lowest to account for infrequent infiltration in the mountain block. Inter-annual deviations were based primarily on the 2010–2013 deviation in precipitation from the 30-yr normal values (appendix B, section B5).

Pumping-Well Withdrawals (PW)

Pumping well withdrawals were estimated based on well type. Well types included domestic, stock, public water supply (PWS), and irrigation wells. Wells within the study area were identified using MBMG's GWIC database and the "Structures and Addresses" shapefile from the Montana Spatial Data Infrastructure dataset (Montana State Library, 2012). Further details on each approach are provided in appendix E.

Domestic well consumptive use was calculated using an average annual consumptive use rate of 435 gallons per day (gpd) per residence (Waren and others, 2012). Consumptive use is the amount of water pumped from the aquifer minus the water that is returned by septic systems. The annual total consumptive use by domestic wells was estimated to be 121 acre-ft/yr for the 249 homes outside of the Town of Boulder's water-service area (appendix E, section E2).

The study area contains 33.5% of the grazing land in Jefferson County, and groundwater withdrawals for livestock in the county was estimated to be 60,000 gpd (67 acre-ft/yr; Cannon and Johnson, 2004). All livestock water was assumed to be consumptively used and was estimated at approximately 23 acre-ft/yr (appendix E, section E3) of groundwater consumptively used for livestock.

Four PWS wells are used to supply water to the town of Boulder (D. Wortman, oral commun., 2012), two of which are used year-round. Based on limited pumping records from the Town of Boulder and extrapolation from more detailed records from Dillon (Abdo and others, 2013), PWS wells were estimated to withdraw 688 acre-ft/yr. Unlike the domestic well estimate, this estimate represents the total volume pumped rather than consumptive use. In the City of Boulder, treated waste-

Table 3. Conceptual model average annual groundwater budget summary (acre-ft/yr).

	Conceptual Model Estimate	Probable Range	
		Min	Max
Irrigation Recharge	6,805	6,125	7,486
Upland Recharge	15,025	12,020	18,030
Canal Leakage	16,568	14,520	17,747
Groundwater Inflow	148	44	443
Total Inflow	**38,546**		
Groundwater Outflow	150	45	451
Riparian Evapotranspiration	7,850	5,055	12,480
Well Withdrawals*	2,951	2,656	3,246
Net River Gains	27,595	24,836	30,355
Change in Storage	0⁺	0	0
Total Outflow	**38,546**		

*Well Withdrawals reflect the net consumptive use, not the pumping rate.
⁺Long-term groundwater levels were stable; however, during the study period levels generally declined. This decline is taken into account in the transient model, but not in the average annual budget.

water is discharged from a lagoon to the river, and so any return to the aquifer was assumed to be through stream infiltration.

Based on water rights, aerial photographs, and GWIC data, five active irrigation wells were identified to irrigate about 1,080 acres within the study area. A combination of side-roll sprinklers and center pivots are used to apply the water. The gross IWR method (appendix E, table E3) resulted in a calculated total groundwater consumptive use of 2,120 acre-ft/yr.

Summing the net withdrawal rates for the different well types gives a total of 2,951 acre-ft/yr. Of these groundwater withdrawals, 72% is for irrigation, 23% is for the Boulder PWS wells, 4% is for domestic water outside of municipal systems, and 1% is for livestock water.

Evapotranspiration by Riparian Vegetation (ET_r)

Local precipitation is insufficient to support the riparian vegetation growing within the floodplain; thus, some portion of the plants' consumptive use is derived from shallow groundwater. Previous work has shown riparian uptake of groundwater as deep as 10 to 13 ft below ground surface (Leenhouts, 2006; Scott, 2004). Data from alluvial wells within the study area indicate the water table is sufficiently shallow for riparian plants to access groundwater throughout most of the floodplain.

Riparian vegetation in the floodplain was divided into two classes: large woody phreatophytes (e.g., cottonwood and willow) and sub-irrigated grasses. Phreatophyte areas were delineated using 2011 infrared NAIP imagery and LANDFIRE plant classifications (USGS, 2010). Grasses, which included riparian grass as well as grass hay grown on sub-irrigated parcels, were delineated using 2011 NAIP imagery and the Montana FLU database (Montana DOR, 2012).

For mixed phreatophytes and Cottonwood, two studies conducted in southwest Montana and west-central Wyoming (Hackett and others, 1960; Lautz, 2008, respectively) reported groundwater consumptive use between 20 and 25 in/yr, and Lautz (2008) reported groundwater consumptive use for meadow grasses at 3 in/yr. Using an average of 22 in/yr for phreatophytes (3,791 acres) and 3 in/yr for grasses (3,603 acres), the annual ET_r rates were multiplied by their respective areas to obtain volumetric estimates for the study area. The resulting average annual consumptive use by riparian vegetation was 7,850 acre-ft/yr.

Changes in Storage (ΔS)

Changes in storage are directly reflected by changes in groundwater levels, with the magnitude of the water-level change being determined by the storativity of the aquifer (Ss if the aquifer is confined, and Sy if it is unconfined). Although many of the long-term (15- to 21-yr) wells show slight water-level declines, the average annual decline (0.07 ft/yr) was small enough to consider the overall trend to be stable. As such the change in storage term in the average annual budget was set to zero (table 3). The short-term trend was more dramatic, however, with groundwater levels during the 2011-2013 study period showing a clear decline. This short-term change in storage was estimated and compared with results of the calibrated transient simulation (Transient Calibration section).

Net River Gain (RIV)

Stream flow measurements were primarily made during the ice-free period. Because there were also substantial irrigation diversions during this time, the effects of irrigation practices needed to be taken into account. The following equation was applied on a monthly basis to each of the seven river reaches to estimate gains or losses in the Boulder River during the irrigation season (fig. 9 and appendix D, table D1):

$$\Delta Q = (Q_{dn} + Q_{div}) - Q_{up},$$

where all values are flows (e.g., cfs) and:

ΔQ is the net gain (negative values are losses);

Q_{dn} is the flow at the downstream end of the reach;

Q_{div} is the amount of water diverted; and

Q_{up} is the flow at the upstream end of the reach.

Evaporation was assumed negligible based on estimates using the Lamoreux–Kohler method (Potts, 1988). Several data sources were used to estimate the timing and rates of diversions in the study area; they included discharge and stage from the two monitored canals, discharge and stage from monitored river sites, groundwater levels on or near irrigated land, and landowner interviews. Diversion amounts were estimated by summing the amount of water the canal needed to deliver (i.e., the gross irrigation water requirement)

and the canal's leakage loss (appendix D, table D2). The monthly distribution of diversions followed the irrigation recharge (IR) approach described above. Results indicated four of the seven reaches were losing, the remaining three were gaining, and on average there was a net gain of 42 cfs (30,427 acre-ft/yr), or 0.96 cfs/mi (appendix D, table D4). These estimates applied to the irrigation season and were not necessarily reflective of conditions between October and April. Also of note is the uncertainty in the estimates; sources of uncertainty include measurement error, a lack of data for many of the canal diversions in the study area, and a lack accounting for run off and return flows (appendix D).

Because changes in storage were considered to be negligible, the net river gain can also be estimated as the difference in the rest of the budget components. This was 27,595 acre-ft/yr (38 cfs), which compares well with the estimate above (30,427 acre-ft/yr or 42 cfs) and is similar to the observed average net increases in the Boulder River from I-15 to Cardwell when irrigation diversions were limited in the fall (mid to late October): 36 cfs (26,080 acre-ft/yr) in 2012 and 43 cfs (31,150 acre-ft/yr) in 2013.

Budget Summary

The groundwater budget analysis indicated that the average annual groundwater inputs and outputs in the Boulder Valley study area totaled about 38,500 acre-ft/yr. Of the groundwater inputs, approximately 43% is from canal leakage, 39% is from upland recharge, 18% is from irrigation recharge, and less than 1% is from groundwater inflow. Of the outputs, approximately 72% flows to surface waters, 20% is used by riparian vegetation, 8% is withdrawn by wells, and less than 1% leaves the study area as groundwater. This average annual budget was used to determine boundary conditions for the steady-state model, and was used to evaluate the calibration.

GROUNDWATER FLOW MODEL CONSTRUCTION

Computer Code

MODFLOW simulates groundwater flow numerically using a finite-difference method, and is a widely accepted groundwater flow program developed by the USGS (Harbaugh and others, 2000). MODFLOW-NWT (version 1.0.8) was used for this project. NWT is a Newton–Raphson formulation for MODFLOW-2005, aimed at providing added stability in nonlinear unconfined flow conditions. NWT must be used in conjunction with the Upstream-Weighting (UPW) flow package, because inter-cell conductance calculations differ from those used in the Layer Property Flow, Block-Centered Flow, and Hydrogeologic-Unit Flow packages. Because the NWT linearization approach generates an asymmetric matrix, the Orthomin χMD solver was used. Groundwater Vistas (Vistas) was the graphical-user interface for MODFLOW (Environmental Simulations Incorporated, 2011; version 6.59 Build1). PEST (version 13.0; Doherty, 2010, 2013a) was used for automated parameter estimation.

Spatial Discretization

The model grid was set to the North American Datum 1983 Montana State Plane coordinate system, in units of International Feet. A rectangular grid frame encompassed the study area, and cells outside of the study area were inactivated (fig. 13). Cell spacing was a uniform 400 ft x 400 ft (3.7 acres), and the model featured one layer, 456 rows, and 285 columns. The model thickness ranged from 192 to 5,150 ft thick, while the saturated thickness ranged from 134 to 3,332 ft. Table 4 provides additional details on the model grid.

The uniform cell spacing of 400 ft x 400 ft allowed for a well-refined grid without significantly compromising computational time. This grid spacing provided a match for the density of available observation data, prevented flow-computation errors in areas of steep gradients, avoided having multiple boundary conditions (e.g., pumping wells) in a single cell, and provided a stable and representative simulation of fine-scale boundary conditions (e.g., streams).

Telescope mesh refinement (TMR) was considered in areas where a finer grid would be advantageous, such as at hydrologically significant features (e.g., the Boulder River) and at closely spaced monitoring sites. Ultimately, TMR was not used due to the potential solution errors introduced by irregular spacing in the block-centered finite difference grid (Anderson and Woessner, 2002). Although these errors are often negligible in relatively small, flat areas, given the Area-Wide Model's regional scale, steep gradients, and the large number of cells requiring refinement, it was decided that such potential errors should be avoided.

A single layer optimized solution stability, pa-

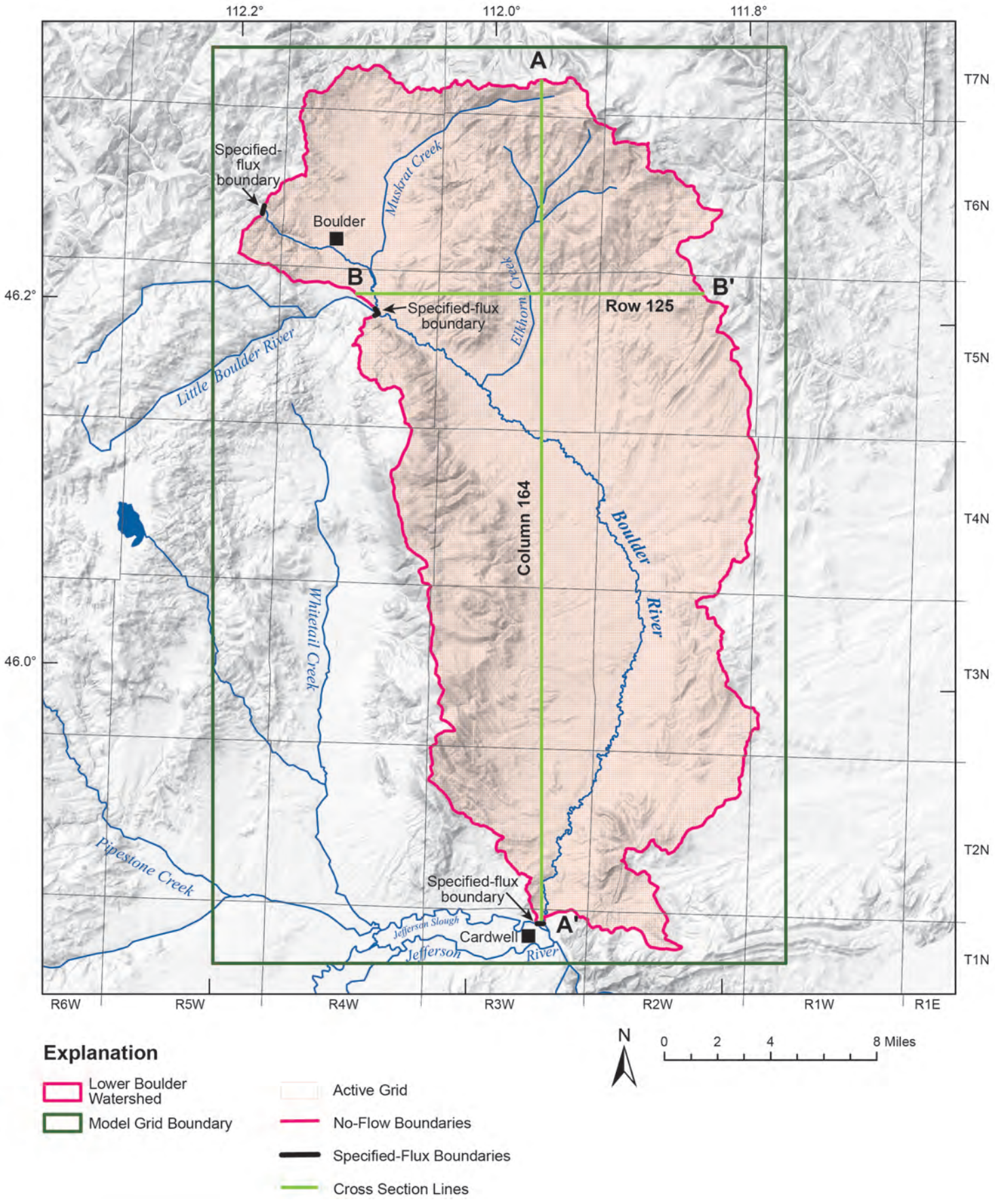

Figure 13. The active grid for the Area-Wide Model has the same extent as the Lower Boulder Watershed. Grid cells are 400 ft by 400 ft in the horizontal dimensions. The edges of the model were primarily modeled as no-flow boundaries; however, specified-flux boundaries were used where groundwater flows into and out of the modeled area through alluvium (fig. 6). Model profiles are shown in figure 14.

Table 4. Details of the model grid.

Rows	456
Columns	285
Layers	1
Total area	745 sq mi
Active area	377 sq mi
Row spacing	400 ft
Column spacing	400 ft
Number of active cells	65,761
Coordinate system	State Plane MT FIPS 2500, International Ft
Vertical datum	NAVD 88
Spatial units	feet
Temporal units	days
X offset	1,281,236.55
Y offset	591,338.58
Rotation	0
Max thickness	5150 ft
Min thickness	192 ft
Max saturated thickness*	3332 ft
Min saturated thickness*	134 ft
No. no flow cells	64,199
No. SFR cells+	3,005
No. WEL cells^	1,392

*Based on steady-state simulation results
+SFR, stream flow routing
^WEL Package cells represent pumping wells, canal leakage, and alluvial groundwater inflow/outflow

rameter estimation, and model run times (fig. 14). Although multiple layers in the floodplain alluvium could have allowed for a finer-scale representation of flux to and from the riverbed, thin, shallow layers would have led to a high rate of cell drying and rewetting at the floodplain/pediment interface, thus increasing numerical instability. Furthermore, a separate, deeper layer would not have any observation points, because wells are typically completed in the shallow alluvium. Multiple layers would also increase model run times substantially.

The top of the grid (fig. 14) was defined using a Digital Elevation Model (DEM) derived from the USGS 1-arc second National Elevation Dataset (U.S. Geological Survey, 2012). The DEM data point spacing was about 98 ft, or roughly a quarter of the 400-ft cell spacing. Top-of-cell elevations were calculated through bilinear interpolation of the more densely distributed DEM data. During the calibration process, 5 ft was added to the top-of-cell elevations to rectify discrepancies between the DEM and monitoring site survey data (see Calibration section).

The bottom of the grid (fig. 14) is a gradual north-to-south sloped plane that was based on the minimum and maximum land-surface elevations in the floodplain. The primary goal in designing the bottom surface was to maintain a relatively uniform saturated thickness of about 200 to 300 ft in the floodplain alluvium to facilitate alluvial aquifer property estimation. Because land-surface elevations generally decrease from north to south in the study

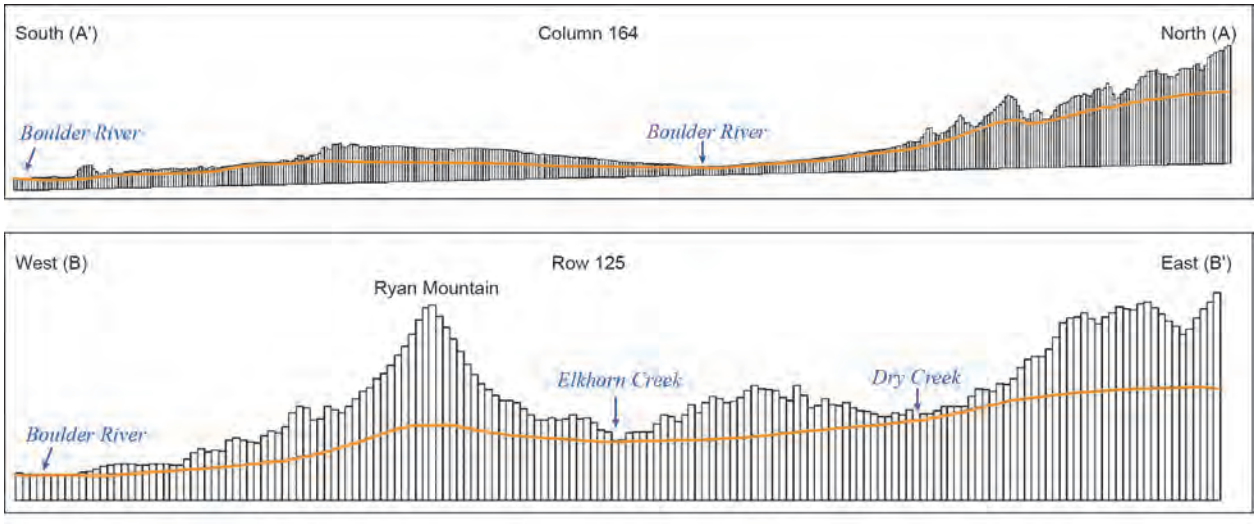

Figure 14. Model cross sectional profiles show the north–south sloped bottom of the model, the top of the model based on the land surface (derived from USGS DEM), and the modeled potentiometric surface. The transect lines used for these profiles are shown in figure 13.

area, the surface was generated by calculating the total change in elevation between the northern- and southern-most points of the floodplain, and dividing by the distance between those points to obtain an average slope. Next, the row containing the southernmost point in the floodplain was set to 300 ft below the land surface at that point, and the remaining bottom elevations were calculated by applying the average slope north and south of that row. The resulting elevations ranged from 3952 to 4728 ft-amsl over the model domain.

Temporal Discretization

The Area-Wide Model's calibrated transient simulation was divided into monthly stress periods to approximate the temporal variation in the aquifer system's seasonal stresses, such as irrigation practices. The number of time steps per stress period was varied during initial transient simulations, and results were insensitive to values greater than five, so each stress period was discretized into five equal time steps (Anderson and Woessner, 2002).

The calibration period for the transient simulation was 3 yr and 1 month (April 2010 to April 2013). The steady-state simulation was added as the first stress period, resulting in a total of 38 stress periods. The simulation began 15 months prior to the start of the study (July 2011) to allow the aquifer system to respond to the dramatic changes in recharge resulting from flooding that occurred before and early in the study period (June–July 2011). The flooding was caused by an excess of high-elevation late season snowpack, as well as high precipitation in the valley. This wet period was followed by below-average precipitation in 2012, and even drier conditions in 2013. These contrasts were advantageous for calibration, in that they represented a wide range of conditions. During the pre-study months, limited calibration was possible by using water-level data from the MBMG's GWAAMON wells (fig. 8), and USGS monitoring of the Boulder River at Red Bridge (USGS 06033000 (GWIC 265943); fig. 9).

Hydraulic Parameters

Hydraulic parameters in the model include aquifer K, Sy, and Ss. Prior to model calibration, parameter values were assigned to polygonal zones in the model based on the aquifer property estimates from aquifer tests performed during this investigation and previous investigations (table 1; Aquifer Properties section). The polygon extents were based on the hydrogeologic units of the conceptual model (Geologic Framework section); the units include the alluvium, the bench sediments, and the upland bedrock. The initial parameter values were modified during the model calibration process (Calibration section).

Boundary Conditions

The boundary conditions in a numerical groundwater model are mathematical expressions of the state of the aquifer system that constrain the model equations; they are assigned to all of the three-dimensional boundary surfaces of the model and to internal sources and sinks (ASTM, 2004). Boundary conditions represent the sources of recharge and discharge, and/or the hydraulic head at the edges of the modeled domain.

The boundary conditions of the Area-Wide Model follow the conceptual model discussions in the Hydrologic Boundaries, Sources and Sinks, and Groundwater Budget sections of this report. This section discusses how they were represented in the numerical model. The boundaries used in the numerical model were either head-dependent flux or specified flux. Specified heads were initially used to develop flux estimates where groundwater flows into/out of the area through the alluvium; however, they were replaced by specified-flux boundaries in the final version of the model.

Active Grid Border

The horizontal edges of the active grid were assigned as specified-flux boundaries. Most of the border was set as a no-flow boundary because it follows the boundary of the lower Boulder River watershed, which is assumed to be a groundwater divide. Only the borders of the floodplain were assigned non-zero flux values, because groundwater flows in and out of the modeled area through the alluvium in the floodplain (figs. 6 and 13). The two areas of inflow (positive flux) are at the alluvium of the Boulder River and Little Boulder River, while the one area of outflow (negative flux) is at the alluvium of the Boulder River near Cardwell. These three portions of the grid boundary were modeled as specified flux cells using the using the WEL (Well) Package. The calibrated rates from the steady-state model were used as constant values in the transient simulation due to the small changes in groundwater gradient and saturated thickness at these locations, which rendered only minor changes in Darcy flux estimates. Additionally, the transient calibra-

tion revealed that the simulated heads were insensitive to the minor variations in flux at these locations.

Internal Sources and Sinks

Sources of recharge to the model include irrigation recharge, upland recharge, canal leakage, and stream infiltration. Irrigation recharge was simulated as a specified-flux boundary with the Recharge Package. The irrigation recharge distribution was primarily derived from the Statewide Final Land Unit classification database [Montana Department of Revenue (MDOR), 2012], and rates varied by irrigation method, crop type, and source water (appendix B, fig. B1 and table B2); further detail on calculating the amount of irrigation recharge is provided in appendix C.

Like irrigation recharge, upland recharge was also applied as a specified-flux boundary using the Recharge Package. As described in the Groundwater Budget section and appendix B, upland recharge was limited to the mountain-block area and was reflective of local precipitation, vegetative ET, slope, and rock type. Conceptual recharge estimates were refined during calibration (see Steady-State Calibration section). Transient rates were applied through the use of recharge multipliers per stress period (appendix B, table B4).

Canal leakage was set as a specified flux boundary using the WEL Package. Leakage from 28 canals were simulated (fig. 15 and appendix D, section D1 and table D2), and a uniform flux was applied across all cells of each canal per stress period. A few low-lying canals were simulated using the Stream-Flow Routing (SFR) Package due to their gaining rather than losing conditions (see Streams section and appendix B, fig. B2 and table B3).

Sinks, or points of discharge within the model, included pumping wells, riparian phreatophyte and grass evapotranspiration, and stream baseflow. Pumping wells were simulated as specified flux boundaries using the WEL Package (fig. 15). Groundwater consumption by riparian vegetation was simulated as a head-dependent flux boundary using the Evapotranspiration Package (EVT). The maximum ETr rates for phreatophytes and grasses were 25 in/yr and 10 in/yr, respectively (fig. 16). The extinction depth was set to 10 ft for both plant groups, and the surface elevation was set to the DEM-interpolated top elevations for each cell. In the transient model, monthly ETr rates were distributed proportional to those of crops from the NRCS IWR Program (NRCS, 2012a).

Streams

Streams serve as both sources and sinks in the study area. Depending on the location, stream water infiltrates to groundwater or groundwater flows into streams. Therefore, streams were simulated as head-dependent flux boundaries using the SFR Package (appendices B and D). This package was used to represent three types of waterways: the Boulder River and its major tributaries (Muskrat Creek and the Little Boulder River), upland creeks, and irrigation diversions (appendix B, fig. B2 and table B3).

SFR requires the specification of several variables, including the segment's starting flow, downstream routing ID, streambed top elevation, streambed vertical hydraulic conductivity (K_v), reach length (L), streambed width (W), streambed thickness (M), and channel slope (S). Additions to and subtractions from stream flow were made via tributaries and diversions, respectively; additions from precipitation and return flow were not explicitly simulated, nor were subtractions from evaporation. Evaporation was assumed negligible based on estimates using the Lamoreux–Kohler method (Potts, 1988). Unsaturated flow was not simulated, and so the streambed was assumed to be in direct contact with the aquifer.

Package outputs include streambed conductance (C, equal to (K_vLW/M)), stream depth, stream flow, and flux to or from the aquifer. Streambed conductance was calculated using constant streambed width and thickness (W and M) per stream network, which were based on average values of field data (table 5). K_v assignments for each stream type are discussed below. For this model the stream depth, which is used to calculate a reach's head elevation and flux, was calculated by applying Manning's equation to determine depth as function of flow and assumes rectangular channel dimensions. Manning's equation is:

$$n = \frac{\Phi}{Q} A R^{2/3} S^{1/2},$$

where:

n is Manning's roughness coefficient (sec/ft $^{1/3}$);

ϕ is 1.486 ft^3/sec (a constant);

Q is stream discharge (ft^3/sec);

A is cross-sectional area (ft^2);

R is hydraulic radius (cross-sectional area divided by the wetted perimeter; ft); and

S is channel slope (ft/ft or unitless).

The roughness coefficient (*n*) was estimated for each flow-monitoring site using the 2012 flow and channel-dimension data, with heavier weight given to the first half of the data record (spring and early summer) because late summer *n* values were biased high due to low-flow conditions. Channel slope (*S*) was estimated in ArcGIS by tracing the stream channel 500 ft above and below each monitoring site and using DEM altitudes at those locations. Results for Boulder River sites were averaged to obtain a single n value for all river segments, whereas the *n* values of its tributaries (Muskrat Creek and Little Boulder River) were based on one site each. SFR segments representing upland creeks, for which data were unavailable, were uniformly assigned the Muskrat Creek *n* value, as their channel properties were most similar to Muskrat Creek (table 5).

Boulder River Network. Starting stream flows were specified only at the start of the Boulder River SFR network, which included the upstream Boulder River and the Little Boulder River inlets (figs. 9 and B2). In the steady-state simulation, estimates of the mean annual flow were specified at each location; the flow estimates were extrapolations based on the data record near each inlet (GWIC 263601 and 265347, fig. 9) and at the one existing long-term USGS station in the study area [USGS 06033000 (GWIC 265943); using data from 1929 to 2013]. Similarly, in the transient simulation, mean monthly flows were estimated and specified. For months in which data were available at GWIC 263601 and 265347, actual site data were used to derive monthly flow estimates. For other months, flow estimates were estimated using the relationships observed during the study between the two sites and the USGS station.

Streambed elevations were specified on a per-reach (i.e., per-cell) basis. At flow monitoring sites in the floodplain, reach elevations were set equal to the available survey data, and USGS 1:24,000-scale topographic maps were used as a guide along other reaches. Specifically, topographic contours were overlaid with SFR segments in ArcMap, and elevations were estimated at the segment endpoints; the elevation difference was then divided by the segment length to derive a bed slope estimate. Slope values generally decreased downstream and ranged from 0.007 at the first river segment to 0.001 at the final river segment. In order for the resulting elevations to fit the survey data at monitoring sites, slight adjustments were made to some segment slopes. As a final step in SFR elevation assignments, top-of-cell elevations were used to refine SFR bed elevations; the two datasets were compared in all SFR cells to ensure that the streambed surface remained below the grid surface in order to avoid flooding.

During the streambed design process, discrepancies were discovered between monitoring site survey data and the topographic map data in the central floodplain, namely at White Bridge, Quaintance Lane, and Dunn Lane (GWIC 265349, 265344, 265343; fig. 9). The surveyed elevations were above the topo-based estimates by 22.4 ft, 2.4 ft, and 7.0 ft, respectively, which had significant effects on the adjacent head values. This became problematic during calibration because heads were consistently higher than the observed groundwater levels, regardless of aquifer property variation. Consequently, the SFR bed elevations were not adjusted to fit the survey data at those three sites. Elevation discrepancies associated with monitoring sites are further discussed in the Calibration section.

Streambed K_v values were estimated through the use of flux calibration targets. Flux targets were set on

Table 5. Input values for the SFR Package.

	Starting Q* (cfs)	K_v (ft/d)	M (ft)	W (ft)	*n* ($sec/ft^{1/3}$);
Boulder River	123	0.2–2.0	3	47	0.065
Muskrat Creek	0	1.4– 2.0	3	8	0.060
Little Boulder River	12	0.7	3	16	0.054
Upland Creeks	0	10	3	5	0.060

*Steady-state value
Kv, Vertical Hydraulic Conductivity
M, Streambed thickness
W, Streambed width
n, Manning's roughness coefficient

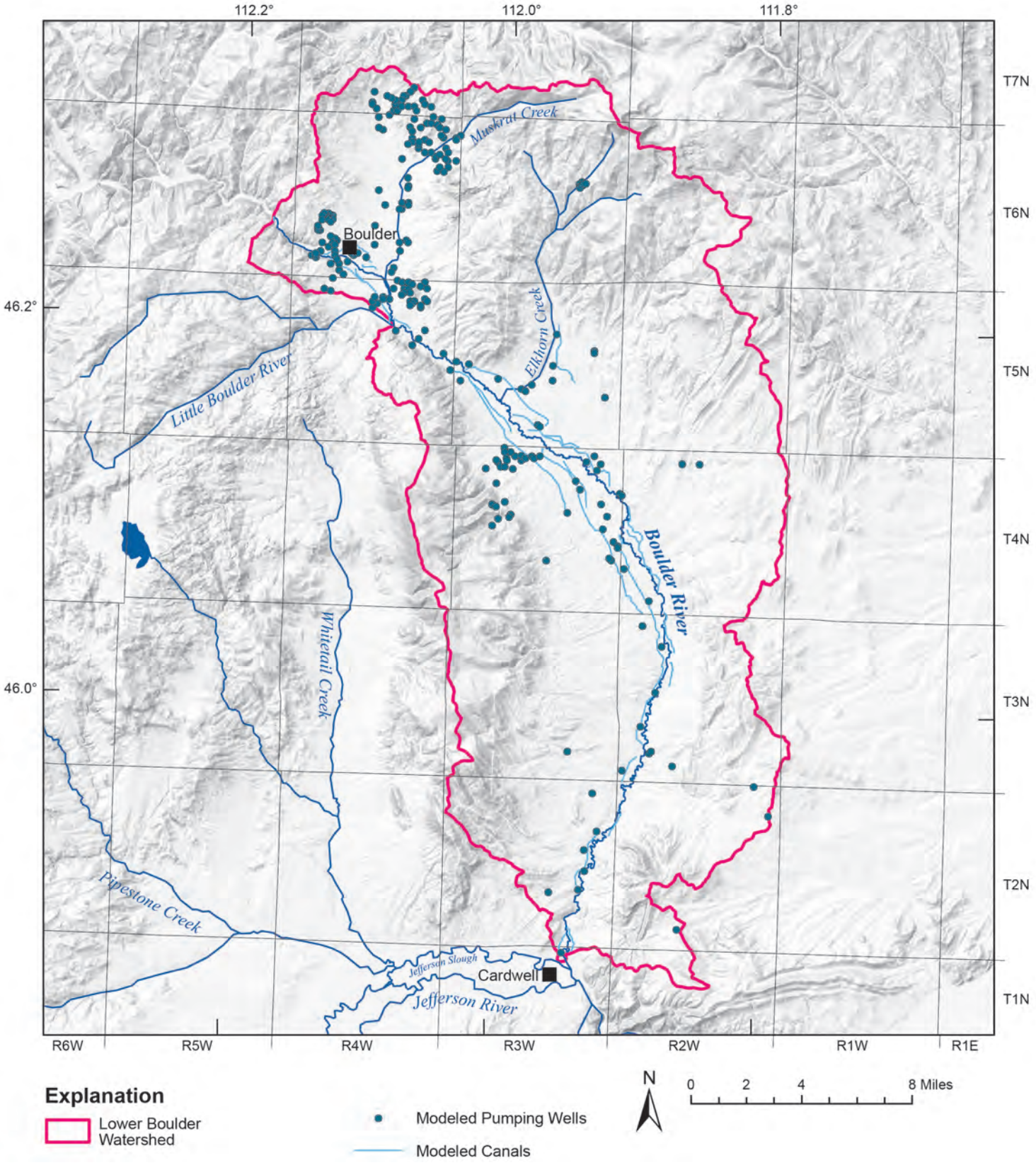

Figure 15. The WEL package was used to simulate pumping well withdrawals and canal leakage. Canal leakage rates were based on monitoring data, channel dimensions, and source water availability (appendix D). Pumping-well rates varied among well types, which included domestic, stock, PWS, and irrigation (appendix E).

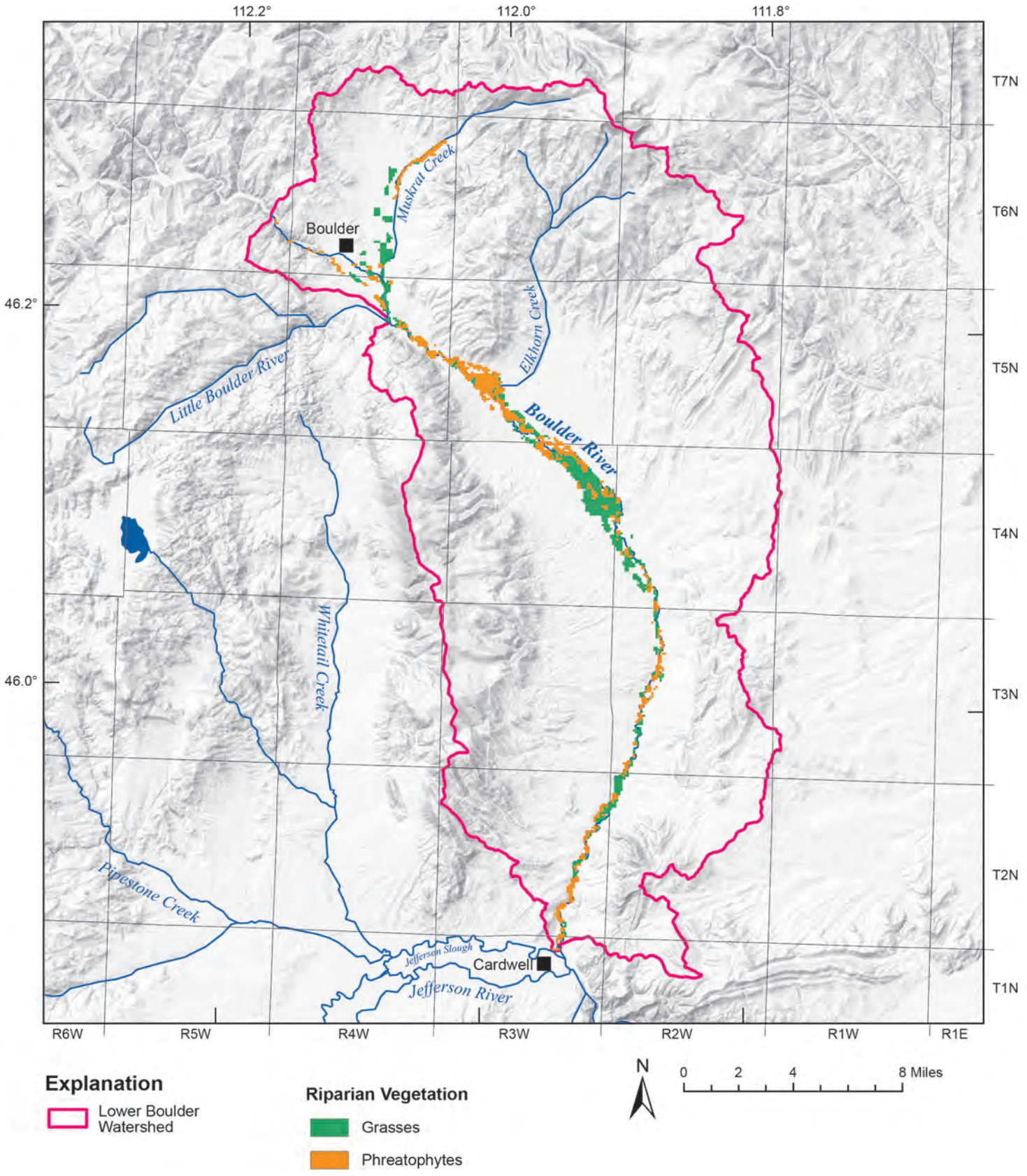

Figure 16. Riparian ET distribution was divided into two plant types: sub-irrigated grasses and woody phreatophytes. The EVT package was used and maximum ET rates were based on the results of studies in similar settings.

a per-segment basis along the river and lower reach of Muskrat Creek. Ideally, the targets would have corresponded with the seven field-based river reaches (fig. 9 and table D1); however, a flux target cannot be assigned to multiple segments in Vistas, and so individual segment fluxes were manually tallied during post-processing. A conceptual range for riverbed K_v was set between 0.1 and 5.0 ft/d based on an a few point estimates where stream flow, stage, and groundwater-level data were available (Carlson, 2013). Segment K_v values were manually varied within this range to achieve optimal flux results. Final K_v values ranged between 1.0 and 2.0 ft/d, except for two segments that were assigned values of 0.1 and 0.2 ft/d. These river segments are located in the town of Boulder, where losing conditions prevail; they were assigned a relatively low K_v because flux results greatly exceeded field estimates of river loss when K_v was within the 1.0–2.0 ft/d range.

Upland Creeks. Upland creek SFR segments were used to represent both stream channel flow and infiltration of stream water along the mountain front. These segments were intended to capture upland recharge within high-relief drainages, where cell flooding would otherwise occur, and then redistribute that recharge along the mountain front, where land slopes lessened and permeability increased. Thus, they were a source of focused recharge in the model, taking in precipitation-derived flow within the mountain block and discharging it to unconsolidated materials at lower elevations.

Streambed K_v values for upland creeks were uniformly set high at 10 ft/d, allowing for easy intake and discharge of flow. Starting flow for all segments was set to zero. Due to the steep and varied gradients within each segment, segments were assigned bed elevations on a per-reach (i.e., per-cell) basis to ensure that the bed remained below the top of the cell and below the elevations of all upstream reaches of the stream network. Modeled creeks were selected based on field observations and an evaluation of 2011 color infrared imagery; those with riparian vegetation and/or observed summertime flow were included in the model. During the calibration process, a few additional intermittent creeks were included to reduce flooding in upland drainages (fig. B2).

Upland creek simulation results showed that most creek networks had no flow at their downstream limits, consistent with field observations. In the steady-state simulation, the remaining flow in those few creeks amounted to less than 0.3 cfs. The only network extending into the floodplain was Muskrat Creek; flow within its upper reaches and tributaries was routed to the segment containing the study's flow-monitoring site (GWIC 265350; fig. 9), where the stream flow was calibrated to field measurements. Flow was calibrated through estimation of streambed K_v values in the portion of Muskrat Creek underlain by alluvium (table 5) and resulted in a steady-state flow of 4.0 cfs, which was comparable to the mean annual field estimate of 4.1 cfs. Transient flow patterns were similar to field data, showing early and late-irrigation season pulses driven by irrigated field recharge (appendix G); peak flows were slightly lower than field measurements, likely due to short-term high-flow events not being captured by the monthly time discretization in the model.

Irrigation Diversions. Diversions from the Boulder River were simulated to represent the effects of irrigation practices on stream flow and groundwater/surface-water interactions. A diversion was also simulated off Elkhorn Creek because of its extensive recharge effects in the area, and observations indicated that it captured all available flow during the irrigation season. Other creek diversions were not simulated, as the surface-water/groundwater interaction objectives of the study were focused on the Boulder River, and data were lacking for upland creeks other than Elkhorn Creek.

Diversions were specified as a single reach (i.e., cell) off the river (appendix B, fig. B2 and table B3), and flow rates were estimated using the approach detailed in the Groundwater Budget section (Canal Leakage) and appendix D (section D1). Field data were used for the Carey Ditch diversion (GWIC 262899). Conditions were set so that flow was diverted from the river unless there was none available. For example, if a diversion rate was set to 100 cfs and only 90 cfs was available at that particular river location, 90 cfs of flow would be diverted.

The leakage from most canals was simulated using specified-flux cells (injection wells in the WEL Package; fig. 15). A few low-lying canals and secondary channels were simulated as SFR segments due to their potentially gaining conditions (appendix B, fig. B2 and table B3).

CALIBRATION

Selection of Calibration Targets

Observed groundwater elevations, measured stream flows, and estimated streambed flux were used as calibration targets (i.e., observations) in the model. Groundwater elevation estimates also served as control points in areas lacking observations. Each of these target types were assigned a group and weight.

Groundwater-level data were collected monthly at 77 monitoring wells during the project, beginning as early as the summer of 2011 and continuing until June 2013 (fig. 8). Of these, 73 had an adequate record to use for the steady-state calibration. Two of the 73 wells (GWIC 51692, 215992) were removed from the calibration dataset because they fell outside of the model domain. Another well (GWIC 262259) was also outside the domain but was still used by mirroring its location on the opposite (west) side of the watershed divide; this approximation of the water level was used to aid calibration in an area otherwise void of observations. Eight additional wells (GWIC 254940, 265167, 265170, 265172, 265176, 266999, 267569, 267570) were removed from the calibration dataset due to their density relative to the model cell size; that is, multiple wells occurred in the same cell. This left 63 wells in the calibration dataset (fig. 17).

Rather than use water levels from a single monitoring event, a mean annual water level was calculated from an annual data record (e.g., Jan 2012–Jan 2013) per well, and that value served as the steady-state head calibration target. This approach was best suited to the steady-state calibration due to the lack of a true steady-state time period during the study. In the transient simulation, the measured monthly heads served as targets.

The calibration criterion was set as a ±5 ft head residual, which was approximately 0.2% of the range of observed groundwater elevations within the modeled area. Head error statistics were also used to aid calibration. These statistics included the residual mean, which should be close to zero in a well-calibrated model (i.e., the positive and negative residuals balance one another); the mean of the absolute value of the residuals, which is a measure of the average error in the model; and the root mean square (RMS) error, which is the square root of the average of the squared residuals.

During certain calibration runs, control points (i.e., imaginary observation wells) were added to better fit heads to observed water levels. They were added after preliminary calibration runs generated an unrealistic hydraulic gradient in certain areas due to a lack of observation data. This occurred in the uplands near the watershed boundary, where sharp contrasts in elevation occur between mountain peaks and alluvial drainages. In these areas, early head configurations varied between extensive flooding in the drainages and unrealistically low heads in the mountains. To resolve these issues, both minimum- and maximum-censored head targets were used. Minimum-censored targets have a residual error of zero when the computed head is above the target. Similarly, maximum-censored targets have an error of zero when the computed head is below the target. Maximum-censored targets were placed in alluvial drainages where flooding was problematic, and the maximum head was set to the land surface (i.e., the DEM value). Minimum-censored targets were placed along ridgelines near the watershed border, and the minimum head was set to 300 ft below the land surface. The number of control points varied between PEST runs, with up to 28 being used in any given run. Note that the head calibration statistics were based only on data measured from the 63 observation wells and did not take these control points into account.

Flux and flow targets were also used in calibration to estimate streambed hydraulic conductivity (K_v), which is one variable in the streambed conductance term. Because the streams were a type of boundary condition, details of the stream package (SFR) design and $K_v$calibration are discussed in the Boundary Conditions section of this report. Vistas supports the use of both flow and flux targets with stream boundary conditions. For this model, surface-water flow (i.e., stream discharge) targets were set at specific SFR nodes, and flux (i.e., streambed leakage) targets were set along SFR segments (fig. B2). The seven field-based river reaches (fig. 9 and table D1) included multiple SFR segments, so after each calibration run, the individual segment fluxes were tallied and compared with field estimates (Boundary Conditions section). Flux was calibrated primarily in the steady-state simulation to (1) approximate the field-based estimate of the net Boulder River gain through the study area; (2) ensure the gain or loss of individual river reaches was reasonable; and (3) ensure that upland creeks achieved a

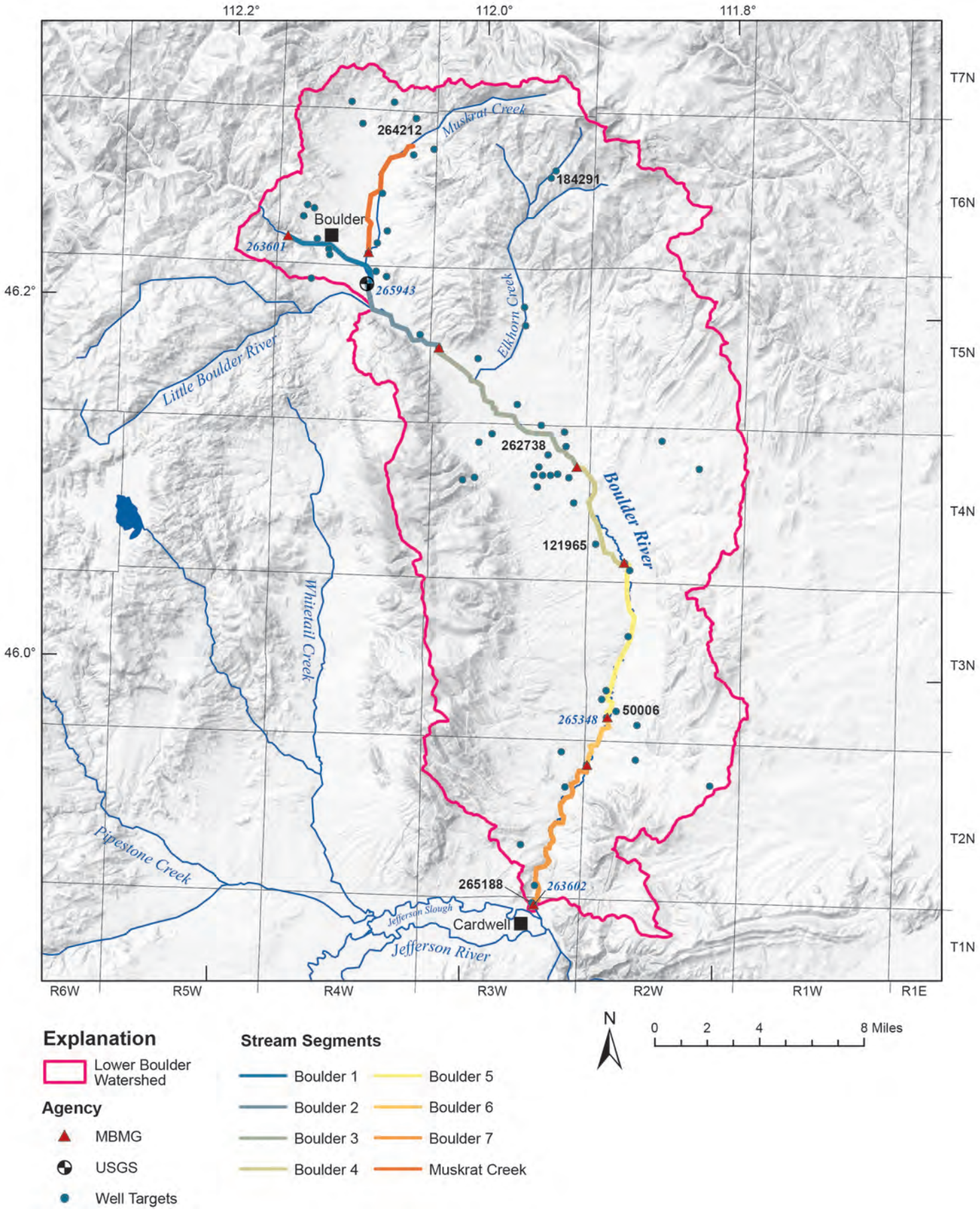

Figure 17. Water levels in 63 monitoring wells served as head targets in the steady–state calibration. Nine surface-water monitoring sites provided stream-flow targets. Estimated gains or losses along stream reaches were also used as targets for the Boulder River and Muskrat Creek. Hydrographs for the numbered sites are show in figures 22 and 25.

net flux of zero (Boundary Conditions section). Only one surface-water flow target was used in the steady-state simulation: at the Muskrat Creek monitoring site (GWIC 265350, fig. 9), a flow target was used to avoid a large over- or underestimation of tributary flow into the Boulder River. Flow at the upstream end of the Boulder River was specified in the model, as was its only other tributary input from outside the study area (the Little Boulder River). In the transient simulation, flow targets were used at the Muskrat Creek site and all eight Boulder River monitoring sites to calibrate to flow measurements.

Observation Grouping and Weighting

The different types of observations were grouped in order to identify their relative contributions to the measurement objective function during a PEST run. The observation groups included (1) head targets representing real monitoring site data; (2) censored head targets representing control points; (3) surface-water flow targets representing monitoring site data; and (4) flux targets representing streambed leakage estimates. Depending on the PEST run, one to four of these groups were used.

These groups were weighted prior to each PEST run in order to ensure roughly equal starting contributions to the objective function, thus preventing a given observation type from overshadowing the others. For instance, a low weight (0.1) was assigned to the censored head targets to reflect their low integrity and keep their contribution to the objective function relatively low; a few were also zero-weighted for a qualitative assessment of calibration results (Doherty and Hunt, 2010). During PEST runs that included both flux and head targets, flux targets were assigned weights orders of magnitude lower than those of the heads so that the head values would still be visible in the objective function despite the difference in units (ft^3/day vs. ft; Doherty and Hunt, 2010). In addition, intra-group weighting was used to penalize the less reliable values of a certain observation type. For example, the heads in two of the 63 monitoring wells (GWIC 50949, 262766) were non-static due to pumping throughout the study period; their targets were assigned a weight of 0.5 rather than 1.0.

Steady-State Calibration

A steady-state simulation is meant to represent average annual conditions for all components of recharge and discharge; it simulates the system in equilibrium with a specified set of stresses. A steady-state simulation can serve several purposes, such as predicting the ultimate impact to the groundwater flow system from a new stress; evaluating the overall groundwater budget; and estimating conductance parameters independently from storage parameters (Doherty and Hunt, 2010). In this model a steady-state simulation was calibrated and then used as the first stress period in the 3-yr transient simulation.

Methods

The steady-state simulation was calibrated to observed values (i.e., the calibration targets) through manual and automated parameter estimation (PEST). Manual calibration involved adjustment of input parameters to minimize the difference between the model output and observations (i.e., to minimize the residuals). Specifically, the calibration goal was to minimize the sum of squared residuals. Typically, only one parameter value was adjusted per model iteration in order to isolate its influence relative to other input parameters. Manually adjusted parameters included aquifer hydraulic conductivity (K), recharge, streambed K_v, and alluvial flux.

PEST was also used to estimate K, upland recharge, and streambed K_v through automated parameter estimation. All parameters were log-transformed to linearize the relationship between each parameter and the model output, and to equalize parameter sensitivities by scaling each parameter relative to its inherent variability (Doherty and Hunt, 2010). Streambed Kv was estimated by SFR segment (Boundary Conditions section). In contrast, upland recharge was estimated zonally. The zonal approach involves polygonal zones that are user-defined throughout the model domain, and PEST yields a single parameter value per zone. The upland recharge polygons generated from precipitation and ET were used in the steady-state calibration (fig. 11; Groundwater Budget and Boundary Conditions sections; appendix B, fig. B1 and table B2). K was held constant during each PEST run in which recharge was estimated; however, relatively high- and low-value K configurations were used in different runs to establish a reasonable range of recharge within the conceptual K estimates.

K was estimated with PEST using a combination of zones and pilot points. The eight hydrogeologic

units discussed in the Geologic Framework section were combined into three groups. All Quaternary and Tertiary bench sediments were combined in one zone; the five bedrock units were combined to form a single bedrock zone; and the Quaternary alluvium in the floodplain remained a distinct unit. The zones were assigned initial values based on the aquifer property estimates discussed in the Aquifer Properties section (table 1).

These simplified zones were partly due to a lack of observations within zones of the original configuration, but also because they were used in conjunction with pilot points. Pilot points allow for intra-zonal variation, because the method generates a parameter value for each model cell. Parameter values between pilot points are based on a user-specified interpolation method. For this model, kriging was used with an exponential variogram model. The default Vistas settings were used and the search radius was set large enough to capture adjacent pilot points within a zone. The K zones allowed for sharp pilot point value contrasts over short distances, such as where bedrock units border the relatively transmissive alluvial floodplain.

Pilot point placement followed PEST guidance documentation (Doherty and Hunt, 2010). A relatively uniform grid was first created to avoid large gaps between points; more were added in areas of dense observations and between the outflow boundary and the closest well (GWIC 265188). The total number and configuration of K pilot points changed throughout the calibration process to improve estimation in various local areas. Pilot point values were constrained by upper and lower bounds, typically within an order of magnitude of the K range (table 1) and textbook values (Freeze and Cherry, 1979; Fetter, 2001). Although K was the estimated parameter, PEST results were evaluated in terms of T because the simulated saturated thickness was generally greater than conceptual estimates, especially in upland areas.

Traditional calibration procedures limit the number of parameters relative to the number of available observations with the goal of creating a well-posed inverse problem (Doherty and Hunt, 2010). In many groundwater modeling problems this goal can only be met by reducing the number of parameters prior to calibration, which can often oversimplify the conceptual model and preclude parameter variability that is potentially important to model predictions. Alternatively, regularized inversion includes a suite of approaches in which parameter simplification is accomplished mathematically as part of the calibration process. The modeler is able to control the degree of parameter variation within a zone through regularization algorithms, which provide greater parameter flexibility and aim to maximize the amount of information extracted from observations (Doherty and Hunt, 2010). For these reasons regularization was used during pilot point PEST runs.

During PEST runs in which K pilot points were regularized, each polygonal zone became its own observation group, with each “pseudo-observation” (Doherty and Hunt, 2010) pertaining to a preferred-homogeneity condition. This preferred-homogeneity condition directs PEST to evaluate not only the fit to head and flux observations within a K zone, but also the departure of each pilot point value from its surrounding values. The approach avoids “bull’s-eye” K configurations and instead favors geologically realistic departures from the background K field. The process was guided by a regularization objective function that was set higher than the measurement objective function. The user specifies the regularization objective function as the value below which PEST is likely over-fitting to observations through unrealistic parameter variation. Regularization variable settings followed those suggested in PEST guidance documentation (Doherty, 2013b).

During calibration calculated groundwater head observations at two wells (GWIC 265183 and 265185) were lowered in proportion to adjacent Boulder River streambed elevations that were also lowered (White Bridge and Dunn Lane; GWIC 265349 and 265343, respectively). As discussed in the Boundary Conditions section, the streambed elevations were lowered because their surveyed elevations were considerably higher than those estimated from topographic maps (22.4 ft and 7.0 ft, respectively). The elevation differences became apparent after local calibration difficulty; specifically, the heads in this part of the central floodplain (GWIC 265183, 121384, 198172, 265072, 51656, 50951, 262738, 262735, 265185) were consistently higher than the observed groundwater levels, regardless of aquifer property variation; thus, the streambed elevations appeared to be anchoring the surrounding heads to an erroneously high datum. The surveyed bed elevations were also problematic because the associated SFR segment slopes were incon-

gruous with adjacent segments that followed the local topographic contours. To resolve these problems, the two bed elevations were calculated using the same topo-based approach as the rest of the simulated riverbed elevations. Once the elevations were lowered to match the topographic map estimates, the head calibration dramatically improved. Additionally, the top grid surface was raised 5 ft from the original DEM-interpolated cell values (Spatial Discretization section) in order to reduce flooding that remained in portions of the central floodplain area. Because the majority of surveyed well elevations were above the DEM in this area, and because of the area's shallow water table, the increase of 5 ft was deemed valid to reduce the flooding.

Results

The resulting modeled potentiometric surface was similar to the observed surface, and errors were reasonably small (figs. 18 and 19). Sixty-one of 63 wells were within the calibration criterion of ±5 ft, with no apparent high or low spatial trends. The observed heads in the other two wells (GWIC 50949 and 262766) were non-static due to pumping, so as expected their simulated heads were above the target values; however, both residuals were within 15 ft of the targets. The RMS error for the steady-state simulation was 2.4 ft; note that this value was calculated from the weighted head residuals, in which the two continuously pumped wells were weighted to 0.5 as described above. The RMS error represents about 0.1% of the observed groundwater-level elevation range of 2,172 ft.

The K distribution resulting from calibration fit well with conceptual estimates for each of the three hydrogeologic unit groups: alluvium, bench sediments, and bedrock (fig. 20, table 1 and table 6). The floodplain alluvium exhibited the highest K and T ranges, as expected, with a mean T value of 4,010 ft^2/day and a range of 299 to 13,818 ft^2/day. Bedrock T values exhibited a mean of 67.1 ft^2/day and ranged from 1.6 to 554 ft^2/day; the relatively young, less-fractured units (e.g., volcanics and granite) were generally at the low end of this range, whereas the relatively older, more-fractured units (e.g., limestone and Belt rock) were at the high end. T values for the bench sediments fell between the bedrock and alluvial values (11 to 2,251 ft^2/day), and had a mean value of 462 ft^2/day (table 8).

Upland recharge values resulting from the steady-state calibration were considerably lower than the upper bound estimates from the conceptual groundwater budget; however, they were similar to values estimated by assuming that about half of the excess water would infiltrate (DP_{ex} = 0.5). The upper bound rates yielded flooding and a poor fit with observations, even when hydraulic conductivity values approached the maximum limit of their reasonable ranges. Recharge values were consequently lowered in order to lower heads and reduce flooding in the mountain block area. The lowering of the initial rates was appropriate because the approach used to derive them was for an upper-bound estimate that did not account for losses other than ET. Losses such as runoff, snow sublimation, and soil moisture retention could be substantial in high-altitude areas with steep gradients, low-permeability bedrock, and deep water tables. The total volume of recharge was lowered to approximately 42% of the upper bound estimate (i.e., DP_{ex} = 0.42). The resulting mean annual recharge was 6.1% of mean annual precipitation. This value is comparable to the 6.5% of precipitation that was applied as mountain-front recharge in the Managed Recharge Model (Carlson, 2013), and to rates applied in studies of similar settings (Huntley, 1979; Maurer and others, 1997; Flint and others, 2002; Bossong and others, 2003; Manning and Solomon, 2005; Flint and Flint, 2007; Magruder and others, 2009).

Upland recharge was also spatially redistributed during the steady-state calibration. Rates were increased along the mountain front and decreased in steep, low-permeability areas of the mountain block, though most recharge still remained in the higher-elevation areas that receive the most precipitation (appendix B, fig. B1). While the primarily goal was to fit computed and observed heads, the shift was also made to qualitatively account for slope and permeability. The recharge redistribution is supported by previous studies on upland recharge, which highlight the effects of such factors on infiltration rates (appendix B, section B4).

Calibrated Boulder River streambed K_v values ranged from 1.0 ft/d to 2.0 ft/d, except for two segments that were assigned values of 0.2 and 0.3 ft/d (Boundary Conditions section). These two river segments are located in the town of Boulder, where losing conditions prevail; they were assigned a relatively low K_v because modeled flux greatly exceeded field estimates of river loss when K_v was within the 1.0–2.0

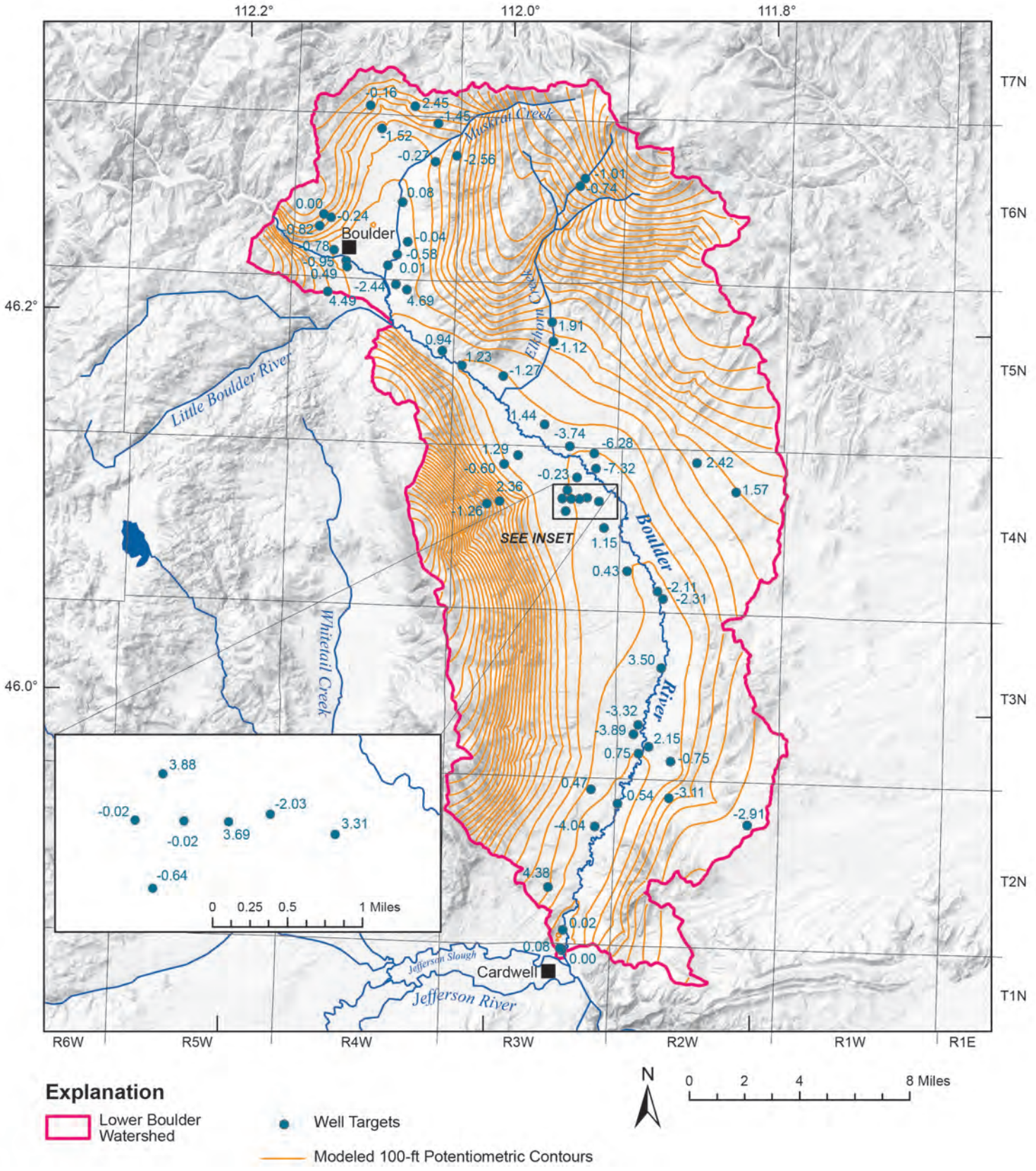

Figure 18. The modeled potentiometric surface from the steady-state calibration was similar to the conceptual surface (fig. 10). The relatively tight contours in upland areas reflect the lower permeability of the bedrock aquifers. Head residuals (blue values) in 61 of the 63 calibration points ranged from -4.0 to 4.7 ft. At the other two sites modeled heads were higher than observed; however, these wells were always pumping when monitored (non-static).

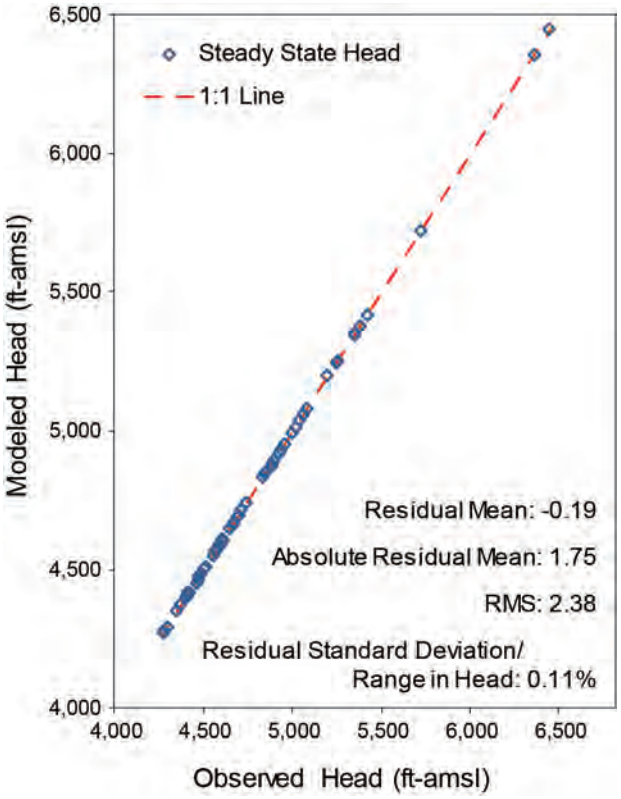

Figure 19. A comparison of observed and computed heads shows no systematic deviation from unity. The root mean square error of the calibrated steady-state model was 2.38 ft.

ft/d range. The net gain simulated within the Boulder River network was 37 cfs, which compares well with the 38 cfs estimate made in the groundwater budget analysis (Groundwater Budget section). The flux result is also comparable to the average net increase in the Boulder River shown during the period of limited diversions (October 15–22), which was 36 cfs in 2012 and 43 cfs in 2013 (Bobst and others, 2016). Additionally, the flux result is similar to the 42 cfs estimate calculated using irrigation-season data (Groundwater Budget section; appendix D, table D4). While the overall net flux difference compares well with field observations, the flux for reaches 3, 4, and 5 did not match well with the field estimates (appendix D, tables D1 and D4), which may result from uncertainty associated with the field estimates. Because of the dramatic seasonal changes in the river's gaining/losing conditions, the results of the transient model were evaluated more closely and are discussed in the next section.

With respect to the streambed K_v of upland creeks, manual calibration resulted in a uniform value of 10 ft/d, which simulated field observations of very little flow reaching the Boulder River (Boundary Conditions section). Total flow from upland creeks to the Boulder River was less than 0.3 cfs.

Calibration to head targets produced alluvial outflow comparable to the conceptual best estimate (Groundwater Budget section). Results of alluvial inflow at the Boulder River and Little Boulder River inlets were at the low end of the estimated inflow range, which suggests relatively low K values and/or thin saturated thicknesses in these areas. The inflow through the Boulder River alluvium at the upstream end of the study area was especially low (11 acre-ft/yr), which reflects its canyon setting (fig. 6); that is, the saturated zone may be entirely within the bedrock underlying the thin layer of alluvium in this area.

The steady-state groundwater budget was comparable to the conceptual annual average groundwater budget for the Boulder Valley (fig. 21; table 7). Differences are primarily due to grid coarseness; for example, the coarseness caused minor variations in the model area vs. the actual study area. The grid

Table 6. Summary of modeled aquifer property values.

	K (ft/day)			T (ft^2/day)		
Hydrogeologic Unit Group	Min	Max	Mean	Min	Max	Mean
Alluvium	0.1	58.8	17.8	299	13,818	4,010
Bench sediments	0.040	14.8	1.8	11.0	2,251	462
Bedrock	0.002	1.74	0.13	1.63	554	67.1
		S_y			S_s (ft^{-1})	
Hydrogeologic Unit Group	Min	Max	Mean	Min	Max	Mean
Alluvium	0.035	0.327	0.145	$1.0x10^{-5}$	$5.0x10^{-4}$	$2.3x10^{-4}$
Bench sediments	0.010	0.295	0.060	$1.0x10^{-6}$	$5.0x10^{-5}$	$1.7x10^{-5}$
Bedrock	0.002	0.052	0.018	$2.5x10^{-8}$	$1.0x10^{-6}$	$3.4x10^{-7}$

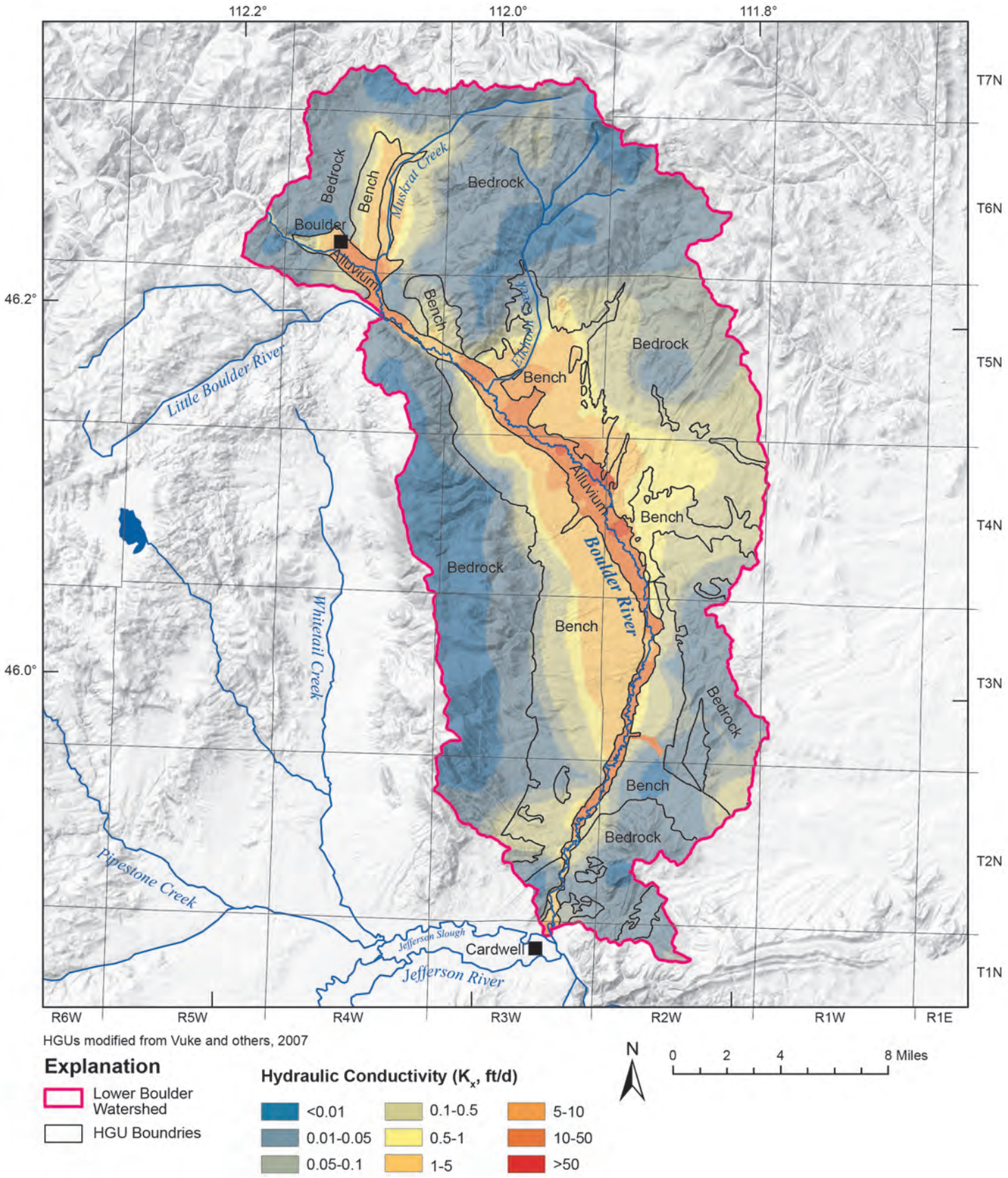

Figure 20. The hydraulic conductivity (K) distribution in the calibrated steady-state model was consistent with conceptual model estimates. The alluvium in the floodplain was the most transmissive, followed by the bench sediments. Bedrock was the least transmissive, and the relatively young, less-fractured bedrock (granite and volcanics) was less permeable than the older bedrock (fig. 6).

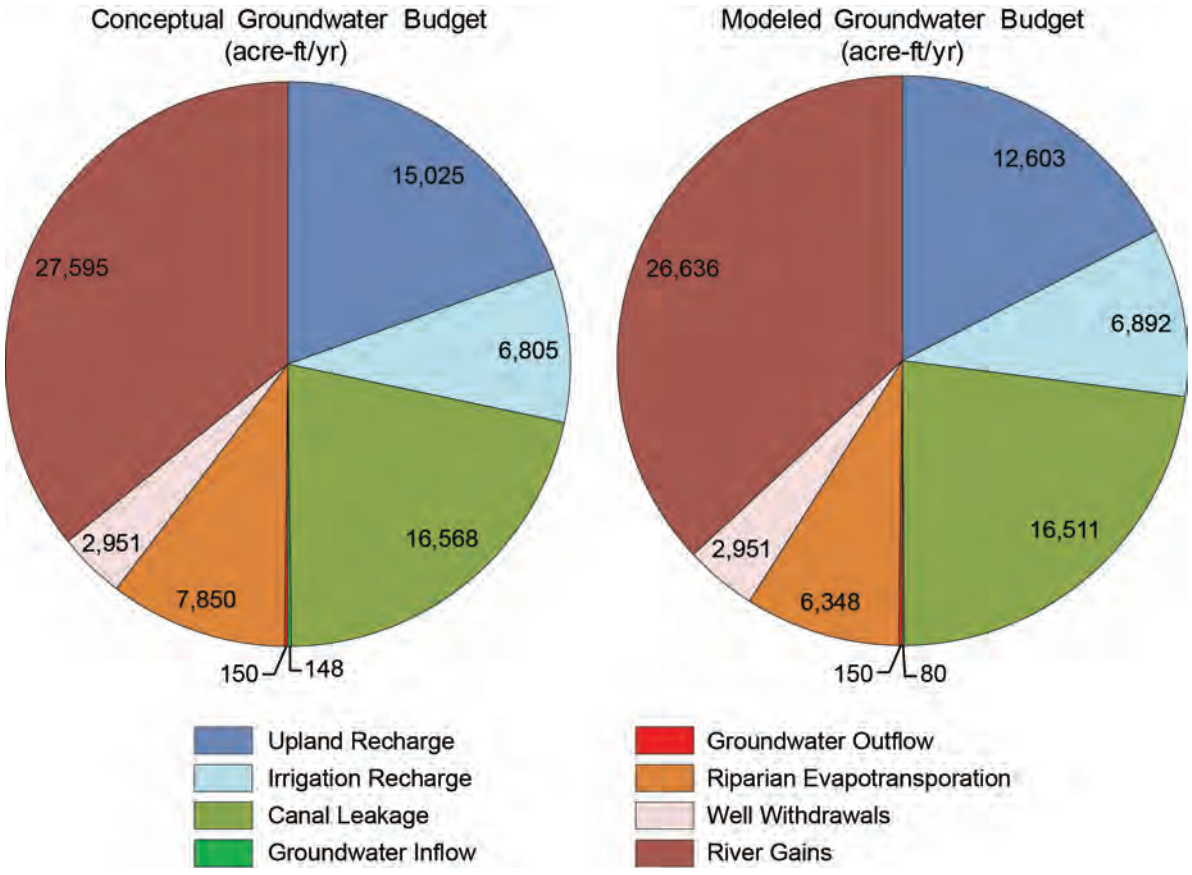

Figure 21. The conceptual and steady-state simulated groundwater budgets were very similar. The greatest difference was in the upland recharge, where the conceptual estimate was poorly constrained by the assumption that half of the excess water would infiltrate (DP_{ex} = 0.5). Minor discrepancies in other components were primarily caused by grid coarseness.

Table 7. Comparison of the conceptual average annual groundwater budget to the steady-state numerical model budget (acre-ft/yr).

	Conceptual Model Estimate	Probable Range		Steady-State Model Budget
		Min	Max	
Irrigation Recharge	6,805	6,125	7,486	6,892
Upland Recharge	15,025	12,020	18,030	12,603
Canal Leakage	16,568	14,520	17,747	16,511
Groundwater Inflow	148	44	443	80
Total Inflow	**38,546**			**36,086**
Groundwater Outflow	150	45	451	150
Riparian Evapotranspiration	7,850	5,055	12,480	6,348
Well Withdrawals*	2,951	2,656	3,246	2,951
Net River Gains	27,595	24,836	30,355	26,636
Change in Storage	0	0	0	0
Total Outflow	**38,546**			**36,086**

*Well Withdrawals reflect the net consumptive use, not the pumping rate.

coarseness also occasionally led to multiple boundary conditions occurring within a single cell, which muted the overall model sum of the individual budget components.

Transient Calibration

Methods

The transient calibration used the results and calibration parameters of the steady-state model, but also adjusted for aquifer storage properties (Sy and Ss) and boundary condition stress rates until observed water-level changes were reasonably replicated by the model. All parameters were manually estimated, and PEST was also used to refine Sy estimates.

The steady-state simulation served as the first stress period of the 3-yr transient simulation. All subsequent stress periods were monthly, beginning with April 2010 and ending in April 2013 (table 8). Each stress period was subdivided into five time steps. April was selected as the first month because its stress rates (e.g., canal leakage, diversions, irrigation recharge, ET, starting river flow) were similar to the steady-state rates, thus providing a relatively smooth transition in model output between the first and second stress periods.

The transient model began 15 months prior to the start of the study to allow the aquifer system to respond to the dramatic changes in recharge that occurred immediately before and during the study. This period of extreme wet/dry contrasts was advantageous for calibration, in that it represented a wide range of aquifer recharge and discharge; aquifer storage properties can often be better estimated when calibration targets show responses to such extreme changes in stress (IDWR, 2013).

While long-term groundwater levels were stable, groundwater levels during the study period (2011–2013) declined in most wells as a result of the shift from wet to dry conditions. Because this declining period was used for the transient calibration, the change in storage was estimated, by comparing March 2012 water levels in monitoring wells to March 2013 levels. In cases where data were not available for March, the starting time was advanced until data were available. In most cases, the same month was used for comparison to remove seasonal influences (i.e., March 2012 vs. March 2013). The only exception was for GWIC 258713 (fig. 8): January and November 2012 values were compared for this well because the data record spanned only that 11-month period. All drawdown values were normalized to 1 yr. For wells without known changes in management (e.g., increased pumping), changes in water levels ranged from an increase of 0.3 ft/yr to a decline of 3.7 ft/yr, with the average change being a decline of 1.05 ft/yr.

Table 8. Stress periods, time steps, and upland recharge multipliers in the 3-yr transient simulation.

Start Date	Stress period length (days)	No. of time steps	Recharge Multiplier
Steady-State	1	1	1.00
4/1/2010	30	5	1.80
5/1/2010	31	5	2.80
6/1/2010	30	5	1.80
7/1/2010	31	5	1.05
8/1/2010	31	5	0.95
9/1/2010	30	5	0.85
10/1/2010	31	5	0.75
11/1/2010	30	5	0.50
12/1/2010	31	5	0.40
1/1/2011	31	5	0.30
2/1/2011	28	5	0.20
3/1/2011	31	5	0.20
4/1/2011	30	5	2.71
5/1/2011	31	5	3.71
6/1/2011	30	5	2.71
7/1/2011	31	5	0.59
8/1/2011	31	5	0.49
9/1/2011	30	5	0.39
10/1/2011	31	5	0.29
11/1/2011	30	5	0.29
12/1/2011	31	5	0.29
1/1/2012	31	5	0.29
2/1/2012	29	5	0.20
3/1/2012	31	5	0.20
4/1/2012	30	5	1.56
5/1/2012	31	5	2.56
6/1/2012	30	5	1.56
7/1/2012	31	5	0.59
8/1/2012	31	5	0.49
9/1/2012	30	5	0.39
10/1/2012	31	5	0.29
11/1/2012	30	5	0.29
12/1/2012	31	5	0.29
1/1/2013	31	5	0.29
2/1/2013	28	5	0.20
3/1/2013	31	5	0.20
4/1/2013	30	5	1.52

The change in storage was estimated by combining the change in head with estimated Sy values. The area of the geologic units and Sy values were based on geologic mapping (fig. 6; Vuke and others, 2007). Quaternary alluvium and gravel, and Quaternary and Tertiary gravels, were assigned an Sy value of 0.1; other Quaternary and Tertiary units were assigned an Sy value of 0.05; bedrock units were assigned an Sy value of 0.01. Using a water-level decline of 1 ft, the amount of water drained from groundwater storage during 2012 was estimated to be about 8,100 acre-ft.

Stress rates in the transient simulation were varied to reflect seasonal and inter-annual variations that occurred between April 2010 and April 2013. These stresses included streamflow entering the study area, streamflow diversions, canal leakage rates, well pumping rates, upland recharge, irrigation recharge, and groundwater use by phreatophytes (ET). Alluvial flux rates were held constant because simulated heads were insensitive to temporal variations in alluvial flux within the range of conceptual estimates (Groundwater Budget section). The only other stress rate held constant was that of stock wells. Stock-well pumping rates were not varied seasonally because field observations and landowner communication indicated that stock wells do not follow consistent seasonal pumping schedules; rather, pumping schedules are quite variable due to factors such as livestock distribution (appendix E, section E3).

Aquifer Storage Properties

The upstream weighting package (UPW) provided a smooth transition in calculating the change in aquifer storage between confined and unconfined conditions. In UPW both Ss and Sy are included for the convertible layer type (i.e., LAYTYP = 1) that was used in this model.

Sy and Ss were estimated through manual calibration using a zonal approach. The zones were initially defined using the eight geologic groups, but the configuration was simplified by combining bedrock zones. PEST was then used to refine Sy estimates. Pilot points were also used, and their placement and bounding values were assigned in a manner similar to the steady-state K calibration (Steady-State Calibration section). The only major difference was that coverage was emphasized near observations that showed large seasonal fluctuations. Following the Sy estimation using PEST, slight manual adjustments of Ss zonal values were applied to optimize results.

Transient Calibration Targets

The transient model was calibrated to the 63 monitoring wells used in the steady-state calibration (fig. 17). The measured monthly water levels served as targets for each monthly stress period (when available). In the 15 monthly stress periods prior to the start of the Boulder Valley study (April 2010–June 2011), water levels in eight GWAAMON wells (fig. 8) and stream flows from the USGS station on the Boulder River at Red Bridge (fig. 9) provided a limited calibration.

Unlike the steady-state calibration, the transient simulation was calibrated to change in heads rather than the monthly head values themselves. Digital filtering (Doherty and Hunt, 2010) was performed by weighting only the representative stress period data from a given well to 1.0; non-static monthly measurements were zero-weighted. Of the 63 monitoring sites used in the steady-state head calibration, 8 were disregarded because of a sparse data record or because pumping influences were apparent through much of the record (GWIC 49040, 49044, 53361, 192602, 239829, 262259, 262766, 267568).

Boulder River stream flows and flux were qualitatively assessed to ensure that their patterns followed observations. The average irrigation-season and non-irrigation season gains and losses were also monitored per river reach as well as through the river length as a whole, and those results were evaluated against conceptual estimates. Because the study-period conditions were not representative of average annual conditions, the transient water budget results were not compared against the average annual water budget estimates developed for the conceptual model (Groundwater Budget section); instead, only the simulated change in storage was compared with the conceptual estimate of the annual (2012–2013) change in storage.

Results

Change in Head. Simulated changes in head were generally a good fit with observations (appendix F). The floodplain head fluctuations were primarily influenced by river interactions (e.g., GWIC 265188; fig. 22) as well as irrigation recharge and canal leakage (e.g., GWIC 262738). Sy results in the floodplain allu-

vium ranged from 0.03 to 0.32 and the mean was 0.14 (fig. 23). Ss values ranged from 1×10^{-5} to 5×10^{-4} ft^{-1} with a mean of 2.3×10^{-4} ft^{-1} (fig. 24). Most head fluctuations within the unconsolidated bench materials were also strongly influenced by irrigation practices (e.g., GWIC 50006, 121965; fig. 22). Sy results in the benches were slightly lower on average than floodplain alluvium, ranging from 0.01 to 0.29 with a mean of 0.06, and Ss values ranged from 1×10^{-6} to 5×10^{-5} ft^{-1} with a mean of 1.7×10^{-5} ft^{-1} (table 6).

Head fluctuations within the upland bedrock were mainly influenced by precipitation-derived recharge (fig. 22) and in a few cases summertime pumping of domestic wells. The range of storage property values was slightly broader than the bench sediments or alluvium, which reflects both the bedrock's greater spatial coverage and its greater variation in rock types; Sy values ranged from 0.002 to 0.052 with a mean of 0.02, and Ss values ranged from 2.5×10^{-8} to 1.0×10^{-6} ft^{-1} with a mean of 3.4×10^{-7} ft^{-1}. During calibration, the minimum bound on Sy was lowered from the minimum value typical of unconfined settings (0.01; Freeze and Cherry, 1979) to a value more typical of semi-confined settings (0.002) in order to better fit the steep head changes observed at some locations. However, as Sy was lowered in these areas, the fit to adjacent sites with less fluctuation was compromised. The wells with less water-level fluctuation were shallower and/or within alluvial drainages, and a close fit to both hydrograph patterns was not feasible due to the single-layer, basin-scale model design. Rather than tightly fitting one or the other, a balance was sought between paired observations (e.g., GWIC 184291 and 264613).

One well near the pediment/bedrock interface along Elkhorn Creek had much greater groundwater levels fluctuations than observed (GWIC 265072; appendix F). As a result of grid discretization this well was located in the same cell as Elkhorn Creek and was strongly influenced by stream leakage. The Kv for this cell, and for all upland streams, was set at 10 ft/day. This relatively high Kv value was uniformly set for all upland creeks because their primary model function was to fully discharge their flow to the aquifer (Boundary Conditions section).

One of the transient calibration goals was to reduce unrealistic flooding within the floodplain during the peak-irrigation season (May–June). In preliminary transient runs, it became apparent that flooding was occurring in the central Boulder River floodplain and the Muskrat Creek floodplain when the rates of all recharge sources—canal leakage, upland recharge, irrigation recharge, and stream infiltration—were at their highest. Flooding was most pronounced in 2011, when extensive flooding did occur in the study area due to an unusually high amount of springtime precipitation. Isolated flooding also occurred within a few upland drainages during the simulation; however, its extent was minor and attention was instead focused on the floodplain area.

To reduce localized flooding in the floodplain the flood-irrigation rate was lowered by assuming an average flood application efficiency of 35% instead of 25% (Groundwater Budget section, appendix C, table C1), and canal-leakage rates were lowered in three canals within the central floodplain from the maximum leakage estimates (1.6 cfs/mi on average) to the mid-range estimates (0.94 cfs/mi on average). These two changes eliminated the majority of flooding; however, some flooding remained in the central floodplain during May and June of 2010 and 2011 due to three factors: 1) the computed river stage remained above the top of some cells because stream channel width remained the same at all flow rates (rectangular channel) when in reality the channel widens during high-flow periods; 2) many of the surveyed well elevations in this area were above the DEM, which was the basis of the top grid surface (Steady-State Calibration section); and 3) these two Spring periods were wetter than average, and extensive flooding occurred in 2011 (R. Sims, oral communication, July 2011).

River Flow. Flow simulations in the Boulder River fit well with observations (fig. 25; appendix G). The river's seasonal net gains and losses throughout the study area were also well matched, with an average non-irrigation season gain of 30 cfs (0.6 cfs/mi) and an average irrigation-season loss of 64 cfs (1.2 cfs/mile; fig. 26). Flux results within each of the seven field-based river reaches show that the two uppermost reaches and lowermost reaches fit fairly well (fig. 17, appendix D, tables D1 and D4); however, reaches 3, 4, and 5 were not as closely matched. These central reaches were estimated to be primarily losing throughout the year, whereas the simulated conditions shift from losing to gaining late in the irrigation season and remain gaining through the rest of each year (table 9).

Muskrat Creek was the only tributary to the Boul-

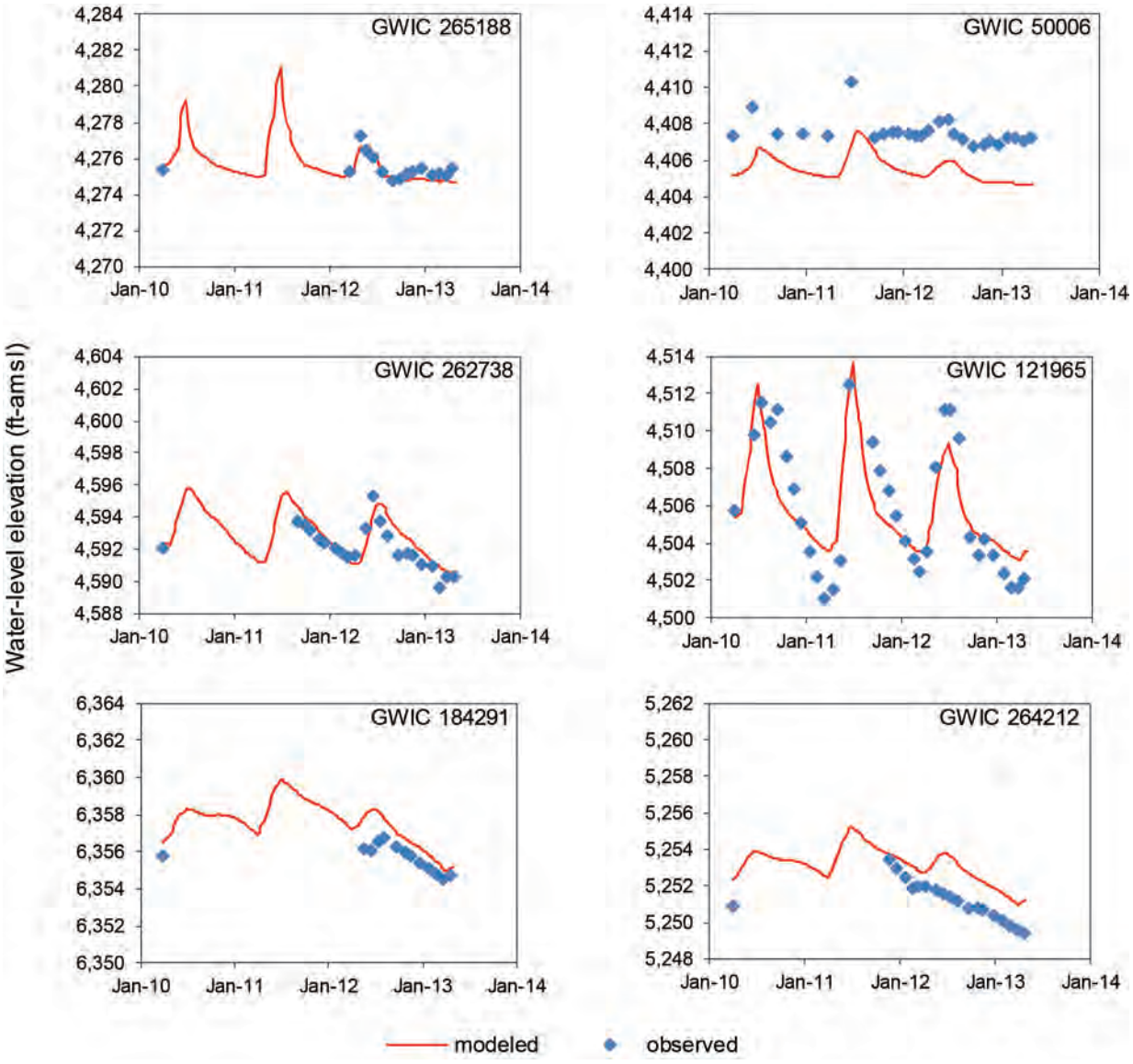

Figure 22. Heads in the calibrated transient simulation were generally a good fit with observations, and showed the influences of surface water near the river (GWIC 265188 and 50006), irrigation recharge near irrigated lands (GWIC 262738 and 121965), and precipitation-derived recharge in the uplands (GWIC 184291 and 264212). Well locations are shown in figure 16.

der River used in the calibration (GWIC 265350). The creek flow is a simulation of the accumulated flow from local upland creeks. While the steady-state flow fit well with the mean annual flow estimate (4.0 cfs and 4.1 cfs, respectively), the transient flow amplitude was more subdued than observations (appendix G). Observed peak flow was 7 cfs, while modeled peak flow was about 5 cfs. Observed low flows were about 3.1 cfs, while modeled low flows were about 3.5 cfs. The subdued amplitude in the simulated flows is likely due to the fact that only groundwater inputs constitute the creek's modeled flow. The sharp peaks in the monitoring site record were primarily caused by surface-water inputs from rapid snowmelt and rainfall events, neither of which are represented in the model. The generally subdued simulation results also may result from the monthly stress periods being too long to capture short-term variations.

Change in Storage. The annual change in storage computed for the transient simulation (April 2012–April 2013) was 5,266 acre-ft/yr. This is lower than the 8,108 acre-ft/yr estimated during conceptual model development (Groundwater Budget section). This discrepancy is acceptable considering the large-scale approach of the conceptual estimate and its inherent uncertainty. The discrepancy is likely attributable to the simulated bedrock Sy values being slightly lower than those used in the conceptual estimate (table 1).

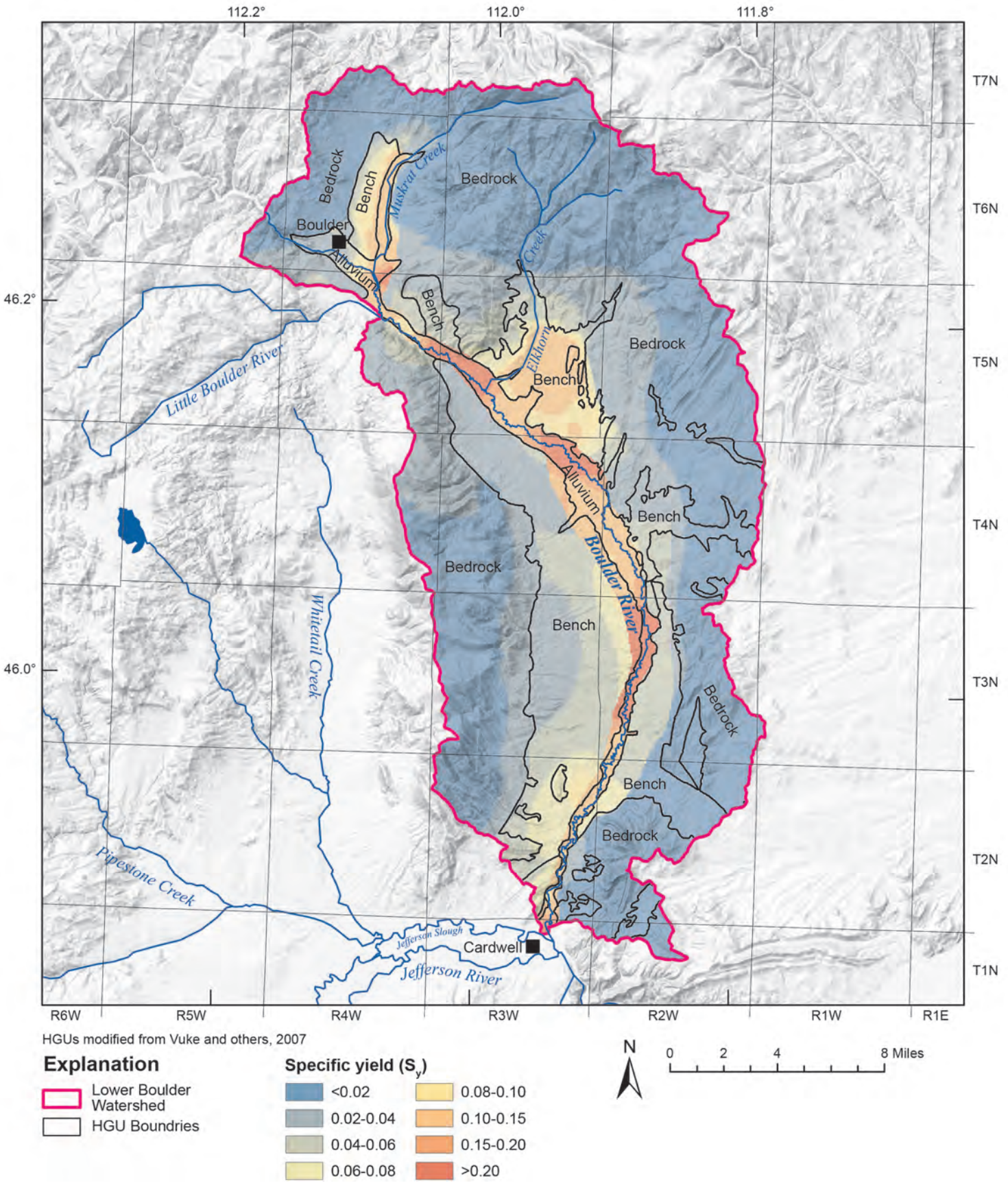

Figure 23. Specific yield (Sy) estimates using PEST in the calibrated transient simulation were similar to conceptual model estimates, and showed a similar pattern to the K distribution (fig. 20).

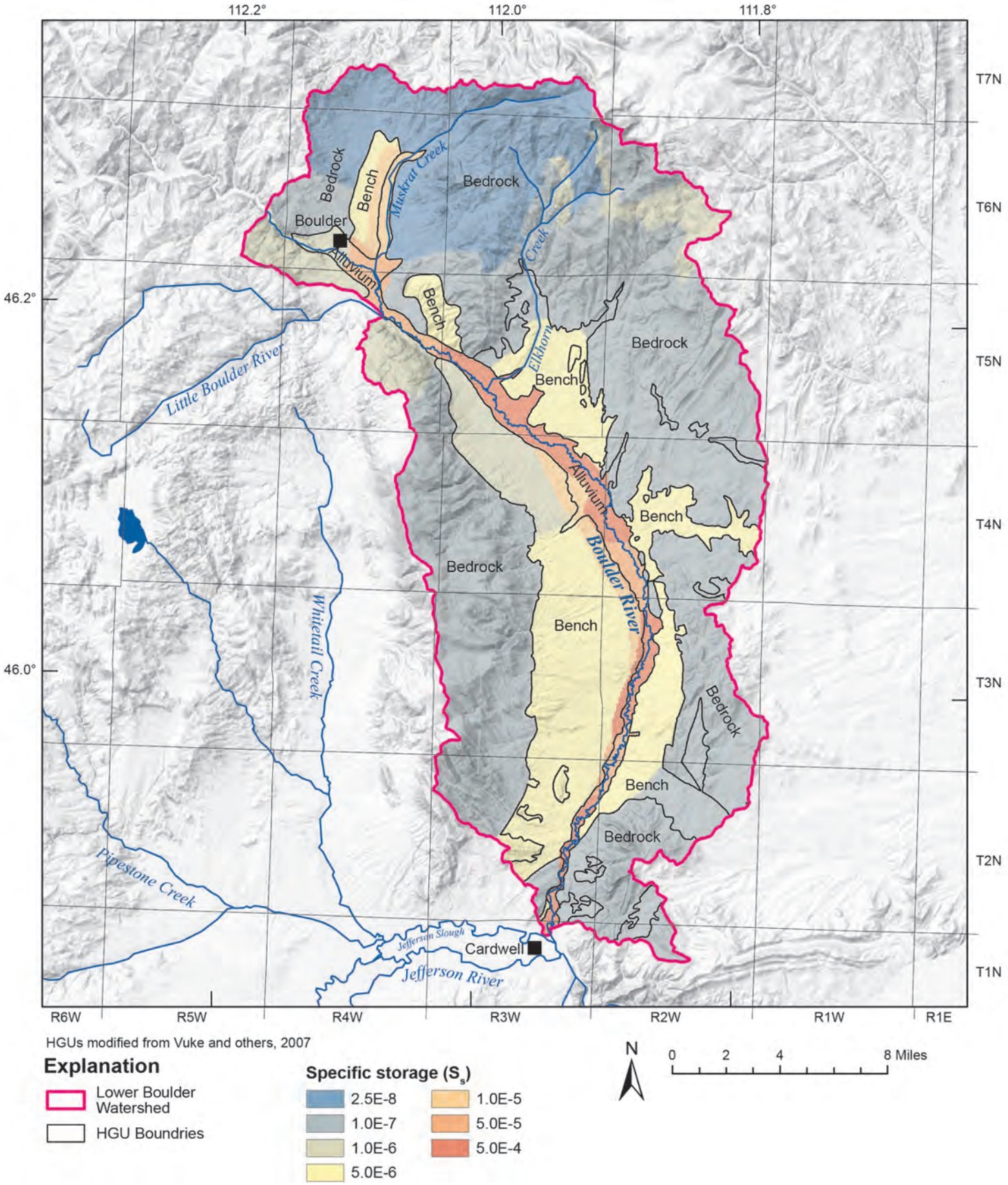

Figure 24. Specific storage (Ss) was estimated using zones rather than the pilot-point PEST approach used for K and Sy. The resulting Ss distribution followed a pattern similar to the K and Sy distributions (figs. 20 and 23).

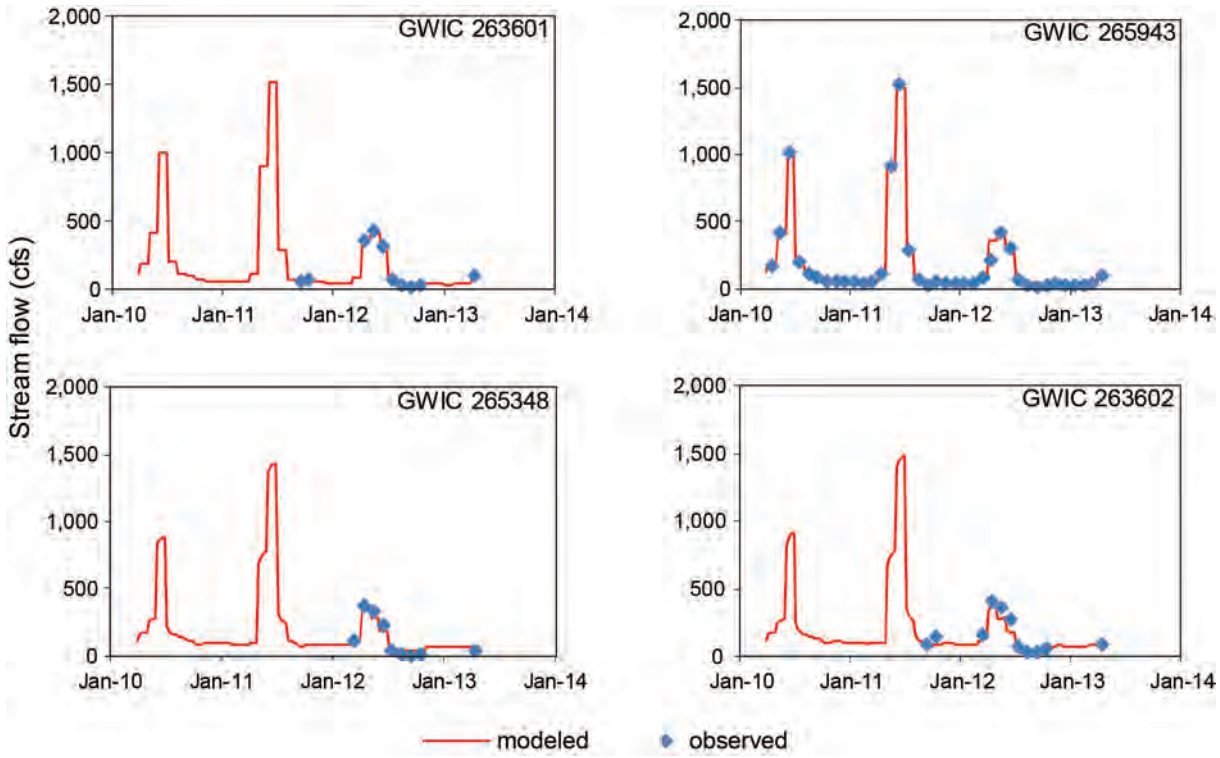

Figure 25. Stream flows in the calibrated transient simulation generally fit well with observed flows. These four sample hydrographs are from Boulder River monitoring sites (fig. 16).

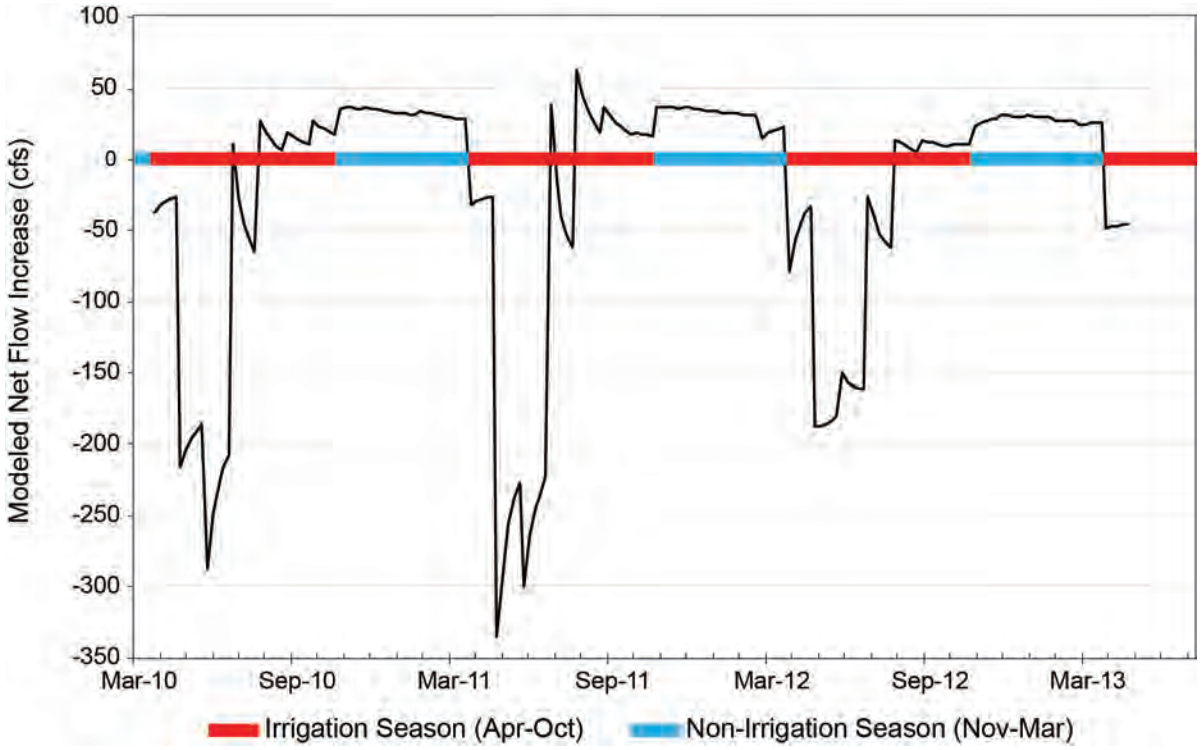

Figure 26. The modeled net change in the flow of the Boulder River as it passes through the study area was consistent with the conceptual model. A dramatic shift from a net flow increase to a net flow decrease occurs at the start of the irrigation season, showing the strong impact of irrigation diversions on the surface-water flow system.

Table 9. Modeled net change in flow for the Boulder River per river reach during the irrigation season and non-irrigation seasons in the 3-yr transient simulation.

Reach No.	River Reach	Mean irrigation season*,** flux (cfs)	Mean irrigation season flux (cfs/mi)	Mean non-irrigation season* flux (cfs)	Mean non-irrigation season flux (cfs/mi)	Predominant Irrigation-Season Conditions	Predominant Non-Irrigation Season Conditions
1	I-15 to Red Bridge	-8.9	-1.8	-0.8	-0.2	Net Decrease	Net Decrease
2	Red Bridge to White Bridge	-3.4	-0.6	2.9	0.5	Net Decrease	Net Increase
3	White Bridge to Quaintance Ln	-41.2	-3.9	9.4	0.9	Net Decrease	Net Increase
4	Quaintance Lane to Dunn Ln	-2.9	-0.4	9.7	1.5	Net Decrease	Net Increase
5	Dunn Lane to Boulder Cutoff	-3.1	-0.3	5.3	0.5	Net Decrease	Net Increase
6	Boulder Cutoff to Cold Spring	-0.7	-0.1	0.9	0.2	Net Decrease	Net Increase
7	Cold Spring to Cardwell	-4.0	-0.3	2.9	0.2	Net Decrease	Net Increase
Net	I-15 to Cardwell	-64.2	-1.2	30.3	0.6	Net Decrease	Net Increase

*The irrigation season is defined as April–October; the non-irrigation season is defined as November–March.
**Note that negative numbers reflect a net decrease in flow, and positive numbers reflect a net increase in flow.

SENSITIVITY ANALYSIS

Methods

A sensitivity analysis was performed to assess the uncertainty in the model solution caused by uncertainty in model parameters. The main objectives were to quantify the model's sensitivity to parameter value changes and to identify the parameters having the most impact on the model solution. Parameters were adjusted systematically, such that one parameter was changed per model run while all other parameters remained at their calibrated values. The change in modeled heads and the sum of squared residuals (SSR) were monitored to evaluate the sensitivity of the head solution to a given parameter. Because the Boulder River gains and losses were a major focus of the model calibration and model predictions, the sensitivity of streambed flux in five river segments was also evaluated (fig. 27).

Modifications were limited to parameters believed to have the greatest influence on the outputs (i.e., stream flux and heads). These parameters included aquifer K, upland recharge, irrigation recharge, canal leakage, streambed K_v, ET, and Sy. The steady-state simulation was used to adjust all parameters except Sy, which was adjusted in the transient simulation. In the streambed K_v sensitivity runs, only the Boulder River and floodplain portion of Muskrat Creek were modified because the predictive focus was on those reaches. For the aquifer property parameters (i.e., K and Sy), values of the three general hydrogeologic groups (alluvium, bench sediments, and bedrock; Geologic Framework section) were modified individually. Other parameters that might affect stream flux, such as streambed elevation, were qualitatively assessed during the calibration process (see Steady-State Calibration section).

The analysis was performed for most parameters through a series of auto-sensitivity-analysis runs (auto-runs) in Vistas. Each auto-run involved a batch process in which a given parameter was incrementally changed by a factor of 0.1, from 0.5 times to 1.5 times its calibrated value, for a total of 11 MODFLOW runs per parameter (table 10). The resulting changes in head, SSR, and streambed flux were evaluated following each auto-run. The only exceptions to this procedure were streambed K_v and Sy. For these two parameters, the incremental change was 0.25 rather than 0.1 due to differences in Vistas post-processing and lengthy run times. For these parameters there were five rather than eleven MODFLOW runs (table 10). In addition, the average change in head statistic was different for Sy than for the other tested parameters because the transient model was used and it represented all heads

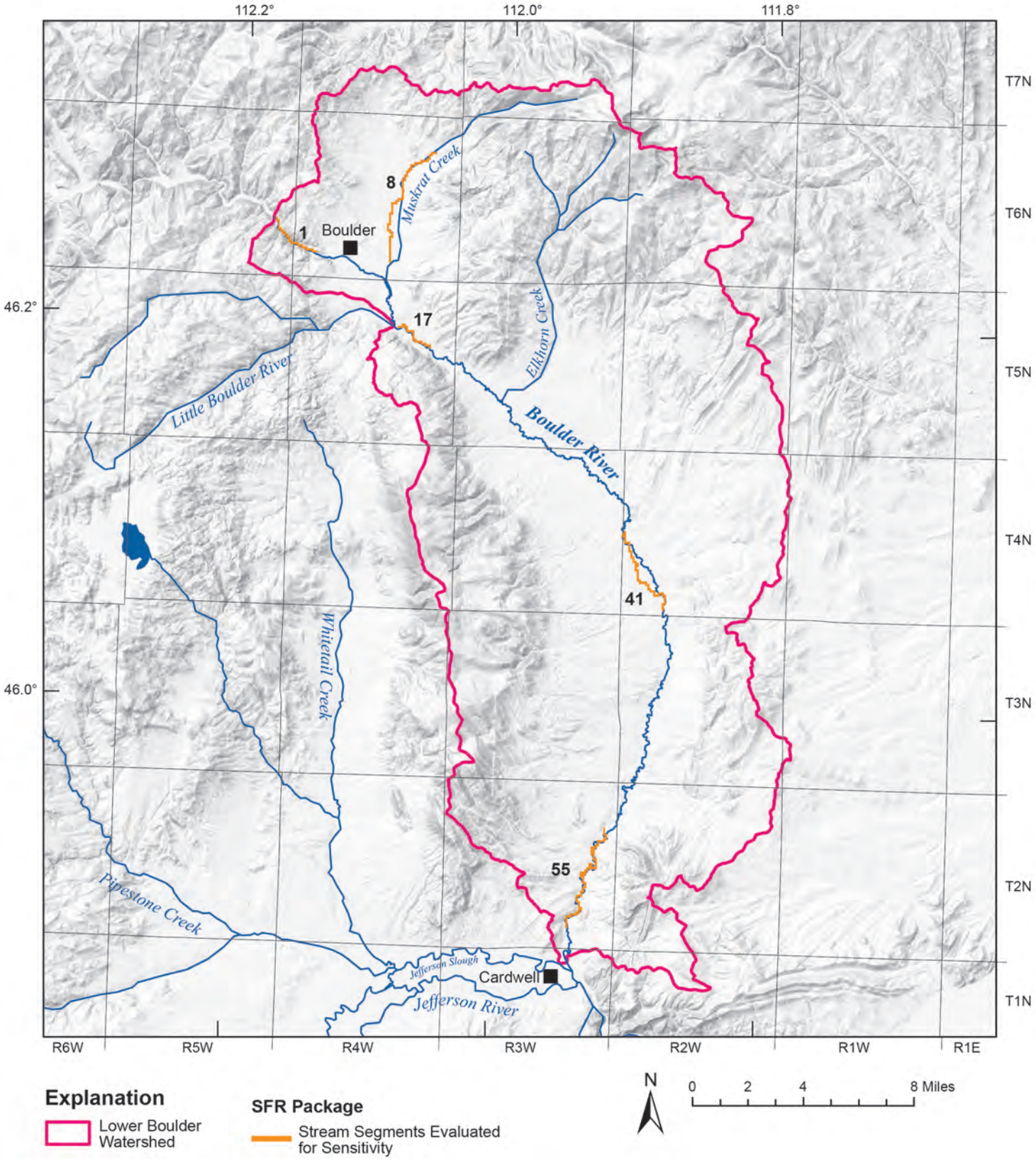

Figure 27. Five SFR segments were evaluated in the sensitivity analysis to determine the effects of parameter changes on stream flow. The results of segment 41 are presented in figures 28 and 29.

Table 10. Sensitivity analysis run summary.

Parameter	Multiplier Range	Multiplier Increment	No. of Runs	Monitored Stream Flux*	Monitored Head Output^
K alluvium	0.5–1.5	0.10	11	Segment 41	SSR, average head change
K bench	0.5–1.5	0.10	11	Segment 41	SSR, average head change
K bedrock	0.5–1.5	0.10	11	Segment 41	SSR, average head change
Canal Leakage	0.5–1.5	0.10	11	Segment 41	SSR, average head change
Upland Recharge	0.5–1.5	0.10	11	Segment 41	SSR, average head change
Irrigation Recharge	0.5–1.5	0.10	11	Segment 41	SSR, average head change
Riparian ET	0.5–1.5	0.10	11	Segment 41	SSR, average head change
Streambed K_v	0.5–1.5	0.25	5	Segment 41	SSR, average head change
S_y alluvium	0.5–1.5	0.25	5	Segment 41	average head change
S_y bench	0.5–1.5	0.25	5	Segment 41	average head change
S_y bedrock	0.5–1.5	0.25	5	Segment 41	average head change

*Additional SFR segments (1, 8, 17, and 55) were evaluated in most runs; Segment 41 was selected as the most representative of river conditions

^SSR: sum of squared residuals (head residuals only)

through the 186 time steps of the transient simulation rather than a single value from the steady-state simulation.

Results

The analysis revealed a wide range of sensitivity to the tested parameters. Not surprisingly, the most dramatic changes in model output resulted from the most dramatic parameter changes, especially from the low end of the spectrum (i.e., 50% of calibrated values).

Steady-state head results indicated that the model solution was most sensitive to changes in upland recharge, bedrock K, and bench K. These three parameters generated the highest SSR and caused the greatest change in head (fig. 28; table 11a). The most notable change occurred when upland recharge was lowered by 50%, which produced a SSR value of 2.7×10^5 and an average head change of 135 ft. Canal leakage and alluvial K changes resulted in smaller responses, while irrigation recharge, streambed K_v, and riparian ET responses were the least influential.

Relative parameter influences were partly a function of spatial scale; that is, parameters such as upland recharge and bedrock K cover a much larger area than other parameters, such as alluvial K and canal leakage. If heads were evaluated only within the floodplain, alluvial K and canal leakage would become more influential due to their prevalence in that portion of the model domain. Likewise, heads are more sensitive to certain parameters by nature of the initial (i.e., calibrated) parameter values; for instance, a decrease in bedrock K will produce more of a response than a proportional change in alluvial K because water levels fluctuate more under lower transmissivity conditions. In addition, the correlation between parameter types is worth noting. Aquifer K values were calibrated based on the values of other parameters such as upland recharge and irrigation recharge; therefore, aquifer K values are correlated to those parameters.

River gain or loss (stream flux) was most sensitive to canal leakage, upland recharge, and irrigation recharge (fig. 28; table 11a). Stream flux was more sensitive to alluvial K than bedrock K. This contrast in sensitivity between heads and stream flux highlights the importance of evaluating multiple components of the model solution, especially with respect to model predictions. The difference in sensitivity likely results from all stream flux observations being located in the floodplain, while groundwater head observations were located throughout the study area.

Sy was adjusted separately within each of the three hydrogeologic groups (alluvial, bench, and bedrock). Results showed heads to be most sensitive to changes in bedrock Sy, similar to their response to K value changes in the steady-state simulation (fig. 29; table 11b). River flux was most sensitive to alluvial Sy changes, because the river flows through the alluvium (fig. 29). The average changes in both heads and flux

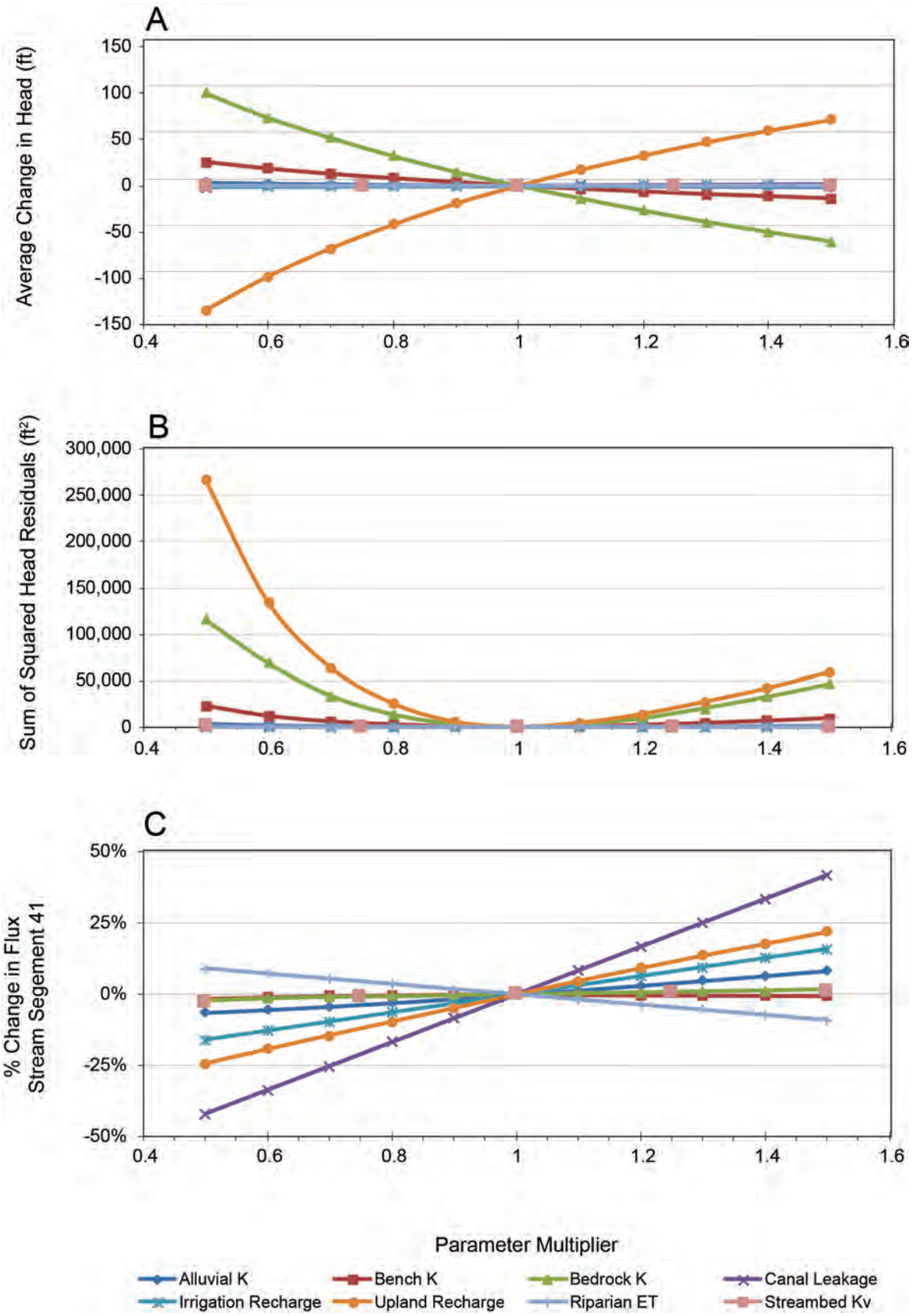

Figure 28. The average head change (A) and the sum of the squared head residuals (B) in the steady-state sensitivity analysis runs showed that head is most sensitive to upland recharge, and bedrock K. Stream flux (C) was sensitive to canal leakage, upland recharge, irrigation recharge, and alluvial K.

Table 11a. Summary of sensitivity analysis results.

	Alluvial K	Pediment K	Bedrock K	Canal Leakage	Irrigation Recharge	Upland Recharge	Riparian ET	Riverbed K_v
Multiplier	**Average % Change in Flux, Stream Segment 41**							
0.5	-6.3%	-1.6%	-2.0%	-42.0%	-15.8%	-24.3%	9.1%	-2.8%
0.6	-5.3%	-1.0%	-1.3%	-33.6%	-12.7%	-19.3%	7.3%	—
0.7	-4.1%	-0.5%	-0.8%	-25.2%	-9.5%	-14.4%	5.5%	—
0.75	—	—	—	—	—	—	—	-1.0%
0.8	-2.9%	-0.2%	-0.6%	-16.8%	-6.3%	-9.6%	3.6%	—
0.9	-1.5%	0.1%	-0.3%	-8.4%	-3.2%	-4.8%	1.8%	—
1	0.0%	0.0%	0.0%	0.0%	0.0%	0.0%	0.0%	0.0%
1.1	1.6%	-0.1%	0.3%	8.4%	3.2%	4.7%	-1.8%	—
1.2	3.2%	-0.2%	0.6%	16.8%	6.3%	9.3%	-3.6%	—
1.25	—	—	—	—	—	—	—	0.7%
1.3	4.9%	-0.2%	0.9%	25.2%	9.5%	13.7%	-5.4%	—
1.4	6.6%	-0.3%	1.3%	33.6%	12.7%	17.8%	-7.2%	—
1.5	8.4%	-0.4%	1.6%	42.0%	15.8%	22.0%	-9.1%	1.2%
Multiplier	**Average Change in Head (ft)**							
0.5	3.36	25.55	100.43	-1.53	-0.60	-134.7	0.11	-0.04
0.6	2.34	18.43	73.73	-1.22	-0.48	-98.3	0.09	—
0.7	1.55	12.74	51.92	-0.91	-0.36	-67.89	0.06	—
0.75	—	—	—	—	—	—	—	-0.01
0.8	0.92	8.06	32.23	-0.61	-0.24	-42.00	0.04	—
0.9	0.42	3.87	15.06	-0.30	-0.12	-19.21	0.02	—
1	0.00	0.00	0.00	0.00	0.00	0.00	0.00	0.00
1.1	-0.35	-3.33	-13.75	0.30	0.11	17.33	-0.02	—
1.2	-0.66	-6.26	-26.92	0.60	0.22	32.88	-0.04	—
1.25	—	—	—	—	—	—	—	0.01
1.3	-0.92	-8.94	-39.11	0.90	0.34	47.07	-0.06	—
1.4	-1.16	-11.35	-50.21	1.20	0.45	59.79	-0.09	—
1.5	-1.36	-13.52	-60.41	1.49	0.56	71.47	-0.11	0.01
Multiplier	**Sum of Squared Residuals (ft^2)**							
0.5	3,410	23,325	115,526	1,441	563	267,040	363	1,010
0.6	1,743	12,371	68,993	1,065	503	134,941	360	—
0.7	913	6,286	33,887	768	453	64,207	358	—
0.75	—	—	—	—	—	—	—	454
0.8	516	3,064	13,731	554	412	25,488	357	—
0.9	365	932	3,159	418	381	5,536	358	—
1	359	359	359	359	359	359	359	359
1.1	439	1,048	2,797	376	346	4,515	361	—
1.2	575	2,544	9,591	475	342	13,969	365	—
1.25	—	—	—	—	—	—	—	400
1.3	750	4,602	20,413	672	347	27,215	369	—
1.4	958	7,045	32,605	959	361	41,794	374	—
1.5	1,183	9,804	46,282	1,272	383	59,044	381	488

Table 11b. Summary of sensitivity analysis results for S_y.

	Alluvial S_y	Pediment S_y	Bedrock S_y
Multiplier	**Segment 41 Average Change in Flux**		
0.5	-0.89%	0.21%	0.001%
0.75	-0.34%	0.09%	0.001%
1	0.00%	0.00%	0.00%
1.25	0.22%	-0.07%	0.000%
1.5	0.37%	-0.13%	-0.001%
Multiplier	**Average Head Change (ft)**		
0.5	0.00	-0.07	-0.38
0.75	0.00	-0.02	-0.14
1	0.00	0.00	0.00
1.25	0.00	0.02	0.09
1.5	0.00	0.03	0.15
Multiplier	**Minimum Average Head Change^ (ft)**		
0.5	-4.39	-13.14	-6.99
0.75	-0.20	-6.01	-2.54
1	0.00	0.00	0.00
1.25	-0.81	-0.21	-0.96
1.5	-1.43	-0.36	-1.68
Multiplier	**Maximum Average Head Change^ (ft)**		
0.5	2.99	1.09	4.33
0.75	1.14	0.36	1.55
1	0.00	0.00	0.00
1.25	0.16	4.85	1.63
1.5	0.30	8.71	2.76

^The minimum and maximum average head changes represent the minimum and maximum values within the model grid for each temporally averaged head change dataset

were low compared with the steady-state results; however, this is partly due to positive and negative values canceling each other out when the mean is calculated. When the results are viewed over time, the change in model output is more pronounced (fig. 29).

PREDICTIVE SIMULATIONS

The calibrated Area-Wide Model was used to predict the impacts of potential increases in groundwater development to surface-water availability. Surface-water availability is often limited in the late-irrigation season in the downstream portion of the Boulder River, and a primary objective of this study was to evaluate the degree to which new groundwater development might further diminish flows in the Boulder River. Predictions were based on increased withdrawals from domestic wells (i.e., "exempt" wells) in the upper portion of the study area connected with the concerns of project stakeholders.

Four hypothetical subdivision development scenarios were modeled in the upper portion of the study area. These examples provide an understanding of the changes in groundwater elevations and baseflow to streams that may result from increased residential development (tables 12 and 13). Potential for development is believed to be higher in these areas, based on land ownership and proximity to similar housing developments that have been built in recent years. Scenario locations differed in their proximity to the Boulder River and its tributaries, and in the transmissivity of local aquifer materials (fig. 30). The subdivision lot sizes in scenarios 1, 2, and 4 were set to 20 acres, which is common among subdivisions in this area. A pumping well was placed in each lot to represent a domestic well, and pumping rates were set equal to those of the domestic wells in the calibrated model

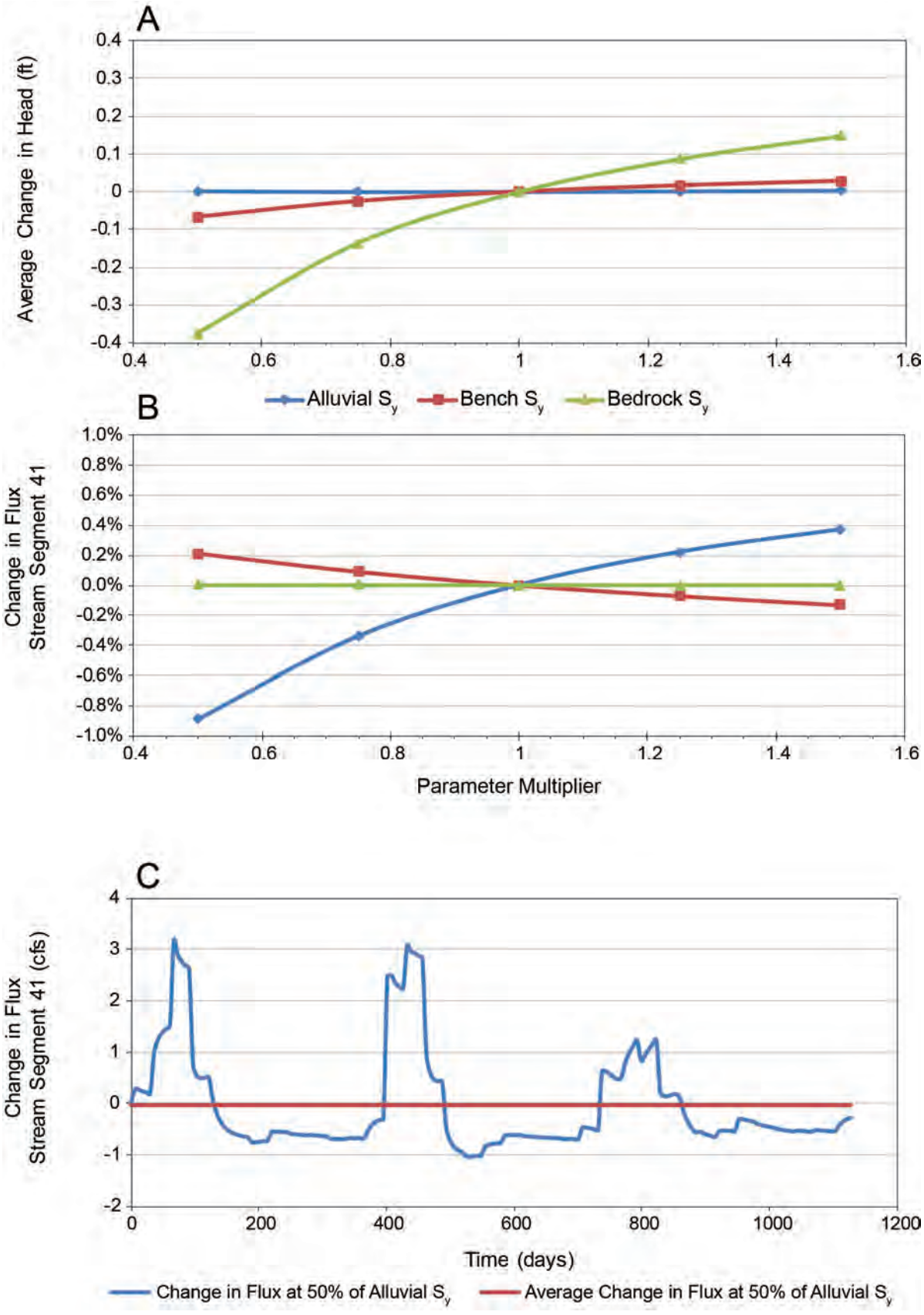

Figure 29. Overall heads were most sensitive to bedrock Sy (A), while river flux was most sensitive to alluvial Sy (B). While the average change values shown (A and B) appear relatively small, it is important to note that transient values can show much more of a response at particular times (C).

Table 12. Predictive scenario setup summary.

Description	Scenario 1 Additions to existing subdivision in North Boulder Valley	Scenario 2 New subdivision on east side of North Boulder Valley	Scenario 3 New subdivision on east side of North Boulder Valley	Scenario 4 New subdivision on west side of Central Boulder Valley
Location	T. 6 N., R. 4 W. Sec. 1, 2, 11, 12	T. 6 N., R. 4 W. Sec. 24, 25	T. 6 N., R. 4 W. Sec. 24, 25	T. 4 N., R. 3 W. Sec. 9, 10
Lot Size	20-acre	20-acre	10-acre	20-acre
Number of New Wells	58	64	128	64

(appendix E, section E2). In Scenario 3 pumping rates were doubled to represent a 10-acre lot size.

Pumping impacts were determined by means of superposition; that is, the results of each scenario were subtracted from a baseline (or reference) scenario. Baseline conditions were set equal to those of the calibrated transient model, with one notable exception: rather than using precipitation data specific to the 2010–2013 simulation period, average rates based on the 1981–2010 normal values were used for all boundary conditions (e.g., upland recharge, canal leakage, starting stream flows, etc.).

All predictive simulations were run for 20 yr to evaluate long-term effects of groundwater withdrawals. As in the calibrated transient model, monthly stress periods and 5 time steps per stress period were used, resulting in a total of 240 stress periods and 1,200 time steps.

The results of each scenario are described below, and a summary is provided in table 14. For groundwater-level evaluation purposes, a drawdown of 1 ft was set as the threshold for defining the zone of influence of the pumping wells. The drawdown results of each scenario were quantified using the maximum radial distance that the 1-ft drawdown contour extended from the point of maximum drawdown. To analyze stream impacts, three depletion factors were evaluated: (1) the change in stream flow over time; (2) the cumulative percent of well discharge derived from

Table 13. Scenario pumping schedules.

			Scenario 1	Scenario 2	Scenario 3	Scenario 4
Number of New Wells			58	64	128	64
Month	Days	gpd/well	Total gal	Total gal	Total gal	Total gal
Jan	31	15	26,970	29,760	59,520	29,760
Feb	28	17	27,608	30,464	60,928	30,464
Mar	31	21	37,758	41,664	83,328	41,664
Apr	30	34	59,160	65,280	130,560	65,280
May	31	523	940,354	1,037,632	2,075,264	1,037,632
Jun	30	964	1,677,360	1,850,880	3,701,760	1,850,880
Jul	31	1,343	2,414,714	2,664,512	5,329,024	2,664,512
Aug	31	1,353	2,432,694	2,684,352	5,368,704	2,684,352
Sep	30	752	1,308,480	1,443,840	2,887,680	1,443,840
Oct	31	126	226,548	249,984	499,968	249,984
Nov	30	26	45,240	49,920	99,840	49,920
Dec	31	10	17,980	19,840	39,680	19,840
Annual Total gal:			9,214,866	10,168,128	20,336,256	10,168,128
Average Annual gpm			17.5	19.3	38.6	19.3

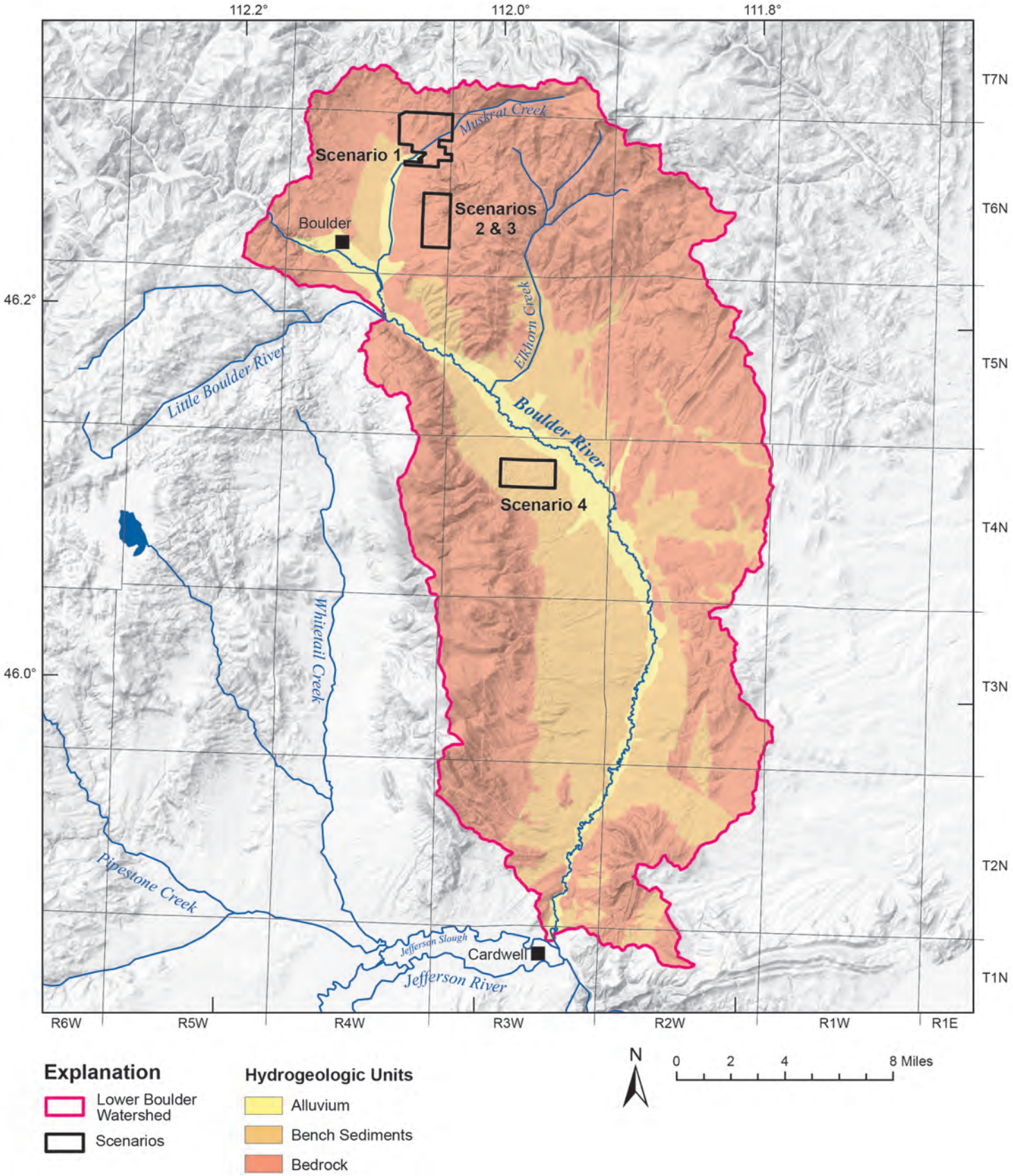

Figure 30. The hypothetical predictive scenarios were located in areas that have potential for future residential development. They included an existing subdivision in the northeast of the North Boulder Valley (scenario 1); a hypothetical subdivision on the eastern side of the North Boulder Valley (scenarios 2 and 3); and a hypothetical subdivision on the west side of the central Boulder Valley (scenario 4).

Table 14. Predictive scenario results.

Scenario	Aquifer Type	Average Total Subdivision Consumptive Use (gpm)	Distance from pumping center to nearest stream (mi)	Maximum radius of 1 ft of drawdown (mi)	Maximum drawdown (ft)	Change in drawdown between first/last 2 years (ft)	Maximum decrease in baseflow (cfs)	Maximum percent of well discharge from stream depletion
1	Granite bedrock	17.5	0.2	1.2*	14.1	1.3/0.19	0.041	65.7%
2	Granite bedrock	19.3	2.0	1.9	11.1	1.4/0.14	0.030	36.3%
3	Granite bedrock	38.6	2.0	2.2	22.3	2.8/0.29	0.060	36.2%
4	Bench sediments	19.3	1.3	1.4	8.2	0.9/0.07	0.041	65.6%

*The maximum radius of the 1-ft drawdown contour was approximated in Scenario 1 due to the grid boundary.

stream flow over time (calculated as the decrease in flow to streams); and (3) the spatial distribution of the change in baseflow to impacted streams at the time of maximum depletion.

The predictive modeling scenarios were not attempts to predict impacts from particular development plans, and the baseline is not an attempt to predict the future with no further development. Rather, the scenarios were intended to predict groundwater levels and stream baseflow under the hypothetical modeled conditions. This analysis assumes that all conditions except for the hypothetical residential developments remain constant. In reality, future conditions will inevitably differ from the modeled conditions due to changes in climate, land use, actual development, and other factors. The value of these projections lies in understanding the types of effects that would result from development similar to the hypothetical scenarios.

Scenario 1

Scenario 1 involved the full development of an incompletely developed subdivision along the northeast border of the North Boulder Valley (fig. 31). Based on the Montana Cadastral owner parcel dataset (Montana State Library, 2013), 58 of the 96 20-acre lots in this area were not developed at the time of these simulations; therefore, wells were added to the model to represent full development of this area. The simulation resulted in a maximum drawdown of 14.1 ft, which occurred in August of the final year of pumping (table 14). The maximum drawdown occurred in the northwest portion of the well field, where modeled K values are the lowest (fig. 31). The increase in drawdown from year to year decreased over time; the difference in maximum drawdown between years 19 and 20 was 0.19 ft as opposed to 1.3 ft between years 1 and 2. The 1-ft drawdown contour extended a maximum of 1.2 mi from the point of maximum drawdown, and it was on the north side of the pumping center. This distance was approximate because the zone of influence reached the edge of the model grid. That boundary was modeled as a no-flow boundary because it is presumed to serve as a groundwater divide (Hydrologic Boundaries section). In reality the groundwater divide would shift northward under these pumping conditions as water is drawn into the cone of depression from beyond the model boundary. Because water would flow in at what is modeled as a no-flow boundary, the actual radius of influence would be slightly less.

Stream flow results for the SFR network indicated a decrease in stream baseflow over time, with a maximum decrease of 0.04 cfs (18.4 gpm) in the final year (year 20) of the simulation (fig. 32). The percentage of the pumped water derived from former baseflow increased over time, with a maximum cumulative percentage of 65.7% at the end of the simulation. The increase in stream depletion with time reflects the fact that aquifer storage becomes less of a source of water. The spatial distribution of depletion shows that the stream segments located closest to the subdivision were most affected, as expected. The mainstem of Muskrat Creek showed the most depletion; within the mainstem, the largest changes in flux occurred in the stream reaches within the subdivision. The only unaffected stream reaches near the well field were those that were dry in the baseline scenario.

Scenario 2

Scenario 2 simulated a hypothetical 20-acre-lot subdivision along the eastern hillside of the North Boulder Valley (fig. 30). Sixty-four wells were included in the pumping scenario. The simulation resulted in a maximum drawdown of 11.1 ft, which occurred in August of the final year of pumping. The increase in drawdown from year to year decreased over time; the difference in maximum drawdown between years 19 and 20 was 0.14 ft as opposed to 1.4 ft between years 1 and 2. The maximum radius of influence was 1.9 mi from the point of maximum drawdown, and it occurred north of the pumping center (fig. 33).

Stream flow results indicated a decrease in stream baseflow over time, with a maximum decrease of 0.03 cfs (13.5 gpm) in the final year (year 20) of the simulation (fig. 34). The cumulative percentage of the pumped water derived from former baseflow increased over time, with a maximum percentage of 36.3% at the end of the simulation. The closest stream segments directly downgradient of the subdivision were most affected. The lower mainstem of Muskrat Creek showed the most depletion. The only unaffected stream reaches near the well field were those that were dry in the baseline scenario.

Scenario 3

Scenario 3 simulated pumping from the same area as Scenario 2 (fig. 30), but the pumping rates were doubled to simulate a 10-acre rather than a 20-acre housing density. The simulation results were propor-

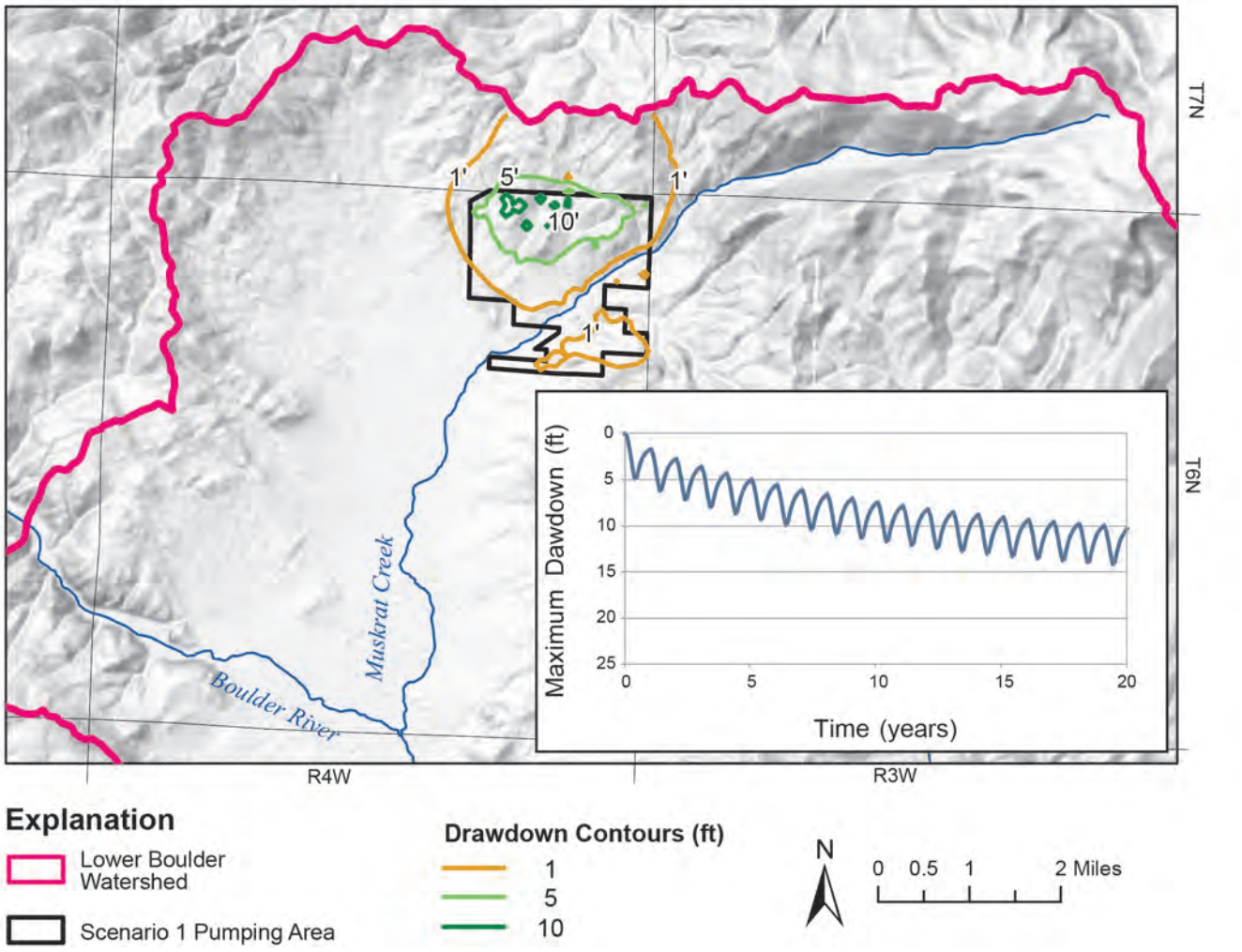

Figure 31. Scenario 1 results show that this type of development would result in a maximum drawdown of about 14 ft (inset), and the 1-ft drawdown contour would extend approximately 1.2 mi from the point of maximum drawdown after 20 yr.

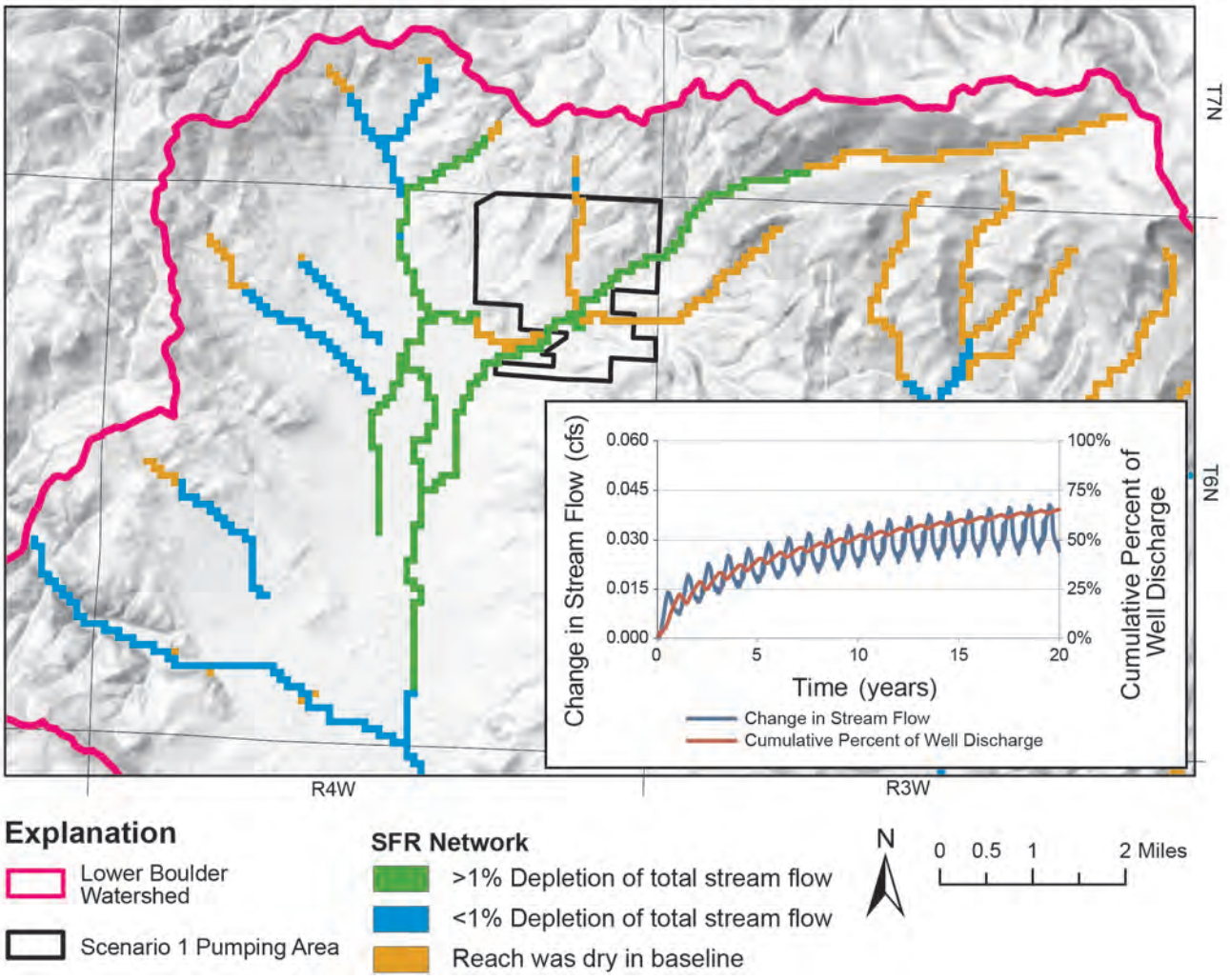

Figure 32. Development under Scenario 1 would cause a decrease in stream flow of about 0.04 cfs after 20 yr, and over time a greater percentage of the water pumped from the wells will be obtained from stream depletion as aquifer storage is depleted (inset). Most of the depletion would occur in Muskrat Creek, with less depletion in other streams near the development.

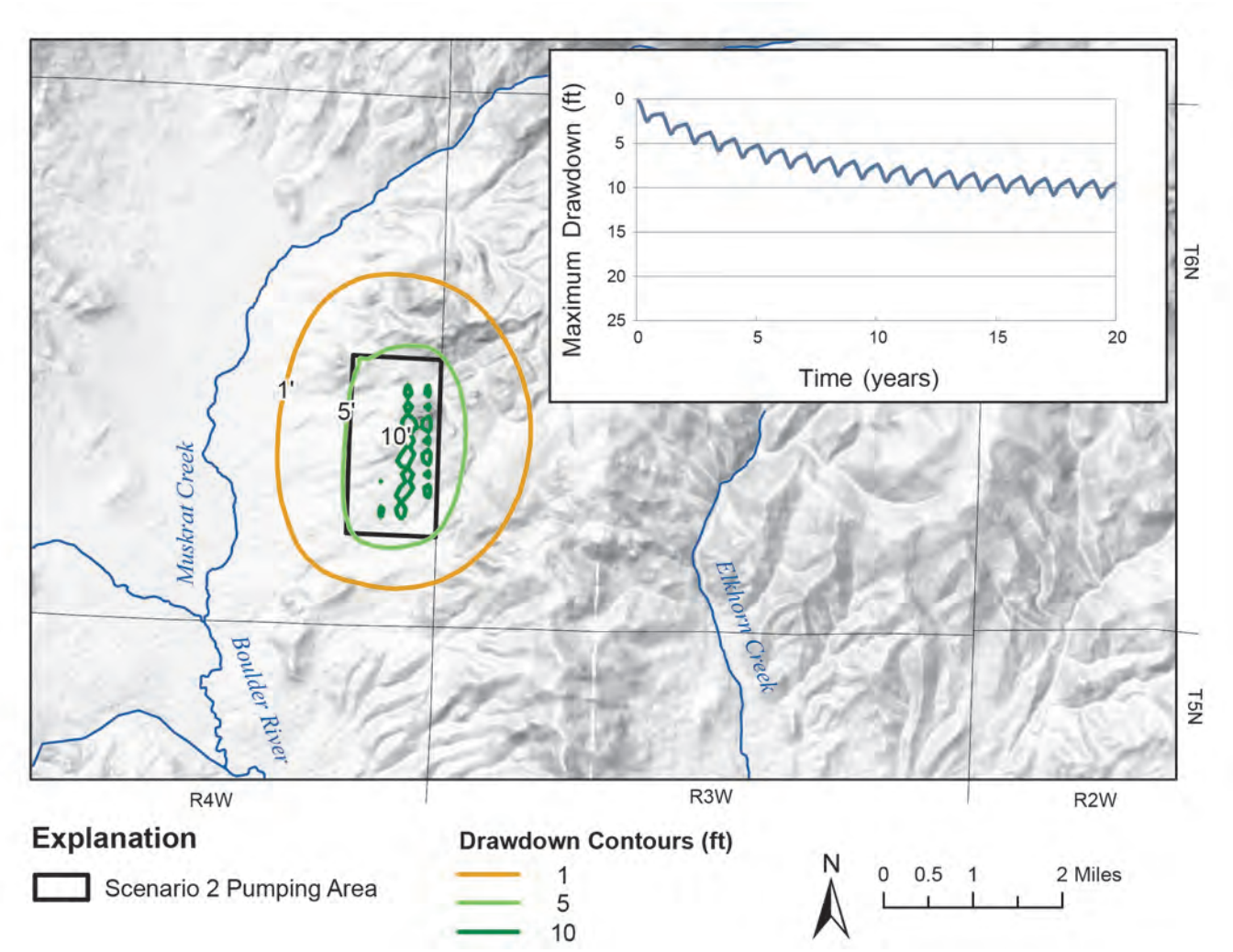

Figure 33. Scenario 2 results show that this type of development would result in a maximum drawdown of about 11 ft (inset), and the 1-ft drawdown contour would extend approximately 1.9 mi from the point of maximum drawdown after 20 yr.

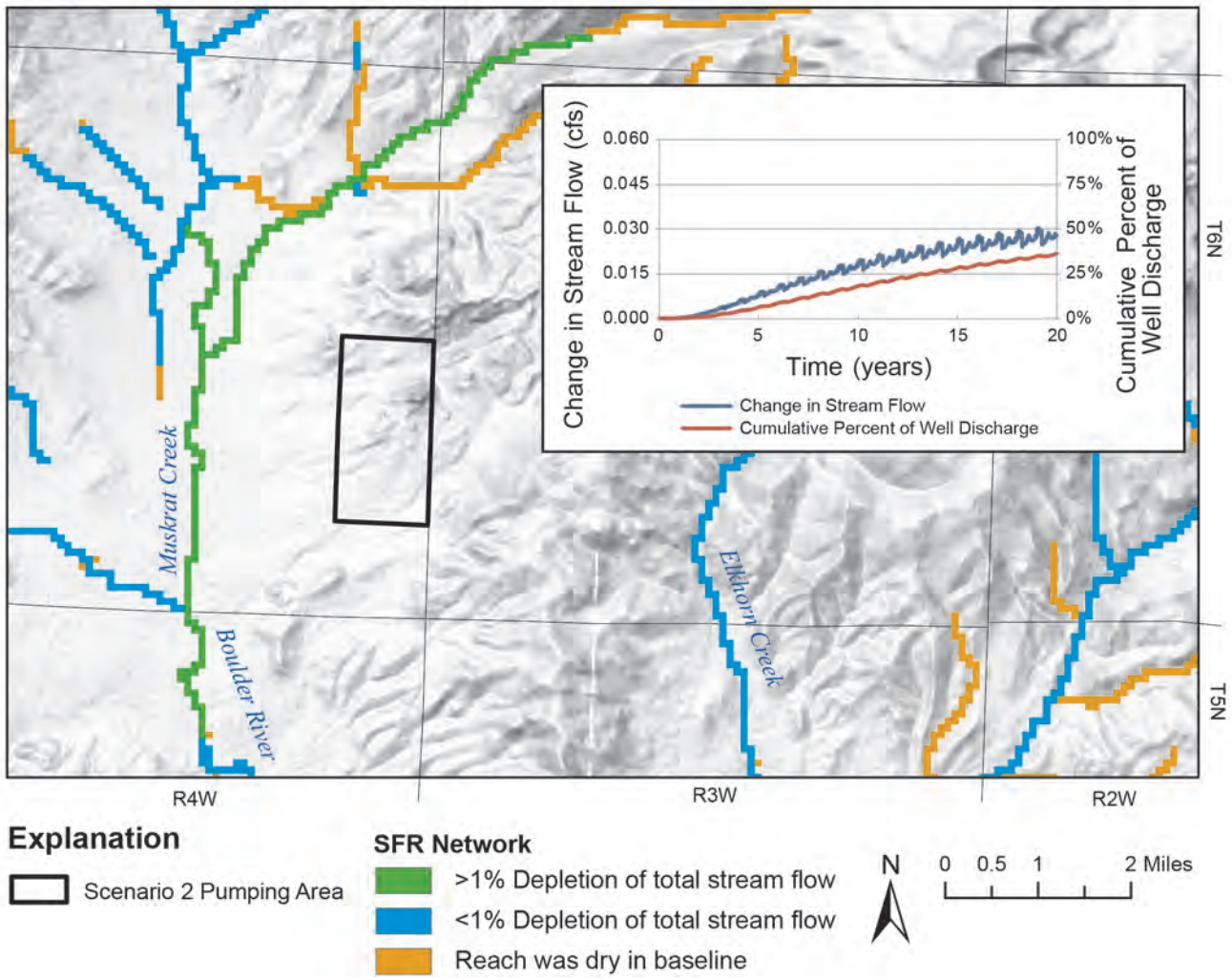

Figure 34. Development under Scenario 2 would cause a decrease in stream flow of about 0.03 cfs after 20 yr, and over time a greater percentage of the water pumped from the wells will be obtained from stream depletion as aquifer storage is depleted (inset). Most of the depletion would occur in Muskrat Creek, with less depletion in other streams near the development.

tional to this increase in pumping rates. For instance, the maximum drawdown was 22.3 ft, or roughly double that of Scenario 2, and it occurred at the same time and location as in Scenario 2. The increase in drawdown from year to year decreased over time; the difference in maximum drawdown between years 19 and 20 was 0.29 ft as opposed to 2.8 ft between years 1 and 2. The maximum radius of influence was 2.2 mi from the point of maximum drawdown, and it occurred north of the pumping center (fig. 35).

Stream depletion results were also proportional to the increased pumping, with a maximum decrease of 0.06 cfs (27.0 gpm) in the final year (year 20) of the simulation (fig. 36). The percentage of the pumped water derived from stream baseflow was very similar to Scenario 2, with a maximum cumulative percentage of 36.2% at the end of the simulation. The closest stream segments downgradient of the subdivision were most affected. The lower mainstem of Muskrat Creek showed the most depletion. The only unaffected stream reaches near the well field were those that were dry in the baseline scenario.

Scenario 4

Scenario 4 was similar to Scenario 2 in that it featured a new 20-acre-lot subdivision with a total of 64 wells. The new development was located along the western pediment of the central Boulder Valley, adjacent to the existing Jack Creek subdivision (fig. 30). Bench sediments underlie the area; therefore, the transmissivity of the aquifer is higher than in scenarios 1, 2, and 3, which were underlain by granite (see Aquifer Properties). The simulation resulted in a maximum drawdown of 8.2 ft, which occurred in August of the final year of pumping. The increase in drawdown from year to year decreased over time; the difference in maximum drawdown between years 19 and 20 was 0.07 ft as opposed to 0.85 ft between years 1 and 2. The maximum radius of influence was 1.4 mi from the point of maximum drawdown, and it occurred west of the pumping center (fig. 37).

Stream flow results indicated a decrease in baseflow over time, with a maximum decrease of 0.04 cfs (18.4 gpm) in the final year of the simulation (fig. 38). The percentage of the pumped water derived from former baseflow increased over time, with a maximum cumulative percentage of 65.6% at the end of the simulation. The closest stream segments downgradient of the subdivision were most affected. The mainstem of the Boulder River showed the most depletion.

Scenarios Summary

The results of the scenarios are summarized in table 14. A few model results were common to all four simulations. For instance, water levels continued to decline throughout each 20-yr scenario, though the annual rate of drawdown decreased by about an order of magnitude by the end of the simulation (table 14). In addition, the location of maximum drawdown was in the lowest-K area of each well field. The maximum drawdown was lowest in Scenario 4 because of the bench sediment's high transmissivity relative to the three bedrock-area scenarios. A larger radius of influence was not always associated with a higher depletion rate; rather, decreases in baseflow were a function of the wells' proximity to affected streams and the duration of pumping.

Results also showed that both drawdown and depletion increased substantially with denser development. In comparing Scenario 2 and Scenario 3, the maximum drawdown and depletion rate were directly proportional to the increase in pumping, in that they both doubled as the pumping rates doubled. The percent of water supplied from base stream flow did not increase with increase pumping rates; rather, at the end of each simulation, the Scenario 2 and 3 percentages were approximately equal (36.3% and 36.2%, respectively). These results correspond well with analytical models of stream depletion (e.g., Jenkins, 1968). These end-of-simulation stream depletion percentages were also substantially lower than those of Scenarios 1 and 4, as was their annual rate of decrease. These results demonstrate that the percentage's magnitude and rate of decrease with time are both proportional to distance from the affected streams, because the Scenario 1 and 4 sites were closer to streams.

Finally, the maximum depletion rate of 0.06 cfs in Scenario 3 may seem rather small; however, the results suggest that the depletion rates will continue to increase with time, especially those farther from the impacted streams, and the wells' water supply will eventually be derived entirely from groundwater flow that formerly discharged to streams. For comparison, the long-term USGS record (1929–2013) at Red Bridge shows a minimum mean monthly flow of 27 cfs. Based on the average annual consumptive use

for Scenario 3, the long-term average effect on stream flow would be a decrease of about 0.09 cfs, with some modest seasonal fluctuations. This would mean that a development of this type could account for about a 0.3% decrease in low flows in the Boulder River.

SUMMARY AND CONCLUSIONS

Assumptions and Limitations

The Area-Wide numerical model served as a useful tool in developing the conceptual model and evaluating the effects of increased groundwater development; however, it has limitations. For example, the model was not intended to accurately simulate hydrogeologic effects at scales finer than the design scale. Certain parameter values, such as irrigation recharge, were assumed to be uniform; in a smaller-area model, such assumptions would not necessarily be appropriate. Likewise, the basin scale of the model precipitated a 1-layer grid in order to optimize solution stability and model run times. If smaller-scale models were developed, multiple layers would allow simulation of aquifer-property changes with depth, allowing for better fitting of upland bedrock water-level observations.

Parameter uncertainty was another limitation on model results, specifically with respect to the Boulder River gains and losses. Parameters influencing river gain/loss results included streambed elevations, stream flow during the non-irrigation season, canal diversions, canal leakage rates, and unsaturated-zone flow. Although estimates of these parameters, and the water-budget estimates, were soundly based; they are still only estimates. A lack of diversion records and historical data as well as the large study area size necessitated assumptions about the duration and flow rates in unmonitored canals, streambed slopes, and the connection between the saturated zone and streambeds.

Model Predictions

The Area-Wide Model evaluated several pumping scenarios in hypothetical residential developments within the northern portion of the lower Boulder River watershed. Results showed that groundwater drawdown and stream depletion were linearly proportional to rates of consumptive use and inversely proportional to aquifer transmissivity. Stream depletion was also proportional to the proximity of streams, both when evaluated as a percentage of the consumptive use rate, and as a decrease in stream baseflow. The timing of maximum drawdown was consistently in late summer, when consumptive use was the highest.

Simulated depletion rates are relatively small compared to surface-water irrigation diversions. Thus, it is unlikely that subdivisions similar to those simulated in this model would introduce a measurable change in surface-water supplies. Larger developments, smaller lot sizes, and more developments would have greater impacts, and those impacts would depend on consumptive use and distance to surface waters.

The predictive scenarios represented system-scale effects of the introduced stresses, and they were based on data available at the time of model construction. There will undoubtedly be new information available for inclusion in future groundwater modeling efforts. Individuals who plan to operate the model should read this report, review the derivation of model parameters, and use caution in interpreting results, especially if any stress is located near the boundaries of the model. Modeling a portion of the current model domain may be appropriate to address local issues with the aquifer characteristics and groundwater fluxes in the present model serving as a starting point for model development. Modifications should be made to incorporate new data.

Recommendations

The residential groundwater development in the simulated scenarios does not appear likely to cause a measurable change in surface-water availability. If new developments are approved, and there is sufficient concern regarding their impacts to surface waters, monitoring could be employed to detect actual changes in groundwater levels, and impact thresholds and management actions could be established to minimize effects to stream flows. Collection of baseline (pre-development) data would greatly aid in differentiating between natural variation and anthropogenic effects.

If a portion of the study area did become a growing population center and residential groundwater use substantially increased, managed recharge could potentially be used to offset groundwater consumption; however, there are several legal and environmental issues that would need to be carefully assessed (Carlson, 2013). An infiltration pilot study would help to identify optimal location(s) and a cost–benefit analysis could be used to determine the economic feasibility. Reducing the consumptive use of water (e.g., xeriscap-

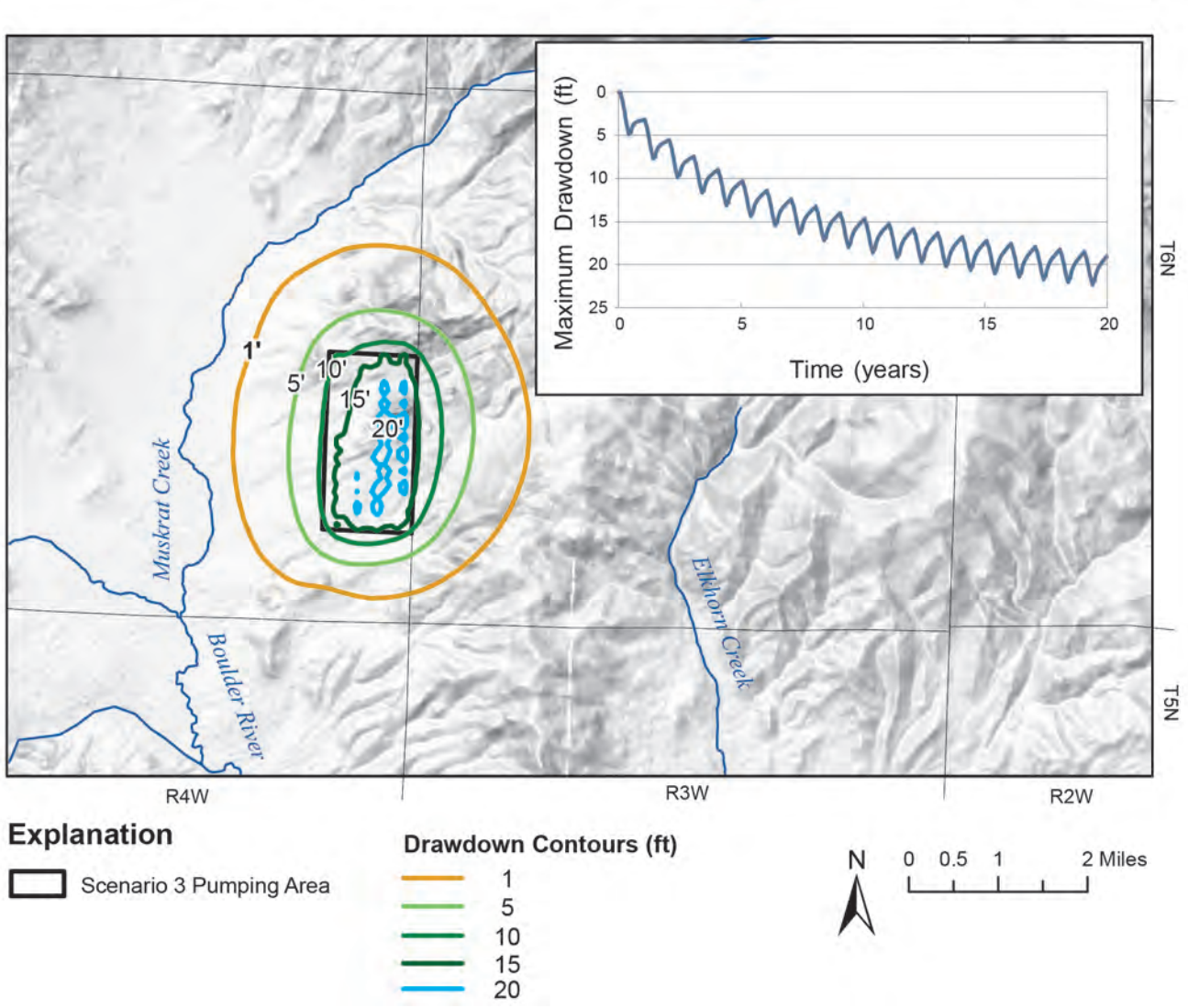

Figure 35. Scenario 3 results show that this type of development would result in a maximum drawdown of about 22 ft (inset), and the 1-ft drawdown contour would extend approximately 2.2 mi from the point of maximum drawdown after 20 yr.

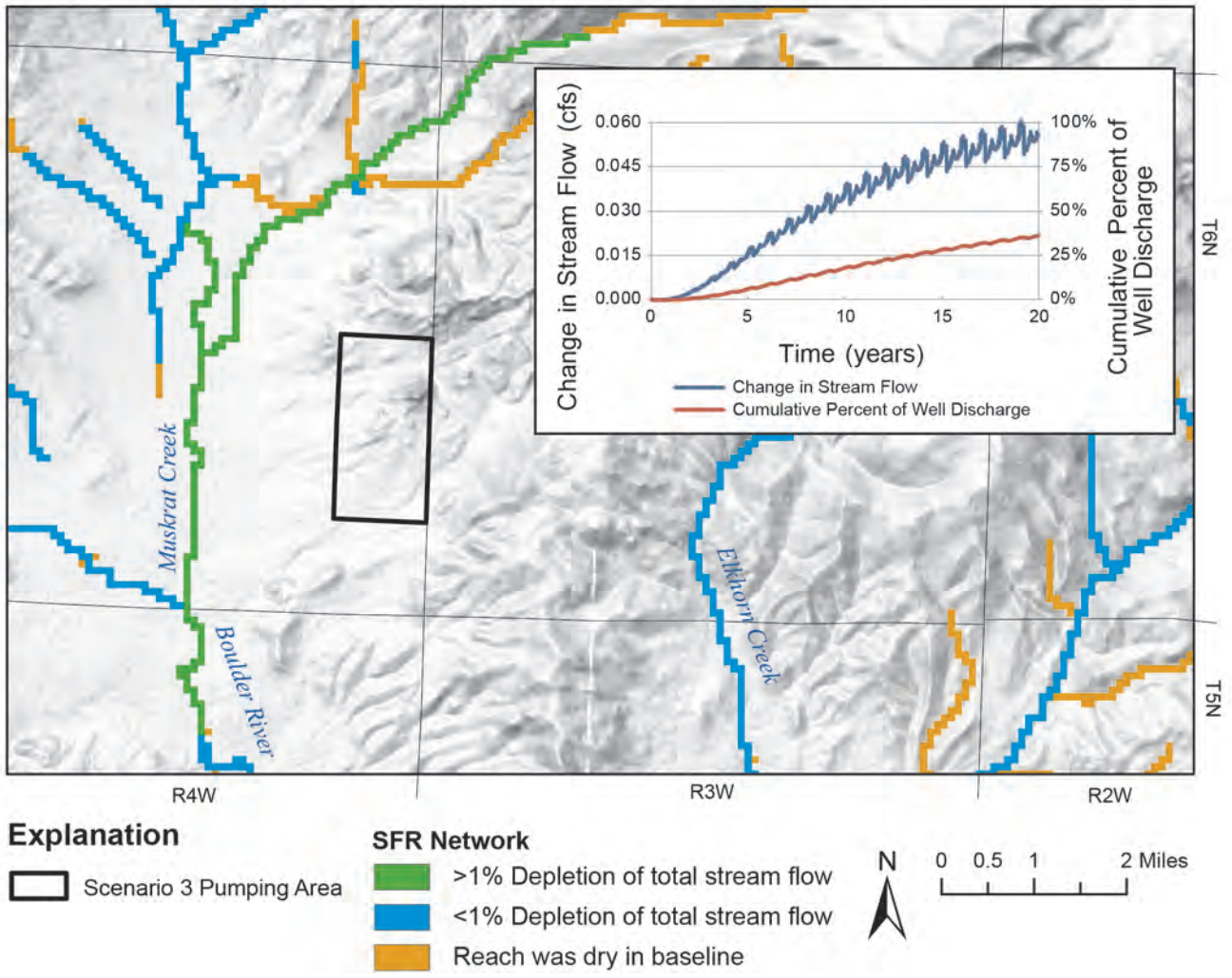

Figure 36. Development under Scenario 3 would cause a decrease in stream flow of about 0.06 cfs after 20 yr, and over time a greater percentage of the water pumped from the wells will be obtained from stream depletion as aquifer storage is depleted (inset). Most of the depletion would occur in Muskrat Creek, with less depletion in other streams near the development.

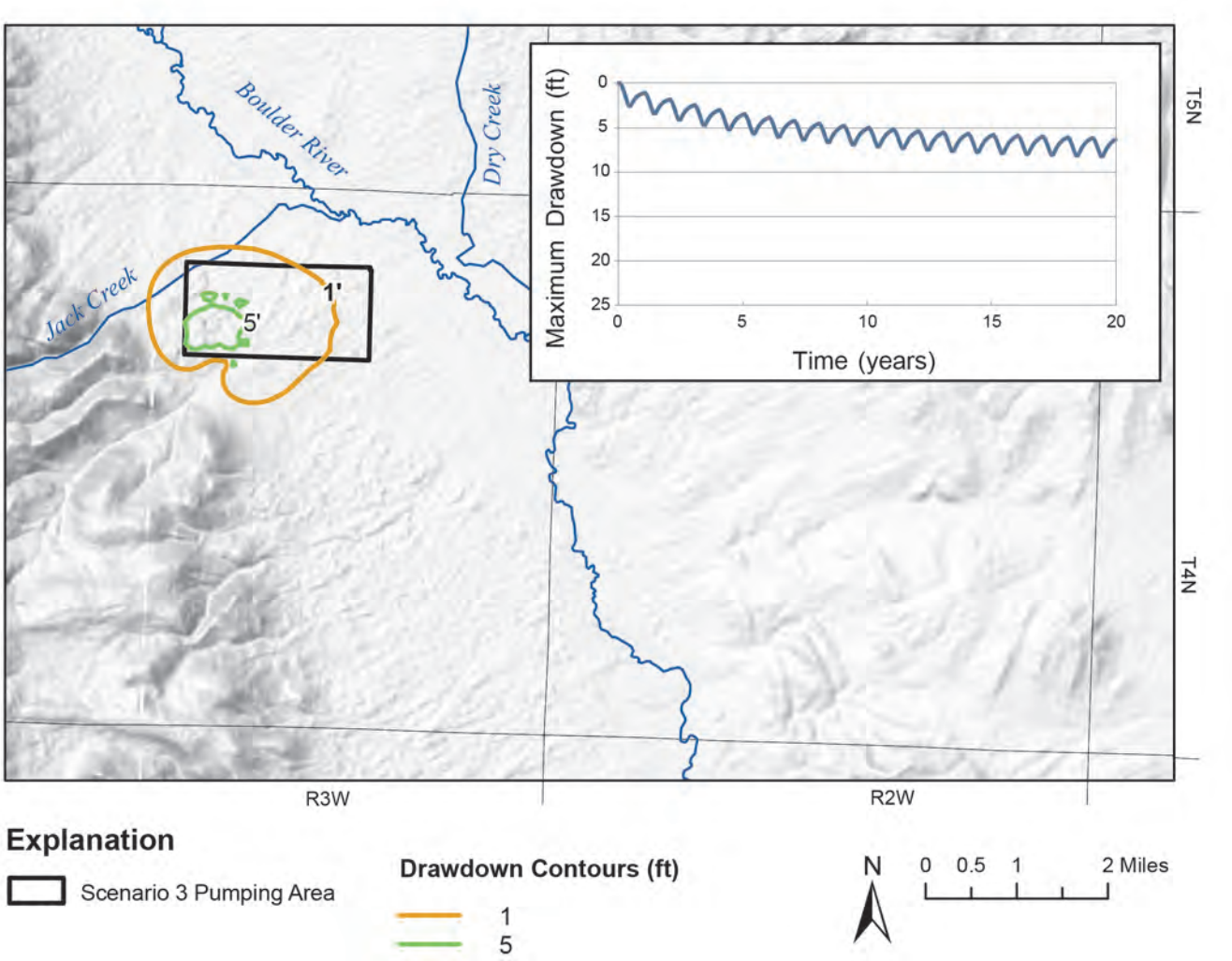

Figure 37. Scenario 4 results show that this type of development would result in a maximum drawdown of about 8 ft (inset), and the 1-ft drawdown contour would extend approximately 1.4 mi from the point of maximum drawdown after 20 yr.

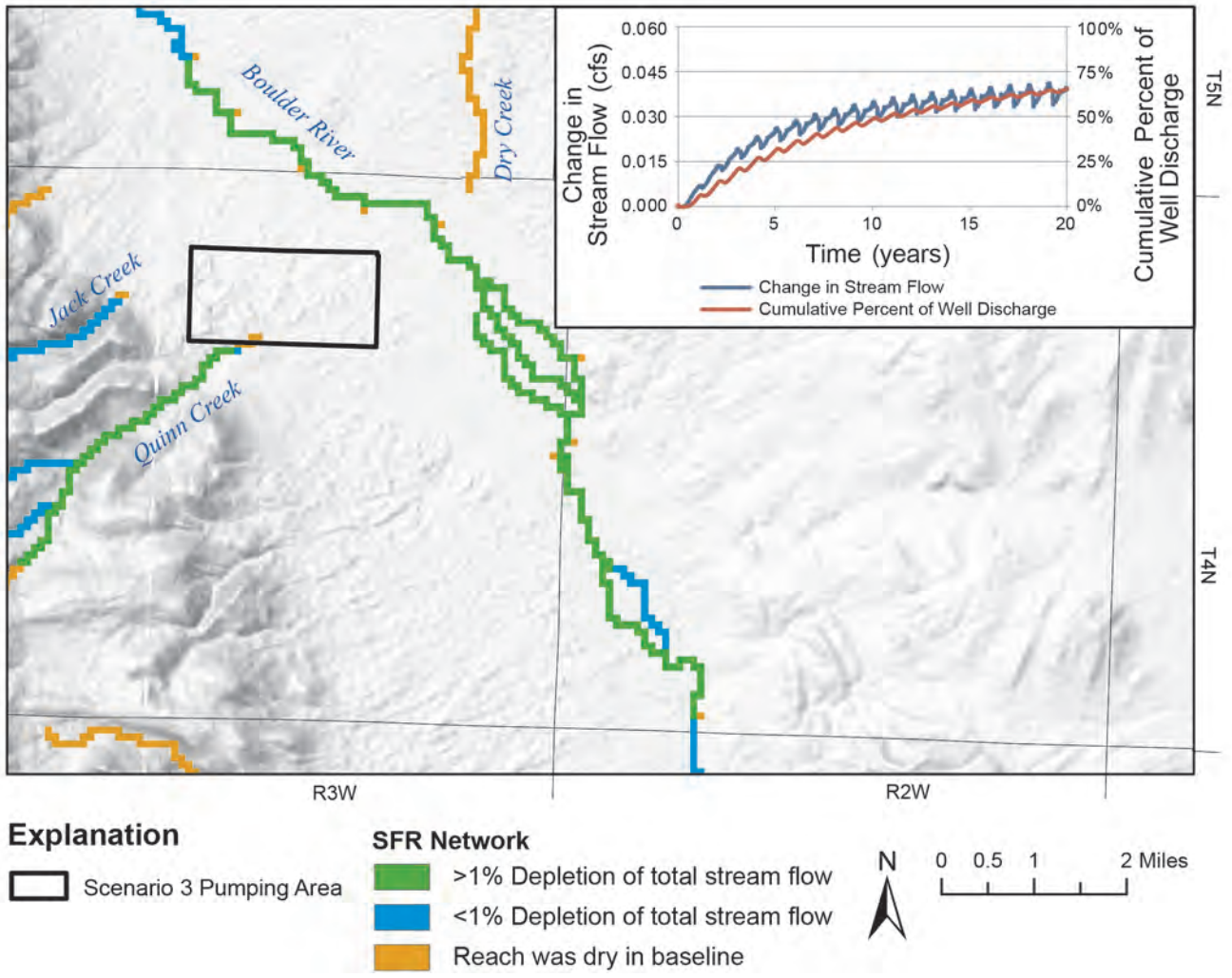

Figure 38. Development under Scenario 4 would cause a decrease in stream flow of about 0.04 cfs after 20 yr, and over time a greater percentage of the water pumped from the wells will be obtained from stream depletion as aquifer storage is depleted (inset). Most of the depletion would occur in the Boulder River, with less depletion in other streams near the development.

ing) is another alternative to minimize groundwater impacts from residential development.

Increased monitoring of surface waters, irrigation diversions, and return flows would greatly aid in understanding the surface-water flow system, and its interaction with groundwater. Identifying the river reaches of most concern would help in developing a monitoring plan. For instance, the lowest flows in the Boulder River typically occur at either Quaintance Lane or Dunn Lane, so stage measurements at one of those sites could be used as a management trigger. In times of severe drought, surface-water modeling may be useful for selecting the most effective water conservation measures.

Reevaluating irrigation practices with the goal of increasing late summer flow in the Boulder River would likely produce significant flow increases. Water lost from the ditches and groundwater recharge below irrigated fields enters the alluvial aquifer and eventually reaches the Boulder River to become the most important source of late summer flows. Therefore, it is not always desirable to line canals, or curtail irrigation. Conversely, increased early season canal use and irrigation would provide additional recharge to the groundwater system. Increasing canal and irrigation efficiency may be desirable in some areas; however, it should be recognized that this will reduce groundwater recharge.

Coordinated actions between irrigators could also improve late summer flow. The drought management plans used in the Upper Jefferson and Big Hole River watersheds could be good models. These plans rely on monitored river flow and temperature to trigger specific actions, including voluntary reductions in diversions. In the Upper Jefferson, VanMullem (2006) showed that the most cost-effective water-saving measures included improving canal system management, canal operating structures, and measuring structures. A similar combination of coordinated action by irrigators and irrigation system improvements would likely also be effective in the Boulder Valley. During low flow periods, such improvements would allow irrigators to more easily regulate the amount of water diverted.

ACKNOWLEDGMENTS

We thank the many landowners and residents of the Boulder Valley for their interest, access to property, and permission to conduct various aspects of the investigation. We especially thank Bob Sims, Pat Carey, and Randy Kirk, who provided many introductions and insight into the hydrogeologic system. We thank Jefferson County, which provided partial funding for this study, and the County Commissioners who provided feedback on the scope of the study. We also thank Tom Harrington from MSU Extension for providing assistance.

Montana Tech students Luke Carlson, John Anderson, Mike Shirley, and Nicole Brancheau greatly assisted with both the field and office aspects of this study. Their help is much appreciated. Figures by Susan Smith, MBMG; editing and layout by Susan Barth, MBMG.

REFERENCES

Abdo, G., Butler, J., Myse, T., Wheaton, J., Snyder, D., Metesh, J., and Shaw, G., 2013, Hydrogeologic investigation of the Lower Beaverhead study area, Beaverhead County, Montana, MBMG Open-File Report 637, 132 p.

Anderson, M.P., and Woessner, W., 2002, Applied groundwater modeling: San Diego, CA, Academic Press, 381 p.

Aquaveo, LLC, 2012, Groundwater Modeling System (GMS), v. 9.0.

ASTM International, 1995, Documenting a groundwater flow model application (D5718-95; reapproved 2006): West Conshohocken, PA, ASTM International.

ASTM International, 2004, Standard guide for application of a ground-water flow model to a site – specific problem (D5447-04): West Conshohocken, PA, ASTM International.

Blaney, H.F., and Criddle, W.D., 1962, Determining consumptive use and irrigation water requirements: U.S. Department of Agriculture Technical Bulletin 1275, 59 p.

Bobst, A.L., Waren, K.B., Ahern, J.A., Swierc, J.E., and Madison, J.D., 2013, Hydrogeologic investigation of the Scratchgravel Hills study area, Lewis and Clark County, Montana, interpretive report: MBMG Open-File Report 636, 63 p.

Bobst, A.L., Butler, J.A., and Carlson, L.D., 2016, Hydrogeologic investigation of the Boulder Valley, Jefferson County, Montana, interpretive report: MBMG Open-File Report 682, 92 p.

Bossong, C.R., Caine, J.S., Stannard, D. I., Flynn, J. L., Stevens, M.R., and Heiny-Dash, J.S., 2003, Hydrologic conditions and assessment of water resources in the Turkey Creek watershed, Jefferson County, Colorado, 1998–2001: USGS Water-Resources Investigations Report: 2003-4034, 140 p.

Botz, M.K., 1968, Groundwater study near Boulder: MBMG unpublished manuscript.

Buck, F.E., and Bille, H.L., 1956, Water resources survey—Jefferson County, Montana: Helena, Mont., Montana State Engineer's Office, 87 p.

Burfiend, W.J., 1967, A gravity investigation of the Tobacco Root Mountains, Jefferson basin, Boulder batholith, and adjacent areas of southwestern Montana: Indiana University, PhD dissertation, 90 p.

Cannon, M.R., and Johnson, D.R., 2004, Estimated water use in Montana in 2000: USGS Scientific Investigations Report 2004-5223, 61 p.

Carling, G.T., Mayo, A.L., Tingey, D., and Bruthans, J., 2012, Mechanisms, timing, and rates of arid region mountain front recharge: Journal of Hydrology, v. 428–429, p. 15–31.

Carlson, L., 2013. Managed recharge and base-flow enhancement in an unconsolidated aquifer in the Boulder River Valley, Montana: Montana Tech, Master's thesis, 174 p.

Chase, Ted, 2012, Montana Department of Revenue, written communication, October 23, 2012.

Chauvin, G.M., Flerchinger, G.N., Link, T.E., Marks, D., Winstral, A.H., and Seyfried, M.S., 2011, Long-term water balance and conceptual model of a semi-arid mountainous catchment: Journal of Hydrology, v. 400, p. 133–143.

Dalton, J.C., 2003, Irrigation Water Requirements user manual, v. 1.0, http://www.nrcs.usda.gov/Internet/FSE_DOCUMENTS/nrcs144p2_013838.pdf [Accessed 9/3/15].

Darr, A., 1975, Boulder water job one step nearer: The Montana Standard, 2/9/1975, p. 17.

Delin, G.N., Healy, R.W., Lorenz, D.L., and Nimmo, J.R., 2007, Comparison of local to regional-scale estimates of ground-water recharge in Minnesota, USA: Journal of Hydrology, v. 334, p. 231–249.

DeVries, J.J., and Simmers, I., 2002, Groundwater recharge—An overview of processes and challenges: Hydrogeology Journal, v. 10, no. 5, p. 5–17.

Doherty, J.E., 2010, PEST model-independent parameter estimation user manual, 5th ed: Watermark Numerical Computing, 336 p, http://www.pesthomepage.org [Accessed 12/19/2013].

Doherty, J.E., 2013a, Addendum to the PEST manual: Watermark Numerical Computing, 266 p, http://www.pesthomepage.org [Accessed 12/19/2013].

Doherty, J.E., 2013b, Getting the most out of PEST, Watermark Numerical Computing, 12 p., http://www.pesthomepage.org/ [Accessed 9/3/15].

Doherty, J.E., and Hunt, R.J., 2010, Approaches to highly parameterized inversion—A guide to using PEST for groundwater-model calibration: USGS Scientific Investigations Report 2010–5169, 59 p.

Dutton, D.M., Lawlor, S.M., Briar, D.W., and Tresch, R.E., 1995, Hydrogeologic data for the northern Rocky Mountains intermontane basins, Montana: USGS Open-File Report 95-143, 94 p.

Environmental Simulations Incorporated, 2011, Guide to using Groundwater Vistas, v. 6, 213 p.

Farnes, P.E., Huddleston, J., and Flynn, K., 2011, Montana electronic precipitation map: Proceedings of the Annual Western Snow Conference, 2011, http://nris.mt.gov/gis/ [Accessed 10/16/14].

Fetter, C.W., 2001, Applied hydrogeology, 4th ed: Englewood Cliffs, N.J., Prentice Hall Inc., 598 p.

Flint, A.L., Flint, L.E., Kwicklis, E.M., Fabryka-Martin, J.T., and Bodvarsson, G.S., 2002, Estimating recharge at Yucca Mountain, Nevada, USA—Comparison of methods: Hydrogeology Journal, v. 10, p. 180–204.

Flint, A.L., and Flint, L.E., 2007, Application of the Basin Characterization Model to estimate in-place recharge and runoff potential in the basin and range carbonate-rock aquifer system, White Pine County, Nevada, and adjacent areas in Nevada and Utah: USGS Scientific Investigations Report 2007-5099, 21 p.

Freeze, R.A., and Cherry J.A., 1979, Groundwater: Englewood Cliffs, N.J., Prentice-Hall Inc., 604 p.

Hackett, O.M., Visher, F.N., McMurtrey, R.G., and Steinhilber, W.L., 1960, Geology and ground water resources of the Gallatin Valley, Gallatin County, Montana: USGS Water-Supply Paper

1482, 282 p.

Harbaugh A., Banta, E., Hill, M., and McDonald, M., 2000, MODFLOW-2000, the U.S. Geological Survey Modular Ground-Water Model—User guide to modularization concepts and the ground-water flow process: USGS Open-File Report: 2000-92, 121 p.

Healy, R.W., 2010, Estimating groundwater recharge: Cambridge, UK, Cambridge University Press, 264 p.

Huntley, D., 1979, Groundwater recharge to the aquifers of northern San Luis Valley, Colorado: Geological Society of America Bulletin, Part II, v. 90, no. 8, p. 1196–1281.

Idaho Department of Water Resources (IDWR), 2013, Enhanced Snake Plain Aquifer Model v. 2.1 final report: Idaho Department of Water Resources, 302 p.

Jenkins, C.T., 1968, Computation of rate and volume of stream depletion by wells: Groundwater, v. 6, no. 2, p. 37–46.

Jerde, E.A., 1984, A structural analysis of a local thrust fault system, southeast Jefferson County, Montana: Washington State University, PhD dissertation.

Johns, E.L., 1989, Water use by naturally occurring vegetation including annotated bibliography (literature review): New York, American Society of Civil Engineers, p. 380–385.

Kendy, E., and Tresch, R.E., 1996, Geographic, geologic and hydrologic summaries of intermontane basins of the Northern Rocky Mountains, Montana: USGS Water-Resources Investigations Report 96-4025, 233 p.

Lautz, L.K., 2008. Estimating groundwater evapotranspiration rates using diurnal water-table fluctuations in a semi-arid riparian zone: Hydrogeology Journal, v. 16, p. 483-497.

Leenhouts, J.M., Stromber, J.C., and Scott, R.L. (eds.), 2006, Hydrologic requirements of and consumptive ground-water use by riparian vegetation along the San Pedro River, Arizona: USGS Scientific Investigations Report 2005-5163, 154 p.

Lerner, D.N., Issar, A.S., and Simmers, I., 1990, Groundwater recharge: A guide to understanding and estimating natural recharge: International Contributions to Hydrology, v. 8, 345 p.

Lewis, R.S. (compiler), 1998, Geologic map of the Butte 1o x 2o quadrangle, south-western Montana: MBMG Open-File Report 363, 16 p., 1 sheet, scale 1:250,000.

Magruder, I.A., Woessner, W.W., and Running, S.W., 2009, Ecohydrologic process modeling of mountain block groundwater recharge. Ground Water, v. 47, no. 6, p. 774–785.

Mahoney, J.B., Kjos, A., Stolz, J., Maclaurin, K., and Kohel, C., 2008, Geologic map of Devils Fence 7.5' quadrangle, west-central Montana: MBMG Open-File Report 565, 1 sheet, scale 1:24,000.

Manning, A.H., and Solomon, D.K., 2004, Constraining mountain-block recharge to the eastern Salt Lake Valley, Utah with dissolved noble gas and tritium data, in Hogan, J.F., Phillips, F.M., and Scanlon, B.R, eds., Groundwater recharge in a desert environment—The southwestern United States: Washington, DC, American Geophysical Union, p. 139–158.

Manning, A.H., and Solomon, D.K., 2005, An integrated environmental tracer approach to characterizing groundwater circulation in a mountain block: Water Resources Research, v. 41, no. 12, 18 p.

Maurer, D.K., and Berger, D.L., 1997, Subsurface flow and water yield from watersheds tributary to Eagle Valley hydrographic area, west-central Nevada: USGS Water-Resources Investigation Report 97-4191, 56 p.

Montana Bureau of Mines and Geology (MBMG), 2011, Montana Groundwater Information Center Water Well Data: http://nris.mt.gov/gis/, updated 7/13/2011.

Montana Department of Revenue (MDOR), 2012, Revenue Final Land Unit Classification, http://mslapps.mt.gov/Geographic_Information/Data/DataList/datalist_Details.aspx?did={4754A734-303D-4920-8CAA-F027D5F3EE58} [Accessed October 2012].

Montana DNRC, 2007, Digitized canal reference data from Montana's Water Resources Survey (http://www.dnrc.mt.gov/wrd/water_rts/survey_books/default.asp), based on the State Engineer's Office WRS publication for Jefferson County, June 1956 [Accessed February 2009].

Montana DNRC, 2011, DNRC general water-use requirements, presented by the DNRC Water Resources Division to the Water Policy Interim Committee on September 13, 2011, http://leg.mt.gov/content/Committees/Interim/2011-2012/Water-Policy/Meeting-Documents/September-2011/water-use-table.pdf.

Montana DNRC, 2013, DNRC Water Right Query System, http://nris.mt.gov/dnrc/waterrights/default.aspx [Accessed April 2013].

Montana State Library, 2012, Montana Structures/Addresses Framework of the Montana Spatial Data Infrastructure, Montana State Library, Helena, Mont., http://mslapps.mt.gov/Geographic_Information/Data/DataList/datalist_Details.aspx?did={56554A37-1684-460C-8792-121D60A64213} [Accessed April 2013].

Montana State Library, 2013, Montana Cadastral, Helena, Mont., http://svc.mt.gov/msl/mtcadastral/ [Accessed April 2013].

Montana Water Resources Board, 1968, Boulder River Project #62.

National Oceanic and Atmospheric Administration (NOAA), 2011, NOAA's 1981–2010 climate normals, http://www.ncdc.noaa.gov/oa/climate/normals/usnormals.html [Accessed 3/4/13].

Nelson, W.L., 1962, A seismic study of North Boulder Valley and other selected areas, Jefferson and Madison Counties, Montana: Indiana University, Master's thesis, 33 p.

Ng, G.H.C, McLaughlin, D., Entekhabi, D., and Scanlon, B., 2009, Using data assimilation to identify diffuse recharge mechanisms from chemical and physical data in the unsaturated zone: Water Resources Research, v. 45, 18 p.

Noble, R.A., Bergantino, R.N., Patton, T.W., Sholes, B.C., Daniel, F., and Schofield J., 1982, Occurrence and characteristics of ground water in Montana, v. 2, the Rocky Mountain region: Montana Bureau of Mines and Geology Open-File Report 99, 132 p.

NRCS, 1993, NRCS National engineering handbook (NEH), Part 623, Chapter 2: Irrigation water requirements: USDA.

NRCS, 2006, USDA Agriculture handbook 296: Land resources regions and major land resource areas of the United States, the Caribbean, and the Pacific Basin, hppt://apps.cei.psu.edu/mlra/, [Accessed January 2013].

NRCS, 2012a, IWR Program, http://www.nrcs.usda.gov/wps/portal/nrcs/detailfull/national/water/manage/irrigation/?&cid=stelprdb1044890 [Accessed October 2012].

NRCS, 2012b, NRCS Web Soil Survey, http://websoilsurvey.nrcs.usda.gov/app/WebSoilSurvey.aspx [Accessed November 2012].

NRCS, 2014, Snow telemetry (SNOWTEL) and snow course data and products, http://www.wcc.nrcs.usda.gov/snow/index.html [Accessed November 2014].

Oregon State University, 2013, PRISM Climate Group, Oregon State University, created February 2004, http://prism.oregonstate.edu [Accessed April 2013].

Parker, J.S., 1961, A preliminary seismic investigation of Tertiary basin fill in the Jefferson Island quadrangle, Montana: Indiana University, Master's thesis, 35 p.

Persson, G., 1995, Willow stand evapotranspiration simulated for Swedish soils: Agricultural Water Management, v. 28, p. 271–293.

Petersen, M.R., and Hill, R.W., 1985, Evapotranspiration of small conifers: Journal of Irrigation and Drainage Engineering, v. 111, no. 4, p. 341–351.

Potts, D., 1988, Estimation of evaporation from shallow ponds and impoundments in Montana: Montana Forest and Conservation Experiment Station Miscellaneous Publication 48, 29 p.

Reynolds, M.W., and Brandt, T.R., 2006, Preliminary geologic map of the Townsend 30' x 60' quadrangle, Montana: USGS Open-File Report 2006-1138, scale 1:100,000.

Rosenberry, D.O., and Winter, T.C., 1997, Dynamics of water-table fluctuations in an upland between two prairie-pothole wetlands in North Dakota: Journal of Hydrology, v. 191, p. 266–289.

Sanford, W.E., and Selnick, D.L., 2012, Estimation of evapotranspiration across the conterminous United States using a regression with climate and land-cover data: Journal of the American Water Resources Association, v. 9, no. 1, p. 217–230.

Scott, R.L., Edwards, E.A., Shuttleworth, W.J., Huxman, T.E., Watts, C., and Goodrich, D.C., 2004,

Interannual and seasonal variation in fluxes of water and carbon dioxide from a riparian woodland ecosystem: Agricultural and Forest Meteorology, v. 122, p. 65–84.

Soil Conservation Service (SCS), 1975, Draft plan and draft environmental impacts statement Boulder River watershed, Jefferson County, Montana.

Sterling, R., and Neibling, W.H., 1994, Final report of the Water Conservation Task Force: Boise, Ida., Idaho Department of Water Resources.

Thiros, S.A., Stolp, B.J., Hadley, H.K., and Steiger, J.I., 1996, Hydrology and simulations groundwater flow in Juab Valley, Juab county, Utah: Utah Department of Natural Resources Technical Publication 114, 101 p.

U.S. Geological Survey (USGS), 2010, LANDFIRE database, http://www.landfire.gov/lf_mosaics.php [Accessed January 2013].

U.S. Geological Survey (USGS), 2011a, National land cover data, http://www.mrlc.gov/nlcd11_data.php [Accessed January 2013].

U.S. Geological Survey (USGS), 2011b, Gap analysis program (GAP), May 2011, National Land Cover, v. 2, http://gapanalysis.usgs.gov/gaplandcover/data/download/ [Accessed January 2013].

U.S. Geological Survey (USGS), 2012, 1/3-arc second national elevation dataset, http://nationalmap.gov/viewers.html [Accessed September 2012].

Vaccaro, J.J., and Olsen, T.D., 2007, Estimates of ground-water recharge to the Yakima River Basin aquifer system, Washington, for predevelopment and current land-use and land-cover conditions: USGS Scientific Investigations Report 2007-5007, 31 p.

VanMullem, J., 2006, Upper Jefferson River irrigation delivery improvement project: Prepared for the Jefferson River Watershed Council and Trout Unlimited.

Vuke, S.M., Coppinger, W.W., and Cox, B.E., 2004, Geologic map of Cenozoic deposits in the Upper Jefferson Valley, southwestern Montana: MBMG Open-File Report 505, 35 p., 1 sheet, scale 1:50,000.

Vuke, S.M., Porter, K.W., Lonn, J.D., and Lopez, D.A., 2007, Geologic map of Montana: MBMG Geologic Map 62-A, 73 p., 2 sheets, scale 1:500,000.

Vuke, S.M., Lonn, J.D., Berg, R.B., and Kellogg, K.S., 2014, Geologic map of the Bozeman 30’ x 60’ quadrangle, southwestern Montana: MBMG Open-File Report 648, 44 p., 1 sheet, scale 1:100,000.

Ward, A.D., and Trimble, S.W., 2004, Environmental hydrology: Boca Raton, Fla., Lewis Publishers, CRC Press, 472 p.

Waren, K.B., Bobst, A.L., Swierc, J.E., and Madison, J.D., 2012, Hydrogeologic investigation of the North Hills study area, Lewis and Clark County, Montana, Interpretive Report: MBMG Open-File Report 610, 99 p.

Wilson, D.A., 1962, A seismic and gravity investigation of the North Boulder River and Jefferson River Valleys, Madison and Jefferson Counties, Montana: Indiana University, Master’s thesis, 43 p.

Wilson, J.L., and Guan, H., 2004, Mountain-block hydrology and mountain-front recharge, in Hogan J.F., Phillips F.M., and Scanlon, B.R., eds., Groundwater recharge in a desert environment—The southwestern United States: American Geophysical Union, p. 113–137.

Woodhouse, B., 2008, Approaches to ET measurement: Southwest Hydrology, v. 7, no. 1, p. 20–21.

APPENDIX A
MODEL FILE INDEX

This appendix indexes the files of the simulations that served as final modeling products. The files include the Groundwater Vistas (Vistas) project file and MODFLOW input and output files. This information is sufficient for a third party to rebuild the model, reproduce model results, and use the model for future purposes (ASTM, 1995). Details on the model's grid, aquifer, and recharge properties are provided in the body of this report. The following simulations are included in the index:

Section A1: Calibration

- Steady-State Calibration: calibrated heads and flows in steady-state mode
- Transient Calibration: calibrated heads and flows in transient mode from April 2010 to April 2013; note that the steady-state simulation was the first stress period

Section A2: Predictive Scenarios

- Scenario 1: evaluated the impacts of increased groundwater withdrawals in an existing 20-acre-lot subdivision (Aspen Valley Ranch) in the North Boulder Valley
- Scenario 2: evaluated the impacts of groundwater withdrawals in a 20-acre-lot subdivision on the east side of the North Boulder Valley
- Scenario 3: evaluated the impacts of groundwater withdrawals in a 10-acre-lot subdivision on the east side of the North Boulder Valley
- Scenario 4: evaluated the impacts of groundwater withdrawals in a 20-acre-lot subdivision on the west side of the central Boulder Valley

Table A1 provides the filename, date, type, and primary action for the simulations listed above; the required supporting files are also included. Table A2 provides the input and output file types for each simulation, including those specific to Vistas. These files are available for download from the Groundwater Investigations Program website (http://www.mbmg.mtech.edu/gwip/gwip.asp).

Table A1. Lower Boulder groundwater model file organization.

Simulation ID	Simulation Date	Simulation Type	Primary Action	File Name	Supporting Files
Steady-State Calibration	9/2/2014	Calibration	Final run of steady-state calibration	BR_SS	BR_SS_head_targets.csv
Transient Calibration	9/3/2014	Calibration	Final run of transient calibration	BR_Transient	BR_Transient_targets.csv
Scenario 1	9/21/2014	Predictive scenarios	Simulated Scenario 1	BR_Scenario_1	
Scenario 2	9/15/2014	Predictive scenarios	Simulated Scenario 2	BR_Scenario_2	
Scenario 3	9/18/2014	Predictive scenarios	Simulated Scenario 3	BR_Scenario_3	
Scenario 4	9/18/2014	Predictive scenarios	Simulated Scenario 4	BR_Scenario_4	

Table A2. Input and output files in the Lower Boulder model.

File Type	File Extension	Vistas Specific
Vistas project file	GWV	Yes
Basic	BAS	
Directory name file	MFN	
Discretization	DIS	
Evapotranspiration Package	EVT	
Name file	NAM	
NWT Solver Package	NWT	
Output Control	OC	
Recharge Package	RCH	
SFR Package	SFR	
Specified Head Package	CHD	
Upstream Weighting (flow property) Package	UPW	
Well Package	WEL	
Horizontal K array	_KX	
Vertical K array	_KZ	
Specific storage array	_S1	
Specific yield array	_S2	
Output Files		
Cell-by-Cell Flows (binary)	CBB	
Heads (binary)	HDS	
Drawdown (binary)	DDN	
List (summary output) file	LST	

APPENDIX B

GROUNDWATER BUDGET METHODOLOGY: UPLAND RECHARGE

Upland recharge (UR) occurs when the amount of precipitation exceeds runoff, evaporation, and plant consumption (Lerner and others, 1990; DeVries and Simmers, 2002; Ng and others, 2009). Upland recharge was evaluated for the parts of the study area that are not irrigated, as irrigation recharge (IR) accounted for diffuse recharge in irrigated areas. Three approaches were used to estimate evapotranspiration (ET) and upland recharge; they included water-balance methods and numerical modeling. Rather than rely on one method alone, using and comparing the results of multiple methods increases the level of certainty in the estimates (Healy, 2010).

Section B1: ET Estimation from Precipitation and Stream Flow Data

Total evapotranspiration for the study area was calculated using the water-balance approach (Ward and Trimble, 2004; Healy, 2010), which begins with the following water budget equation:

$$PCP + SW_{in} + GW_{in} = ET + SW_{out} + GW_{out} \pm \Delta S,$$

where:

PCP is total volume of precipitation received within the area of interest;

SW_{in} is surface water flowing in;

GW_{in} is groundwater flowing in;

ET is evapotranspiration;

SW_{out} is surface water flowing out;

GW_{out} is groundwater flowing out; and

ΔS is changes in storage.

It is then assumed that if a long-term average is used, the system is at steady state ($\Delta S = 0$). For this analysis, 30-yr normal precipitation and long-term average surface-water flows were used. The equation can be rearranged to solve for ET as:

$$ET = PCP + SW_{in} - SW_{out} + GW_{in} - GW_{out}.$$

Mean annual precipitation was calculated for the study area by using the 30-yr (1981–2010) normal 800-m PRISM precipitation dataset (Oregon State University, 2013; fig. 3). Evaluation of these data shows that annual average precipitation ranges from 11.4 in to 38.2 in, and the area receives 325,485 acre-ft/yr of precipitation on average (an area-weighted average of 16.2 in/yr).

As discussed in Bobst and others (2016), the long-term average surface-water flow for different stations was calculated based on extrapolation of the long-term record from the USGS station (Boulder River near Boulder; 06033000) and monitoring conducted during this study. The average surface-water inflow to the study area was calculated to be about 97,909 acre-ft/yr (GWIC 263601, 89,525 acre-ft/yr; GWIC 265347, 8,384 acre-ft/yr). Surface-water outflow was calculated to be about 80,049 acre-ft/yr (GWIC 263602) on average.

Groundwater underflow to and from the study area was estimated based on Darcy flux through the alluvium. For the Boulder River and Little Boulder River alluvium at the upstream end of the study area, the groundwater flux was estimated to be 148 acre-ft/yr. At Cardwell the Boulder River alluvium was estimated to discharge 150 acre-ft/yr from the study area.

Using the equation above, it was calculated that the mean annual ET flux in the study area is about 343,343 acre-ft/yr. The fact that total ET is greater than precipitation is not surprising given the extent to which surface water from outside the study area is used for irrigation.

Section B2: ET and UR Estimation from Precipitation and Vegetation Data

Although the water balance approach provides a reliable estimate of the total annual ET rate for the study area, it provides no information on how ET is spatially distributed. Distributed ET values were estimated in order to use them in conjunction with the precipitation distribution to estimate the magnitude and geographic distribution of groundwater recharge.

The distribution of ET was calculated by using the LANDFIRE vegetation dataset (30-m pixels, USGS, 2010). Three other datasets were also evaluated and contained vegetation classes similar to those of LANDFIRE (USGS, 2011a; USGS, 2011b; NRCS, 2006); the LANDFIRE dataset was selected due to its superior resolution and detailed vegetative descriptions. Over 40 vegetative classes were grouped into 11 plant types based on their altitude and geographic distribution in the study area (fig. 5, text). Literature values were used to estimate actual ET rates of the different plant types (Chauvin and others, 2011; Hackett, and others, 1960; Lautz, 2008; Persson, 1995; Rosenberry and Winter, 1997; Scott and others, 2004; Woodhouse, 2008; Leenhouts and others, 2006; Sanford and Selnick, 2012; Petersen and Hill, 1985; Johns, 1989). The ET values ranged from 12 in/yr (lowland grass and sagebrush) to 28 in/yr (riparian phreatophytes; table B1). This approach assumes that site-specific ET rates are similar to ET rates in similar settings; furthermore, because most literature values were based on 1- to 2-yr studies, this method assumes that short-term rates are representative of longer-term average rates.

The spatial distribution of plant types relative to precipitation was also used to constrain ET rates; that is, a plant type's average annual ET rate was limited to the average annual precipitation rate of the plant location (with the exception of irrigated crops and riparian phreatophytes, which consume other sources of water). Plant groupings generally fell within discrete elevation ranges, with higher-elevation groups exhibiting higher ET rates. This spatial pattern mirrored that of the precipitation distribution.

The vegetation-based ET estimates resulted in an area-wide ET rate of 326,002 acre-ft/yr. This value is 95% of the water balance approach, which was considered a good match given the uncertainties inherent in both approaches.

Geographically distributed upland recharge was estimated by subtracting the distributed ET values from precipitation. These values were averaged based on 1-in precipitation polygons (fig. B1), in which an average ET rate was calculated per polygon. The results were applied as upland recharge where they were positive. The highest groundwater recharge rates occurred at higher elevations such as Elkhorn Peak (maximum of 14.1 in/yr) and Bull Mountain (maximum of 4.5 in/yr). No upland recharge resulted on the pediment (grass and sagebrush), and strongly negative values were either irrigated or contained phreatophytic vegetation. Phreatophyte ET rates were expected to exceed precipitation, as their consumptive use is partly derived from shallow groundwater (Groundwater Budget section). This approach assumes that all precipitation in excess of ET has the potential to become groundwater recharge. In reality not all of the excess water will infiltrate through the root zone. For instance, in flood-irrigated settings the NRCS often assumes that about half of the excess water infiltrates (DP_{ex} = 0.5; appendix C).

Table B1. Evapotranspiration values for different vegetation types.

Vegetation Group	Acres	Evapotranspiration Rate (ft/yr)	Acre-ft/yr
Upland Sagebrush	64,734	1.1	70,124
Douglas Fir	49,790	1.4	68,457
Shrub/Grass Lowlands	40,393	1.0	40,391
Mixed Evergreen	27,186	1.8	49,839
High Xeric Grass	20,988	1.2	24,484
Agricultural	15,161	2.1	31,078
Mesic Meadow	12,926	1.7	21,543
Whitebark Pine	4,179	2.2	9,054
Alpine Rangeland/Deciduous Shrubs	2,818	2.0	5,635
Developed	1,971	1.0	1,971
Riparian	1,468	2.3	3,426
Total	**241,616**		**326,002**

Section B3: Refining UR Estimates through Numerical Modeling

Numerical modeling helped to further refine UR estimates in the study area. The results of the vegetative approach noted above were input as the preliminary UR rates in the steady-state model. Through the calibration process these preliminary values were lowered, most notably at higher elevations. The initial rates yielded flooding and a poor fit with observations, even when hydraulic conductivity values approached the maximum limit of their reasonable range. UR values were consequently lowered in order to lower heads and reduce flooding in the mountain block area. The lowering of the initial rates was deemed valid because the approach used to derive them (section B2) did not account for losses other than ET; losses due to other factors (e.g., runoff, snow sublimation, soil moisture retention) could be substantial in high-altitude areas with steep gradients, low-permeability bedrock, and deep water tables. The total volume of UR lowered to approximately 42% of the upper bound estimate (i.e., $DP_{ex} = 0.42$). UR was 6.1% of mean annual precipitation within the area of applied recharge, while the upper bound estimate was 11%. The range of UR values also narrowed through the calibration process. Upper bound values ranged from 0.3% to 37% of mean annual precipitation (0.1–14.1 in/yr), while the revised rates ranged from 1.7% to 12% (0.25–3.0 in/yr).

Furthermore, UR was spatially redistributed during model calibration. In particular, rates were increased along the mountain front and decreased in steep, high-altitude and low-permeability areas of the mountain block (fig. B1). While the primarily goal was to fit computed and observed heads, these changes were also made to qualitatively account for influential factors such as slope and permeability. The recharge redistribution is supported by previous studies on upland recharge, which highlight the effects of such factors on infiltration rates (section B4). The final upland recharge values used in the model varied from 0.25 to 2.93 in/yr (fig. B1 and table B2).

Upland streams were also simulated in the model to represent focused recharge in streams and stream sediments. Stream cells functioned to gain flow in their upper reaches within the mountain block area, and recharge the aquifer in their lower reaches within the mountain front zone near or on the pediment (fig. B2; table B3). Steady-state model results showed that approximately 24% of the applied UR took the form of focused recharge, which is comparable to previous work (Flint and Flint, 2007).

Section B4: Spatial Distribution of Upland Recharge

Precipitation within the mountainous regions is the dominant source of recharge to the basin-fill aquifer, which is common among semi-arid intermontane valleys of the western U.S. (Healy, 2010). Some of the precipitation-derived recharge flows into the basin-fill via bedrock flow paths, and is referred to as mountain-block recharge. Another portion of the recharge becomes streamflow and results in focused recharge at the mountain front where the streambed transitions from bedrock to alluvial fan materials (Wilson and Guan, 2004). The focused stream leakage and diffuse infiltration that ultimately recharge the basin-fill aquifer are collectively referred to here as mountain front recharge (MFR). The mountain front is the transition zone in an alpine watershed marked by changes in slope, vegetation, soil type, and/or the presence of faults (Wilson and Guan, 2004). In developing the Lower Boulder conceptual groundwater budget, focused and diffuse recharge were not individually estimated (and are herein referred to as “upland recharge”) because most upland streams in the study area quickly infiltrate upon reaching the unconsolidated basin-fill deposits, which were the primary focus of the study; as noted above, however, a rough estimate of the focused-to-diffuse recharge ratio was obtained through numerical modeling.

Quantifying MFR is difficult due to a limited understanding of subsurface flow mechanisms as well as local variability in slope, aspect, vegetation, fracture and fault distributions, climate, and vadose-zone thickness. To help improve study-area estimates, results were compared with previous work in similar settings to ensure that they were reasonable. Previous studies (Huntley, 1979; Maurer and others, 1997; Flint and others, 2002; Bossong and others, 2003; Manning and Solomon, 2004; Flint and Flint, 2007; Magruder and others, 2009)

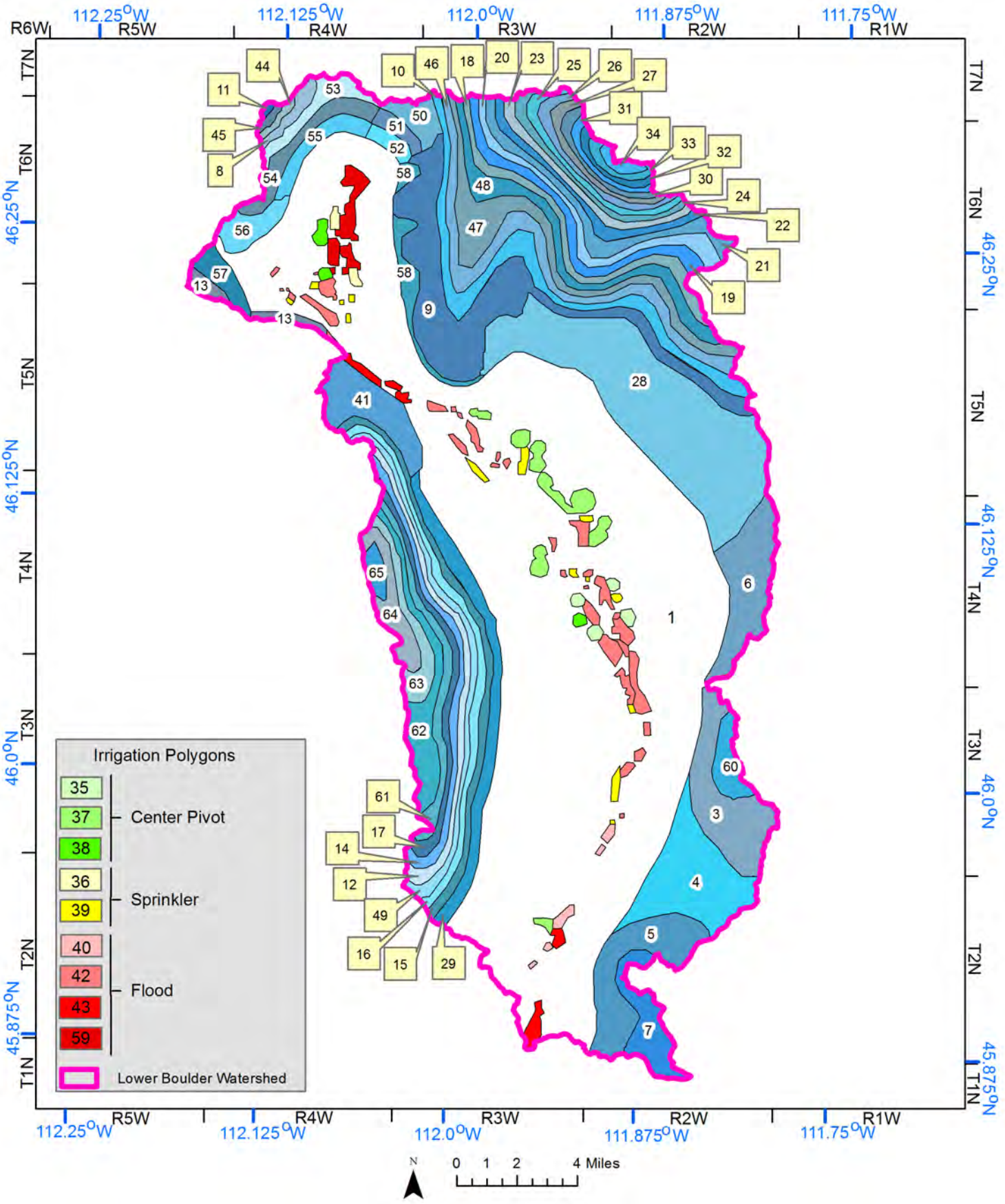

Figure B1. The recharge applied to the Area-Wide model includes upland recharge in the mountain block, mountain front recharge along the boundary between the bedrock and unconsolidated valley fill deposits, and irrigation recharge. See table B2 for additional details.

Table B2. Boulder Valley Area-Wide Model Recharge Values by Zone (page 1 of 2)

Zone	Zone Description	Precip (in/yr)	Recharge (ft/d)	Recharge (ft/yr)	Area (acres)	Recharge (acre-ft/yr)
1	No recharge - non-irrigated valley bottom	10-14	0.0000000	0	336,815	0
2	NONE (unused)	---	0	0	0	0
3	Diffuse Recharge - South Elkhorns	14-15	0.0000562	0.02	4,852	100
4	Diffuse Recharge Boulder Cutoff Pass	13-14	0.0000626	0.02	6,332	145
5	Diffuse Recharge Doherty Mountain	14-15	0.0000960	0.04	4,657	163
6	Diffuse Recharge South Elkhorns	14-15	0.0001239	0.05	4,375	198
7	Diffuse Recharge Doherty Mountain	15-16	0.0001277	0.05	2,545	119
8	Diffuse Recharge NW of Muskrat Valley	17-18	0.0002112	0.08	646	50
9	Diffuse Recharge/Mountain Front Recharge Elkhorn Mountains	13-19	0.0002112	0.08	10,637	821
10	Diffuse Recharge Elkhorn Mountains	19-20	0.0002226	0.08	4,364	355
11	Diffuse Recharge NW of Muskrat Valley	20-21	0.0002295	0.08	92	8
12	Diffuse Recharge - Bull Mountain	20-21	0.0002455	0.09	2,108	189
13	Diffuse Recharge S & SW of Muskrat Valley	15-16	0.0002112	0.08	977	75
14	Diffuse Recharge - Bull Mountain	21-22	0.0002556	0.09	2,171	203
15	Diffuse Recharge - Bull Mountain	17-18	0.0002226	0.08	2,869	233
16	Diffuse Recharge - Bull Mountain	18-19	0.0002340	0.09	2,556	218
17	Diffuse Recharge - Bull Mountain	22-23	0.0002568	0.09	1,855	174
18	Diffuse Recharge - Elkhorn Mountains	23-24	0.0002683	0.10	2,288	224
19	Diffuse Recharge - Elkhorn Mountains	24-25	0.0002797	0.10	2,336	239
20	Diffuse Recharge - Elkhorn Mountains	25-26	0.0002911	0.11	2,105	224
21	Diffuse Recharge - Elkhorn Mountains	26-27	0.0003025	0.11	2,413	267
22	Diffuse Recharge - Elkhorn Mountains	27-28	0.0003139	0.11	1,491	171
23	Diffuse Recharge - Elkhorn Mountains	28-29	0.0003253	0.12	1,219	145
24	Diffuse Recharge - Elkhorn Mountains	29-30	0.0003368	0.12	1,102	136
25	Diffuse Recharge - Elkhorn Mountains	30-31	0.0003482	0.13	1,062	135
26	Diffuse Recharge - Elkhorn Mountains	31-32	0.0003596	0.13	1,021	134
27	Diffuse Recharge - Elkhorn Mountains	32-33	0.0003710	0.14	878	119
28	Diffuse Recharge/Mountain Front Recharge Elkhorn Mountains	14-19	0.0004277	0.16	17,473	2,730
29	Diffuse Recharge - Bull Mountain	15-17	0.0004277	0.16	3,871	605
30	Diffuse Recharge - Elkhorn Mountains	33-34	0.0004562	0.17	676	113
31	Diffuse Recharge - Elkhorn Mountains	36-37	0.0006527	0.24	503	120
32	Diffuse Recharge - Elkhorn Mountains	35-36	0.0005168	0.19	500	94
33	Diffuse Recharge - Elkhorn Mountains	34-35	0.0004832	0.18	525	93
34	Diffuse Recharge - Elkhorn Mountains	37-38	0.0006695	0.24	419	102
35	Center pivot irrigation - central valley	---	0.0007297	0.27	1,660	442
36	Muskrat Valley Sprinkler Irrigation	---	0.0020745	0.76	253	192

Table B2. Boulder Valley Area-Wide Model Recharge Values by Zone (page 2 of 2)

Zone	Zone Description	Precip (in/yr)	Recharge (ft/d)	Recharge (ft/yr)	Area (acres)	Recharge (acre-ft/yr)
37	Center pivot irrigation - central valley	---	0.0009157	0.33	426	143
38	Center Pivot Irrigation - Muskrat Valley	---	0.0009843	0.36	826	297
39	Sprinkler Irrigation along Boulder River	---	0.0015378	0.56	918	516
40	Flood Irrigation along Boulder River	---	0.0019299	0.70	338	238
41	Diffuse Recharge North end of Bull Mountain	15-17	0.0002226	0.08	3,603	293
42	Flood Irrigation along Boulder River	---	0.0024922	0.91	3,331	3,033
43	Flood Irrigation along Boulder River	---	0.0031322	1.14	441	504
44	Diffuse Recharge NW of Muskrat Valley	18-19	0.0002112	0.08	268	21
45	Diffuse Recharge NW of Muskrat Valley	19-20	0.0002226	0.08	187	15
46	Diffuse Recharge - Elkhorn Mountains	20-21	0.0002340	0.09	4,268	365
47	Diffuse Recharge - Elkhorn Mountains	21-22	0.0002454	0.09	4,606	413
48	Diffuse Recharge - Elkhorn Mountains	22-23	0.0002568	0.09	3,126	293
49	Diffuse Recharge - Bull Mountain	19-20	0.0002454	0.09	2,314	207
50	Diffuse Recharge NE of Muskrat Valley	16-17	0.0002226	0.08	1,179	96
51	Diffuse Recharge NE of Muskrat Valley	15-16	0.0002112	0.08	591	46
52	Diffuse Recharge NE of Muskrat Valley	14-15	0.0003195	0.12	573	67
53	Diffuse Recharge NW of Muskrat Valley	16-17	0.0002112	0.08	1,491	115
54	Diffuse Recharge NW of Muskrat Valley	15-16	0.0002112	0.08	1,921	148
55	Diffuse Recharge NW of Muskrat Valley	14-15	0.0003195	0.12	1,282	150
56	Diffuse Recharge SW of Muskrat Valley	14-15	0.0004277	0.16	1,399	219
57	Diffuse Recharge SW of Muskrat Valley	14-15	0.0003195	0.12	1,157	135
58	Mountain Front Recharge E of Muskrat Valley	---	0.0004277	0.16	1,561	244
59	Flood Irrigation - Muskrat Valley	---	0.0033679	1.23	1,245	1,532
60	Diffuse Recharge South Elkhorns	15-16	0.0001239	0.05	1,308	59
61	Diffuse Recharge - Bull Mountain	23-24	0.0002911	0.11	1,972	210
62	Diffuse Recharge - Bull Mountain	24-25	0.0003139	0.11	3,074	352
63	Diffuse Recharge - Bull Mountain	25-26	0.0003368	0.12	1,686	207
64	Diffuse Recharge - Bull Mountain	26-27	0.0003596	0.13	2,017	265
65	Diffuse Recharge - Bull Mountain	27-28	0.0003710	0.14	595	81

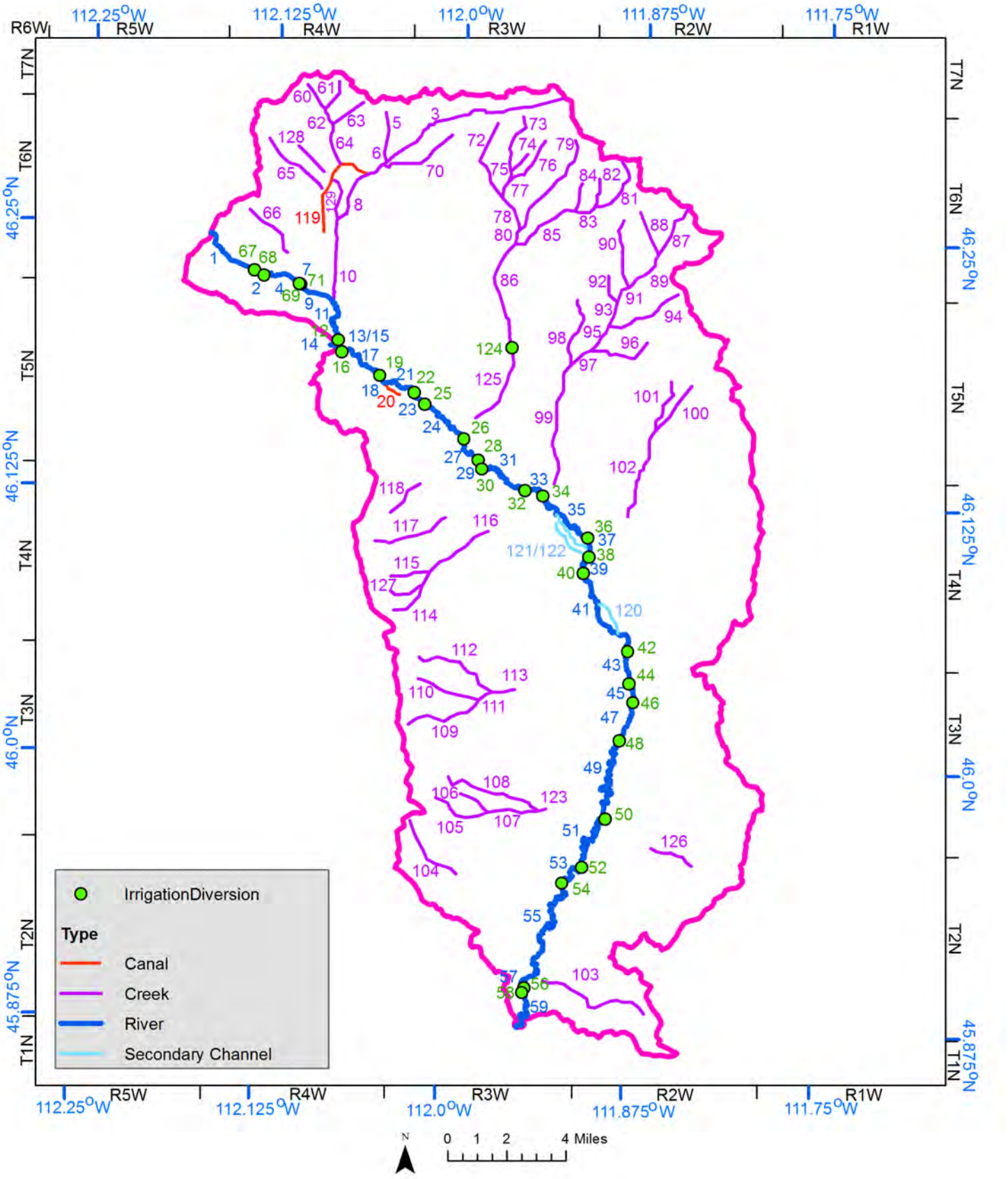

Figure B2. Stream segments were used to represent the Boulder River, Muskrat Creek, the Little Boulder River, secondary channels which periodically gain water, irrigation diversions, some irrigation canals (where they may be gaining), and upland creeks. The upland creek segments typically gained water in their upper reaches within the mountain block area, and recharged the basin-fill aquifer in their lower reaches within the mountain front zone near or on the pediment. See table B3 for additional details.

Table B3. Descriptions of Stream segments for the Boulder Valley Area-Wide Model (page 1 of 3)

Segment	Description	Upstream End		Number of Reaches (cells)
		Row	Column	
1	Boulder River - Upstream boundary to Butler Canal	82	27	36
2	Boulder River - Butler Canal to Phelan Canal	99	46	8
3	Muskrat Creek - Headwaters to Wood Creek	22	182	108
4	Boulder River - Phelan Canal to State Canal	100	53	17
5	Wood Creek	28	104	26
6	Muskrat Creek - Wood Creek to Rawhide Creek	50	104	2
7	Boulder River - State Canal to Slope Canal	104	66	1
8	Muskrat Creek - Rawhide Creek to Muskrat Road	51	103	79
9	Boulder River - Slope Canal to Muskrat Creek	105	66	20
10	Muskrat Creek - Muskrat Road to Mouth	104	81	8
11	Boulder River - Muskrat Creek to Franchi Canal	111	80	27
12	Irrigation Diversion - Franchi Canal	129	83	1
13	Boulder River - Franchi Canal to Little Boulder River	130	82	4
14	Little Boulder River	132	82	2
15	Boulder River - Little Boulder to Killiam (Franchi) Canal	133	83	3
16	Irrigation Diversion - Killiam (Franchi) Canal	135	84	1
17	Boulder River - Killiam (Franchi) Canal to McCauley Canal	134	85	28
18	Boulder River - McCauley Canal to Murphy Canal	145	100	1
19	Irrigation Diversion - McCauley Canal	144	101	1
20	Irrigation Diversion - Murphy Canal	146	100	19
21	Boulder River - Murphy Canal to Smith Canal	145	101	27
22	Irrigation Diversion - Smith Canal	154	117	1
23	Boulder River - Smith Canal to Clark Canal	155	116	11
24	Boulder River - Clark Canal to Quinn Canal	159	123	35
25	Irrigation Diversion - Clark Canal	160	122	1
26	Irrigation Diversion - Quinn Canal	175	140	1
27	Boulder River - Quinn Canal to Howard Canal	176	139	14
28	Irrigation Diversion - Howard Canal	183	146	1
29	Boulder River - Howard Canal to Carey Canal	184	145	17
30	Irrigation Diversion - Carey Canal	191	155	1
31	Boulder River - Carey Canal to Quantance Canal	190	156	15
32	Irrigation Diversion - Quantance Canal	197	164	1
33	Boulder River - Quantance Canal to Wickham Canal	196	165	13
34	Irrigation Diversion - Wickham Canal	199	175	1
35	Boulder River - Wickham Canal to Twohy Canal #1	200	174	39
36	Irrigation Diversion - Twohy Canal #1	218	195	1
37	Boulder River - Twohy Canal #1 to Twohy Canal #2	219	194	15
38	Irrigation Diversion - Twohy Canal #2	230	194	1
39	Boulder River - Twohy Canal #2 to Carey-Twohy Canal	230	192	3
40	Irrigation Diversion - Carey-Twohy Canal	232	191	1
41	Boulder River - Carey-Twohy Canal to Carey East Side Canal	232	193	64
42	Irrigation Diversion - Carey East Side Canal	269	212	1
43	Boulder River - Carey East Side Canal to Dawson Canal #1	270	211	17
44	Irrigation Diversion - Dawson Canal #1	286	212	1
45	Boulder River - Dawson Canal #1 to Dawson Canal #2	285	213	12
46	Irrigation Diversion - Dawson Canal #2	293	215	1
47	Boulder River - Dawson Canal #2 to Sheehy Canal	293	213	26

Table B3. Descriptions of Stream segments for the Boulder Valley Area-Wide Model (page 2 of 3)

Segment	Description	Upstream End		Number of Reaches
		Row	Column	(cells)
48	Irrigation Diversion - Sheehy Canal	309	207	1
49	Boulder River - Sheehy Canal to Mooney Canal	309	209	53
50	Irrigation Diversion - Mooney Canal	339	200	1
51	Boulder River - Mooney Canal to Carey-Dawson Canal	340	201	44
52	Irrigation Diversion Carey-Dawson Canal	365	192	1
53	Boulder River - Carey-Dawson Canal to Downs Canal	366	191	23
54	Irrigation Diversion - Downs Canal	373	181	1
55	Boulder River - Downs Canal to Cardwell Canal #1	373	183	88
56	Irrigation Diversion - Cardwell Canal #1	420	166	1
57	Boulder River - Cardwell Canal #1 to Cardwell Canal #2	421	165	2
58	Irrigation Diversion - Cardwell Canal #2	423	165	1
59	Boulder River - Cardwell Canal #2 to Mouth	422	166	22
60	Upper Spencer Creek	15	69	19
61	unnamed tributary of Spencer Creek (N)	14	82	21
62	Middle Spencer Creek	26	77	10
63	unnamed tributary of Spencer Creek (S)	23	93	23
64	Lower Spencer Creek	33	80	23
65	Amazon Creek above Reider Canal	39	52	46
66	unnamed tributary northwest of Boulder	71	43	37
67	Irrigation Diversion - Butler Canal	98	47	1
68	Irrigation Diversion - Phelan Canal	101	52	1
69	Irrigation Diversion - Evens Canal	105	65	1
70	Rawhide Creek	38	133	47
71	Irrigation Diversion - Slope Canal	104	67	1
72	Upper Turnley Creek	33	154	51
73	Upper Sourdough Creek	30	165	35
74	unnamed tributary of Sourdough Creek	47	167	14
75	Middle Sourdough Creek	54	160	7
76	Greyback Gulch	41	175	35
77	Lower Sourdough Creek	59	158	9
78	Lower Turnley Creek	66	156	21
79	Upper Elkhorn Creek	41	188	66
80	Middle Elkhorn Creek	80	163	9
81	Upper Queen Gulch	50	208	42
82	DuBois Gulch	58	199	15
83	Middle Queen Gulch	71	197	12
84	Hobo Gulch	60	191	15
85	Lower Queen Gulch	72	188	42
86	Lower Elkhorn Creek - Queen Gulch to Dulaney Canal	87	161	64
87	Upper East Fork Dry Creek	72	238	31
88	Turman Creek	73	217	27
89	Lower East Fork Dry Creek	91	226	29
90	West Fork Dry Creek	77	210	37
91	Dry Creek - West Fork Dry Creek to Stull Gulch	106	212	11
92	Stull Gulch	102	203	14
93	Dry Creek - Stull Gulch to Hunting Gulch	112	207	14
94	Hunting Gulch	110	234	47

Table B3. Descriptions of Stream segments for the Boulder Valley Area-Wide Model (page 3 of 3)

Segment	Description	Upstream End		Number of Reaches
		Row	Column	(cells)
95	Dry Creek - Hunting Gulch to unnamed eastern tributary	123	204	19
96	unnamed eastern tributary of Dry Creek	131	220	39
97	Dry Creek - unnamed eastern tributary to Horse Gulch	134	196	17
98	Horse Gulch	112	189	42
99	Dry Creek - Horse Gulch to Mouth	141	186	67
100	Upper Cabin Gulch	149	231	30
101	unnamed tributary of Cabin Gulch	151	240	35
102	Lower Cabin Gulch	170	224	53
103	Cottonwood Canyon	431	219	67
104	Conrow Creek	344	114	46
105	Upper South Fork Cottonwood Creek	334	127	33
106	unnamed tributary of South Fork Cottonwood Creek	333	136	23
107	Lower South Fork Cottonwood Creek	341	149	29
108	North Fork Cottonwood Creek	325	132	58
109	South Dunn Canyon	301	114	48
110	Upper Dunn Canyon	281	119	37
111	Middle Dunn Canyon	290	145	9
112	North Fork Dunn Canyon	271	119	52
113	Lower Dunn Canyon	287	151	12
114	South Fork Quinn Creek	250	108	32
115	North Fork Quinn Creek	235	106	19
116	Lower Quinn Creek	233	123	45
117	Jack Creek	219	99	46
118	Clarke Gulch	206	106	26
119	Irrigation Diversion - Reider Canal	53	99	66
120	Boulder River - secondary channel above Dunn Creek	248	200	19
121	Boulder River - secondary channel below Quinn Creek	208	180	31
122	Boulder River - secondary channel below Quinn Creek	212	180	27
123	Cottonwood Creek	340	171	2
124	Irrigation Diversion - Dulaney Canal	133	161	1
125	Lower Elkhorn Creek - Dulaney Canal to Mouth	134	160	49
126	Negro Hollow	365	240	28
127	Middle Fork Quinn Creek	241	106	20
128	unnamed tributary west of Muskrat Creek	42	65	24
129	Spencer Creek below Reider Canal	57	80	26

have yielded MFR estimates ranging from 1% to 19% of mean annual precipitation in variably-fractured crystalline and carbonate bedrock within the western U.S. MFR within this study area ranged from 1.7% to 12% of mean annual precipitation and was 6.1% on average; thus, results were within the range of previous estimates. Results were also comparable to those of the Managed Recharge Model that was created for this study, in which 6.5% of the mean annual precipitation was applied as MFR (Carlson, 2013).

Section B5: Temporal Distribution of Upland Recharge

B5.1 Intra-Annual Variation

In addition to estimating upland recharge on an annual basis, it was also estimated seasonally to more independently estimate aquifer storage properties (Transient Calibration section). Groundwater-level hydrographs were qualitatively evaluated as a first step to estimating the seasonal distribution. Many water-table fluctuation methods quantitatively analyze hydrographs to estimate recharge; however, most require prior knowledge of specific yield (Healy, 2010, Delin and others, 2007). These methods were not used because estimating specific yield was a main objective. The qualitative hydrograph analysis revealed common seasonal patterns among upland sites, namely a sharp spring peak followed by a decrease from summer through fall, with small peaks periodically occurring outside of the spring. Because precipitation is the primary source of recharge in the study's upland bedrock areas, monthly 30-yr normal PRISM precipitation data were also evaluated and each month's contribution to the total annual precipitation was calculated. Recharge estimates were made on a monthly time scale to match the PRISM data availability and the temporal discretization of the numerical model.

To help estimate the timing of spring recharge, snowpack data were evaluated from the Tizer Basin SNOTEL site (elevation 6,880 ft asl), which is 4.4 mi northeast of Elkhorn Peak and is the closest SNOTEL site to the study area (NRCS, 2014). The snowmelt period in both years of the study ranged from mid-April to early May. Comparing this timing to that of rising water levels in upland wells shows that groundwater recharge timing is variable for a given year; for instance, snowmelt occurred in mid- to late April of 2012, and the timing of maximum groundwater levels ranged from mid-May to early August. These data illustrate a major challenge in estimating recharge distribution in upland portions of alpine watersheds; namely, that neither the timing nor quantity of recharge can be clearly determined from a single SNOTEL station at this study's spatial scale.

A literature review revealed little research on quantifying seasonal precipitation-derived groundwater recharge in alpine watersheds, where the snowpack persists through much of winter. Notable studies included two that used the USGS Precipitation-Runoff Modeling System (PRMS) to simulate watershed dynamics and estimate groundwater recharge, among other hydrologic water-budget components. Bossong and others (2003) ran PRMS simulations of the Turkey Creek Watershed, which was classified into four subsurface reservoirs capable of receiving recharge. Study period (1999–2001) results showed that each reservoir received the vast majority of its annual allotment during spring months (March–May), with much smaller peaks occurring through the rest of the year (fig. B3).

Vaccaro and Olsen (2007) used PRMS to estimate monthly groundwater recharge in the Yakima River Basin over a 42-yr period (1960–2001). For the purposes of this investigation, 10 of the study's simulated water years were evaluated in the undeveloped, higher-elevation (approximately 5500–7500 ft asl) recharge zones, where precipitation was the primary recharge source. Results were similar those of Bossong and others in the predominant spring recharge values and the smaller periodic peaks throughout the rest of the year. Relatively little or no recharge occurred in mid- to late summer, when ET often exceeded precipitation (fig. B4).

Based on the above findings as well as other work (Delin and others, 2007; Carling and others, 2012), the vast majority (approximately 60–75%) of recharge in the lower Boulder conceptual model was applied in the spring. Fall and winter rates were lowest to account for infrequent infiltration in the mountain block, as indicated by the Tizer Basin SNOTEL data.

Summer rates were set higher than the near-zero rates of the two PRMS studies in order to account for the slow, steady infiltration that appears to occur in some upland portions of the study area, as shown in water-level hydrographs (appendix F). The inability to account for this slow infiltration has been noted as

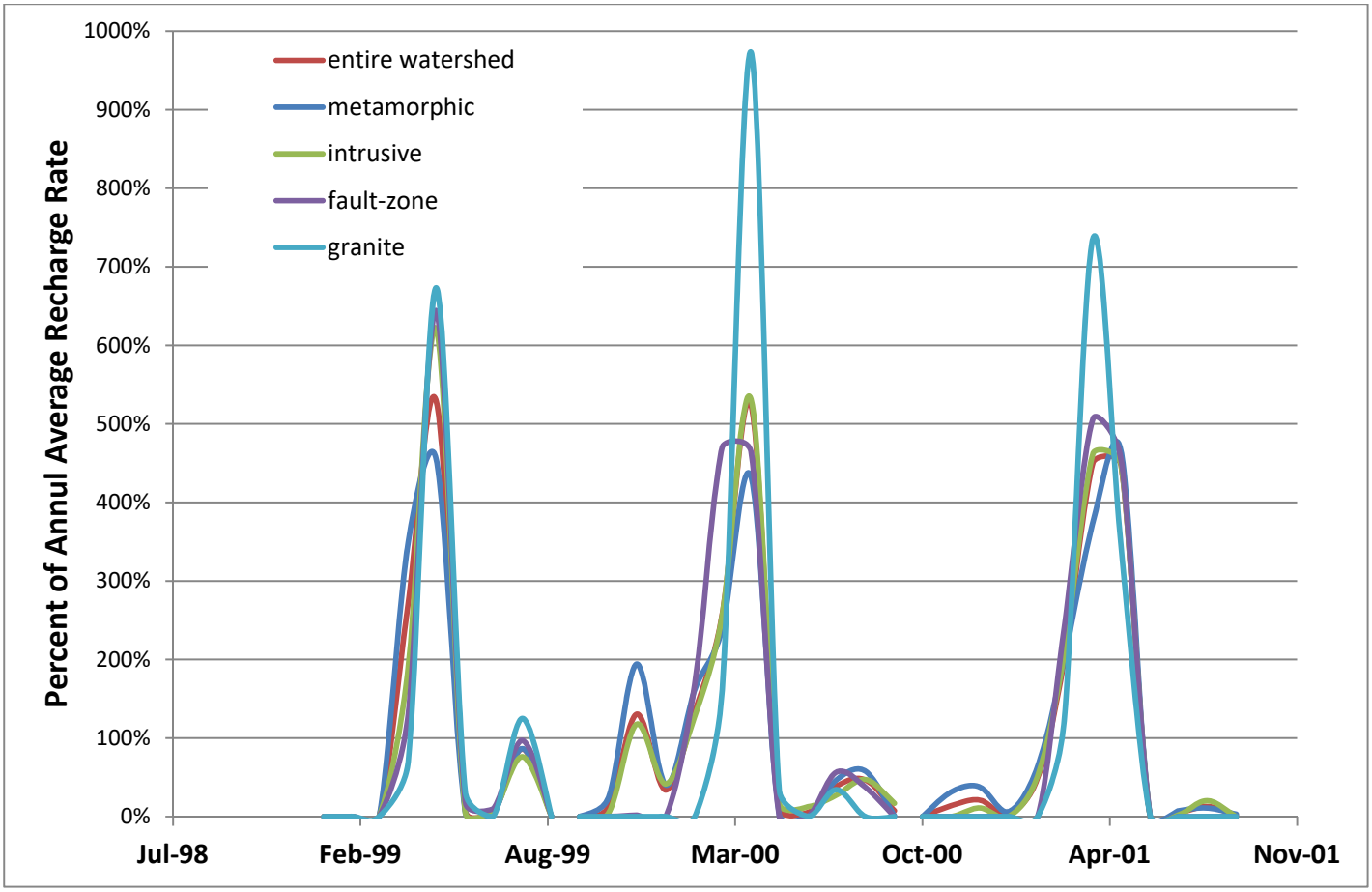

Figure B3. Water available for groundwater recharge per month from 1999 to 2001 as a percent of the average annual rate (modified from Bossong and others, 2003).

a limitation of many recharge-estimation approaches (Delin and others, 2007). Furthermore, despite ET being at its peak in summer, recharge can occur given the right combination of soil moisture and precipitation conditions.

B5.2 Inter-Annual Variation

Precipitation during the study period varied from well above the 30-yr normal (2011) to well below it (2013), as reflected in groundwater levels strongly influenced by upland recharge (fig. 22 in text, appendix F). This relatively extreme inter-annual variability was useful, because aquifer storage properties can be better estimated with data that show responses to extreme stresses.

As in previous studies, deviations in precipitation were used as a metric for deviations in UR over the study period (Thiros and others, 1996; Carling and others, 2012). Similar to the seasonal-variation approach (section B5.1), monthly PRISM datasets were evaluated; however, for the purpose of estimating inter-annual deviations, study period data were used rather than the 30-yr normal monthly data. Each raster image was clipped to the study area, and its mean value was calculated as a percent deviation from the 30-yr normal value for the given month (table B4). PRISM data were used because they proved more representative of study-wide conditions when compared with data from individual weather stations.

Rather than directly correlating monthly PCP deviations to monthly recharge values, the monthly PCP deviations were averaged over seasonal periods. Three seasonal periods were defined based on hydrograph trends: a winter period that included November through March; a spring period that included April through June; and a summer/fall period that included July through October. Each seasonal average was volumetrically weighted based on the period's 30-yr normal precipitation values relative to the mean annual precipitation; for instance, the spring months were 164% of the mean monthly precipitation rate, on average, so a factor of 1.64 was applied to recharge estimates in the spring period. Winter months were not

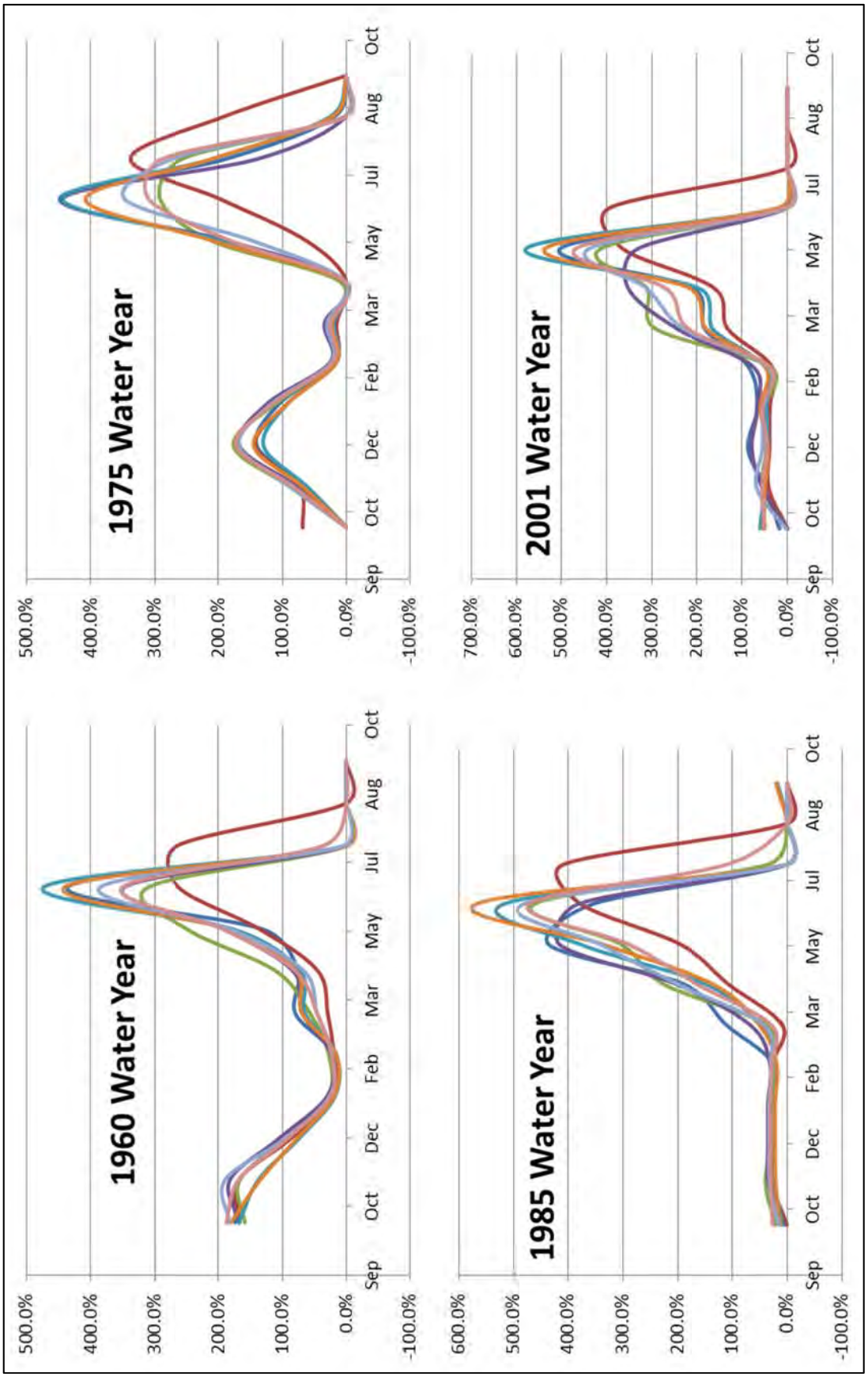

Figure B4. Monthly groundwater recharge results as a percentage of the annual average rate for the given water year (modified from Vaccaro and Olsen, 2007).

adjusted because it was assumed that deviations in winter precipitation affected spring recharge; thus, the winter period deviation was added to the spring period deviation, and the sum was applied evenly over the spring period. Finally, these seasonal deviation values were added to the normal year seasonal percentages described above (section B5.1). The results became the monthly recharge percentages throughout the study period. These monthly percentages were multiplied by the annual average recharge rate to obtain monthly recharge rates; the percentages were similarly applied as recharge multipliers in the transient model (Transient Calibration section). Table B4 provides the 2011 calculations and results as an example of this two-part approach, and table 8 (text) lists the monthly recharge multipliers.

Section B6: Limitations

Each of the approaches used in estimating upland recharge includes limitations. The monthly time discretization is one example, as previous work has shown large discrepancies between recharge estimates when switching from a daily or hourly time scale to a monthly time scale (Healy, 2010; Delin and others, 2007). Another major limitation is that site-specific factors such as soil moisture, weather conditions, and depth-to-water were not accounted for in a quantitative manner. Lastly, a lack of simulation of land-surface and vadose-zone processes adds further uncertainty to the estimates.

Table B4. 2011 Lower Boulder monthly recharge calculations to account for seasonal variation and deviation from the 30-year normal values.

A	B	C	D	E	F	G	H	I	J	K	L	M	N	O	P
Month	2011 Avg PCP (100 x mm)	2011 Avg PCP (in)	1981-2010 Monthly Normal (in)	Normal monthly PCP as % of annual	Normal seasonal Avg	2011 as a % of 30-yr normal	Days/ month	Days/ month as % of year	UR as % of 30-yr normal annual value	Monthly UR as % of year	2011 % deviation from 30-yr normals	Volume-weighted deviation	Time lag adjusted % above or below normal	2011 monthly UR % = seasonal % + deviation from normal	Resulting UR Multiplier
November	3006	1.18	0.92	68%		129%	30	8.2%	50%	4%			0%	50%	**0.50**
December	2146	0.84	0.75	56%		113%	31	8.5%	40%	3%			0%	40%	**0.40**
January	1554	0.61	0.68	50%	60%	90%	31	8.5%	30%	3%	108%	5%	0%	30%	**0.30**
February	1861	0.73	0.65	48%		113%	28	7.7%	20%	2%			0%	20%	**0.20**
March	2518	0.99	1.07	80%		92%	31	8.5%	20%	2%			0%	20%	**0.20**
April	5641	2.22	1.53	113%		146%	30	8.2%	200%	16%			71%	271%	**2.71**
May	8735	3.44	2.50	186%	164%	138%	31	8.5%	300%	25%	139%	64%	71%	371%	**3.71**
June	8744	3.44	2.58	192%		133%	30	8.2%	200%	16%			71%	271%	**2.71**
July	2071	0.82	1.60	119%		51%	31	8.5%	100%	8%			-41%	59%	**0.59**
August	2009	0.79	1.42	106%	102%	56%	31	8.5%	90%	8%	59%	-41%	-41%	49%	**0.49**
September	791	0.31	1.33	99%		23%	30	8.2%	80%	7%			-41%	39%	**0.39**
October	3047	1.20	1.12	83%		107%	31	8.5%	70%	6%			-41%	29%	**0.29**

See column descriptions below.

A–Month of the Year: November 2010 to October 2011

B–2011 Average PCP (100 x mm): Average precipitation over the study area, as reported by PRISM. Units are 1/100th of a mm (or 1/100,000th of a m). The PRISM data were clipped to the study area, converted to a total volume, and divided by the total area.

C–2011 Average PCP (in): Column B multiplied by (1/(100*25.4 mm/in)) = 0.000394

D–1981–2010 Monthly Normal (in): PRISM reported Monthly Normal precipitation for the study area based on the record from 1981 to 2010. The PRISM data were clipped to the study area, converted to a total volume, and divided by the total area.

E–Monthly PCP as % of annual: Values in Column D divided by Annual Normal precipitation from PRISM divided by 12. The Annual Normal is the sum of the Monthly Normal values in Column D, which is 16.15 in. The Annual Normal divided by 12 is 1.34 in.

F–Seasonal Average: The sum of the grouped months, divided by the Annual Normal divided by 12 and multiplied by the number of months.

G–2011 as a % of 30-yr normal: Column C divided by Column D.

H–Days per month: The number of days in each of the months.

I–Days/ month as % of year: Column H divided by 365 days.

J–UR as % of 30-yr normal annual value: Upland recharge as a percentage of the total that would occur in a Normal year. Values based on previous studies in snow dominated systems (Bossong and others, 2003; Vaccaro and Olsen, 2007; Delin and others, 2007; Carling and others, 2012) and professional judgement.

K–Monthly UR as % of year: Column I times Column J.

L–2011 % deviation from 30-yr normal: Average of the grouped months (Column G).

M–Volume-weighted deviation: 2011 deviation from the 30-yr seasonal normal, weighted by each season's volume relative to the annual average–(Column L minus 1) times Column F

N–Time lag adjusted % above or below normal: Adjusts the timing of seasonal precipitation deviations (Column M) to account for upland recharge lag times. The November–March seasonal deviation was assumed negligible in real time and was applied to the April–June period in conjunction with the April–June real-time deviation. Effects of July–October precipitation deviations were assumed to be real-time.

O–2011 monthly UR % = seasonal % + deviation from normal: Column J plus Column N.

P–Resulting UR Multiplier: Conversion of Column O to a decimal.

APPENDIX C

GROUNDWATER BUDGET METHODOLOGY: IRRIGATION RECHARGE

This appendix details the methods used to estimate groundwater recharge derived from irrigating parcels in excess of crop needs. The approach was based on NRCS Irrigation Water Requirements program (IWR) output (NRCS, 2012a), previous MBMG methodology (Bobst and others, 2013; Waren and others, 2012), techniques employed by the Idaho Department of Water Resources (IDWR, 2013), interviews with local NRCS staff, and water-level and flow observations in the study area.

Section C1: Preliminary IWR Approach

The IWR program computes monthly crop ET rates. A monthly net irrigation water requirement (NIR) is also calculated, which is equal to the ET rate minus the effective precipitation received by the crop and any carryover moisture at the beginning and end of each season (Dalton, 2003). The Blaney–Criddle (Soil Conservation Service Technical Release 21) method is commonly used by the NRCS in western Montana (L. Ovitt and R. Pierce, oral and written commun., 2012) and was used in IWR calculations for this study.

The following equation was used to calculate irrigation recharge (IR):

$$IR = [(NIR/IME + P_{eff} - ET) \times DP_{ex}], \qquad \text{Equation C1}$$

where:

NIR is net irrigation water requirement (an IWR output), in/month;

IME is irrigation method application efficiency, in/month;

P_{eff} is effective precipitation (an IWR output), in/month;

ET is evapotranspiration (an IWR output), in/month; and

DP_{ex} is portion of applied water in excess of ET that results in deep percolation (i.e., groundwater recharge) rather than runoff, unitless.

IR was calculated for each of the three irrigation methods used in the study area (pivot, flood, and sprinkler) and each crop type (alfalfa and pasture grass/grass hay). IR was then multiplied by the total acreage per irrigation method based on land-use data (Montana Department of Revenue, 2012), and these were summed to obtain a volumetric irrigation recharge estimate for the study area. That study-area value served as the IR best estimate in the conceptual groundwater budget analysis (table 7, text). In the numerical model, IR rates were spatially distributed according to the irrigation method per parcel. Monthly IR values are provided in table C1. Note that the (NIR/IME) term in equation C1 is equal to the gross irrigation water requirement, which was used in estimating canal diversions (appendix D) and irrigation well withdrawals (appendix E).

Section C2: Considerations in IWR Approach

The IWR variables in equation C1 depend on many factors, such as soil type, crop type, growing season length, weather data availability, and irrigation method. To best estimate each variable, the following considerations were made with respect to these factors:

1. Weather stations—Local weather station data served as inputs to the IWR Program and were provided by NRCS staff (R. Pierce, written commun., 2012). Thirty-year normal datasets were required, so only weather stations with a complete 30-yr record (1971–2000) were viable data sources. The Boulder NOAA station was the only weather station within the study area, which is in the northern portion. Trident was the closest station to the southern end of the study area (Cardwell) with a sufficient data record. Weather conditions between Trident and Cardwell were assumed comparable. IWR values were obtained using both the Boulder and Trident climate data, and two sets of IR values were calculated.

2. Soil type—Local NRCS staff specify silty loam in their IWR calculations, as it is believed to be the predominant soil type in a region that includes the study area (L. Ovitt, oral and written commun., 2012). A

Table C1. Preliminary IWR-based irrigation recharge estimates and associated assumptions. The mid-range efficiency was used for sprinkler and pivot, and the min value was used for flood irrigation (blue). These values were modified to reflect the availability of water (table C2).

Irrigation Method:	Flood (grass only)			Sprinkler (grass-alfalfa average)			Pivot (grass-alfalfa average)		
Application Efficiency:	Min 35%	Mid-range 25%	Max 15%	Min 75%	Mid-range 65%	Max 60%	Min 85%	Mid-range 80%	Max 70%
	(in)	(in)	(in)	(in)	(in)	(in)	(in)	(in)	(in)
January	0.00	0.00	0.00	0.00	0.00	0.00	0.00	0.00	0.00
February	0.00	0.00	0.00	0.00	0.00	0.00	0.00	0.00	0.00
March	0.00	0.00	0.00	0.00	0.00	0.00	0.00	0.00	0.00
April	0.00	0.00	0.00	0.02	0.02	0.03	0.02	0.02	0.03
May	1.11	1.92	3.81	0.20	0.48	0.66	0.04	0.16	0.46
June	3.15	5.09	9.62	1.30	2.09	2.59	0.75	1.06	1.82
July	4.68	7.56	14.28	1.88	3.03	3.75	1.04	1.48	2.54
August	4.14	6.69	12.64	1.63	2.64	3.27	0.91	1.29	2.21
September	1.67	2.77	5.35	0.37	0.75	0.99	0.11	0.26	0.62
October	0.00	0.00	0.00	0.04	0.07	0.09	0.03	0.04	0.07
November	0.00	0.00	0.00	0.00	0.00	0.00	0.00	0.00	0.00
December	0.00	0.00	0.00	0.00	0.00	0.00	0.00	0.00	0.00
Annual	14.75	24.04	45.69	5.44	9.09	11.37	2.90	4.31	7.75

Assumptions:

1. The predominant soil type in the study area is silt loam.
2. Only grass is grown in flooded parcels.
3. Sprinkler and pivot parcels are an even mix of alfalfa and grass.
4. Study-area weather conditions reflect an average of the Boulder and Trident weather station conditions.
5. Flood irrigation estimates assume that 50% of excess water goes to runoff. No attempt is made to model this runoff as surface-water gains in stream segments.

detailed inspection of the irrigated lands within the Boulder study area was performed using the NRCS Web Soil Survey and SSURGO data (NRCS, 2012b). The inspection revealed that sandy loam also constitutes a substantial (30%–40%) portion of the soils, so sandy loam was input in the IWR program and recharge rates were recalculated and compared to the silty loam rates. Due to a slightly lower available water capacity in sandy loam, recharge rates were 0.2 to 0.3 in/yr greater per irrigation type, and the overall annual volumetric recharge for the entire study area increased by 3% (or 559 acre-ft/yr). Because this difference was deemed insignificant, silty loam was used for all IWR calculations.

3. Crop type—Field observations and discussions with ranchers and local NRCS staff indicated that irrigated lands in the study area include considerable amounts of both alfalfa and pasture grass, though their exact proportions were unknown (L. Ovitt, oral commun., 2012). Three land-coverage datasets were inspected for crop information (USGS 2010, 2011a, b). Two of the three datasets included crop types, and the two were in good agreement in distinguishing between pasture grass/hay and other crop types suggestive of alfalfa (e.g., small grains, cultivated crops, and close-grown crops); however, as neither dataset explicitly identified alfalfa as a crop type, they were not used for recharge estimation purposes. Instead, a 50/50 mix of alfalfa and pasture grass was assumed for pivot- and sprinkler-irrigated parcels, and only pasture grass was assumed to grow on flood-irrigated parcels. Alfalfa and pasture grass IWR values were applied accordingly in recharge calculations.

4. Irrigation method—During the study, irrigated land consisted of 56% wild flood, 32% pivot, and 12% wheel line. Irrigated acreages and methods were obtained from land-use data published by the Montana Department of Revenue (DOR; Montana Department of Revenue, 2012). “Irrigated Land” is one land use in the

Table C2. Monthly percentages of irrigation recharge distribution per irrigation period. These percentages were also applied to the diversion rates of canals associated with individual irrigated parcels, as detailed in appendix D. These percentages were used to redistribute the diversion and application of water based on water availability rather than crop demand.

Month	Apr–Oct Annual %	Apr–Sept Annual %	Apr–July Annual %
January	0%	0%	0%
February	0%	0%	0%
March	0%	0%	0%
April	5.5%	6.1%	7.6%
May	23.8%	26.8%	34.8%
June	23.4%	26.4%	34.2%
July	16.0%	18.0%	23.3%
August	10.5%	11.8%	0%
September	9.8%	11.0%	0%
October	11.0%	0%	0%
November	0%	0%	0%
December	0%	0%	0%
Annual	100%	100%	100%

dataset and is divided into three subclasses based on irrigation method (pivot, sprinkler, and flood). All Irrigated Land parcels were included in IR calculations. "Hay" is another land use in the dataset and is classified as non-irrigated; however, while evaluating canal use in the study area (appendix D), it was observed that a few active canals coincided with only hay parcels, suggesting that the parcels are irrigated in at least some years. The DOR database defines Irrigated Land as being irrigated the majority of the time (e.g., 2 of 3 years), and land in an irrigation district is not classified as irrigated unless it is charged an irrigation fee. Because of these stipulations, it was deemed plausible that parcels classified as "hay" are sometimes irrigated, and hay parcels coinciding with active canals were included in irrigation recharge calculations.

Because irrigation methods have changed in the study area in recent years, such as flood to pivot irrigation (L. Ovitt, oral commun., 2012), the frequency of data updates was verified with DOR staff. DOR staff reported that land-use classifications are updated annually by DOR county appraisal staff. The updates are based on landowner feedback, ground truthing, and new imagery analysis. Although landowners are not required to report land-use changes to DOR, many do in order to ensure their property appraisals are correct. (T. Chase, Montana Department of Revenue, written commun., October 23, 2012).

5. Application efficiency (IME)—The NRCS National Engineering Handbook (1993) provides a range of efficiencies for most irrigation methods. For methods not discussed in the Handbook, efficiency estimates were obtained from interviewing local NCRS staff and reviewing previous work (L. Ovitt, oral commun., 2012; Sterling and Neibling, 1994). The following values were selected for each method:

- Wild flood efficiencies range from 15% to 35%; 35% was used for IR calculations;
- Sprinkler efficiencies range from 60% to 75%; 65% was used for IR calculations; and
- Pivot efficiencies range from 70% to 85%; 80% was used for IR calculations.

6. Other IWR inputs—The values of several other IWR data inputs were verified with NRCS staff to ensure they were appropriate for study-area conditions (L. Ovitt and R. Pierce, oral and written commun., 2012). They included carryover moisture, seasonal duration, site elevation, wetting cycles, haying periods, and effective precipitation (P_{eff}).

7. DP_{ex}—This term was a multiplier used to account for the portion of excess applied water that results in deep percolation (i.e., groundwater recharge) rather than runoff; it can range from 0 to 1. In a model of the eastern Snake Plain Aquifer, the Idaho Department of Water Resources (DWR) assigned a similar term to irrigated lands on a site-specific basis. In areas without surface-water return flows, the term was set to 1.0, signifying that all excess water recharged the aquifer. In areas with evidence of return flows, the term was calibrated to the observed return flow rates (Idaho DWR, 2013).

For the purposes of irrigation recharge estimation in the Lower Boulder study, DP_{ex} values were assigned based on irrigation type, where DP_{ex} was set to 0.5 for flood parcels and 1.0 for pivot and sprinkler parcels. This

approach assumes that excess flood irrigation water results in substantial (50%) runoff, whereas very little runoff results from pivot and sprinkler applications.

Section C3: Modifications to IWR Approach

In order to more realistically represent the timing of irrigation recharge, the temporal recharge distribution was modified to follow water availability rather than the theoretical crop needs calculated in IWR. The vast majority of irrigated land in the study area is surface-water irrigated (L. Ovitt, oral commun., 2012), and surface-water availability is much greater in the early season (e.g., April–June). Consequently, irrigation water is often applied in excess of crop demand during this period, and water applied later in the season falls short of crop demand.

Monthly recharge rates were redistributed to be consistent with the timing of irrigation canal diversions. Canal diversion rates and durations are detailed in appendix D and were based on field observations, water-level and discharge hydrographs, and landowner interviews (P. Carey, oral commun., 2013). Irrigation season duration was divided into three periods: April–October (full season), April–September, and April–July. Multipliers were devised and applied to monthly recharge values to redistribute recharge within these periods (table C2; appendix D, section D4). Finally, each irrigation parcel was assigned to one of the three periods based on the canal from which it derived its water. Groundwater-irrigated parcels were assigned to the full-season period (April–October) based on water-level data from a well adjacent to an irrigation well (GWIC 262766) and the assumption that water availability is not a factor when groundwater is the supply source. The final irrigation recharge values are provided in table C2.

APPENDIX D

GROUNDWATER BUDGET METHODOLOGY: RIVER GAINS AND LOSSES

This appendix details the methods used to estimate the Boulder River's gains and losses (i.e., baseflow and infiltration) through the study area. Because estimates were based on data from the irrigation season, the methodology involved estimation of canal leakage rates (section 1); irrigated-parcel water requirements (section 2); the associated Boulder River diversions (section 3); and the timing of those diversions (section 4). Section 5 outlines the resulting river gain/loss estimates.

Section D1: Canal Leakage

Active canals within the Montana DNRC irrigation records (Montana DNRC, 2007) were identified based on field observations and an inspection of 2011 NAIP imagery. Irrigation diversions off the Boulder River were then grouped by river reach, with each reach bounded by flow-measurement stations (fig. 9, table D1). As noted in table D2, a few shorter canals were combined to fit the numerical model's grid discretization; that is, some canals were grouped if they overlapped in a given grid cell.

An average seasonal leakage rate per canal was estimated as a flux per unit length of canal (i.e., cfs/mi). Leakage rates of canals monitored during the study, namely the Murphy and Carey canals, were estimated using the data collected; their leakage estimation is detailed in Bobst and others (2016). Leakage rates of unmonitored canals were estimated from two data sources: (1) the rates of canals monitored during the study, and (2) canal width. Canal width estimates were approximated from field observations and a detailed inspection of 2011 NAIP imagery. Based on a canal's width relative to the Murphy and Carey canals, it was assigned a leakage rate equal to that of the Murphy Ditch (0.26 cfs/mi), Carey Ditch (1.61 cfs/mi), or the mean of the two (0.94 cfs/mi).

The length of each canal was measured (table D2) and then multiplied by its leakage rate to obtain a volumetric (i.e., discharge) rate per canal. This volumetric rate was applied as a specified-flux boundary in the numerical model. The total volumetric rate was multiplied by its estimated flow duration per month, and all months were summed to obtain a total seasonal volume per canal. Calculations were made in monthly time increments in order to fit the monthly time scales of the IWR output and the transient model. April irrigation practices were assumed to commence in the final 10 days of the month, and July calculations were based on a 21-day period to account for haying.

Table D1. Estimated river reach conditions and associated canal flow durations based on observed water levels and non-irrigation season flows.

Reach No.	River Reach	Length (mi)	Predominant Irrigation-Season Conditions	Estimated Canal Flow Duration
1	I-15 to Red Bridge	4.9	Losing	April–July
2	Red Bridge to White Bridge	5.4	Gaining	April–September
3	White Bridge to Quaintance Lane**	10.5	Losing	April–July
4	Quaintance Lane to Dunn Lane	6.5	Losing	April–July
5	Dunn Lane to Boulder Cutoff	10.2	Losing	April–July
6	Boulder Cutoff to Cold Spring	5.0	Gaining	April–September
7	Cold Spring to Cardwell	11.8	Gaining	April–September
**	Carey Ditch	N/A	N/A	April–October
	Groundwater-irrigated parcels	N/A	N/A	April–October

** The Carey Ditch was treated differently from other canals within Reach 3 based on available data

Table D2. Data used to estimate gross IWR and canal leakage rates.

River Reach No.	Canal	Length (mi)	Estimated Leakage Rate (cfs/mi)	Irrigated Parcel Acreage	Estimated Flow Duration
1	Frascht-Smith/State-East*	1.17	0.26	387	April–July
1	Harper/State-Wahle*	1.83	0.26	251	April–July
1	Slope	0.4	0.26	5	April–July
1	Evans/State-West*	0.66	0.26	118	April–July
2	Murphy	8.27	0.26	360	April–September
2	Killiam	1.39	0.26	99	April–September
2	Franchi	1.43	0.13	62	April–September
2	McCauley	1.01	0.94	51	April–September
3	Carey**	8.57	1.61	738	April–October
3	Murphy-Quaintance	5.05	0.26	103	April–July
3	Wickham	3.32	0.26	283	April–July
3	Quinn	3.59	0.26	224	April–July
3	Hoops	5.96	0.26	468	April–July
3	Howard	3.58	1.61	242	April–July
3	Clark/Dawson*	3.94	0.26	209	April–July
4	Carey-East (North of Dunn Ln)	3.09	0.26	382	April–July
4	Carey-Twohy	5.39	0.94	517	April–July
4	Twohy	2.55	0.26	560	April–July
5	Carey-East (South of Dunn Ln)	1.81	0.94	56	April–July
5	Dawson-West	2.25	0.94	93	April–July
5	Dawson-East	2.11	0.94	136	April–July
5	Sheehy	2.49	0.94	333	April–July
6	Brenner	1.31	0.94	142	April–September
7	Carey-Dawson	1.38	0.94	148	April–September
7	Downs	2.91	1.61	295	April–September
7	Cardwell-West	1.01	0.94	86	April–September
7	Cardwell-East	1.29	0.94	68	April–September
N/A	Groundwater-irrigated parcels	N/A	N/A	555	April–October

*Canal lengths and parcel acreages were combined in order to avoid overlap in model grid.

**The Carey Ditch was treated differently from other canals within Reach 3 based on available data.

Section D2: Gross IWR per Canal

Each irrigated parcel in the study area (Montana Department of Revenue, 2012) was evaluated and matched to the canal most likely to be irrigating it. The acreage per irrigation method (flood, pivot, and sprinkler) was then summed for each canal.

Gross irrigation water requirements were calculated from IWR program output (appendix C). The IWR program generates a net irrigation water requirement (NIR). The gross irrigation water requirement accounts for the application efficiency of each irrigation method (IME); it is equal to net irrigation water requirement divided by the irrigation method's application efficiency, or NIR/IME (appendix C, equation C1).

Section D3: Diversions (Section 1 + Section 2)

Each canal's volumetric leakage rate (section 1) was summed with the total gross IWR of its respective parcels (section 2). This sum was equal to the canal diversion rate, which was calculated for each month of the irrigation season. As described below (section 5), these diversion rates were grouped into one of the seven river reaches in the study area (table D1). The total diversion rate for a given reach sometimes included water demands from parcels outside of the reach; for instance, parcels downstream of the reach were included in diversion calculation if they were irrigated by a canal diverted within the reach. Likewise, parcels within a given reach were excluded from diversion calculation if they were irrigated by a canal diverted upstream of the reach.

Section D4: Seasonal distribution of diversions

Diversion timing and rates were initially proportional to IWR output, which is determined by theoretical crop demand through the irrigation season. However, as in the irrigation recharge approach (appendix C), the temporal distribution of diversion rates was adjusted to reflect observed irrigation practices in the lower Boulder River valley, which are strongly influenced by water availability in addition to crop demand. The vast majority (approximately 90%) of irrigated land in the study area is irrigated by surface water (L. Ovitt, oral commun., 2012), and surface-water availability is much greater early in the season (e.g., April–June). Consequently, irrigation water is typically applied in excess of crop demand during this period, whereas water applied late in the season often falls short of crop demand.

Several data sources were used to estimate the timing and rates of diversions in the study area. They included discharge and stage from the two monitored canals, discharge and stage from monitored river sites, groundwater levels on and near irrigated land, and landowner interviews.

D4.1 Canal Data

Two canals were monitored throughout the study period: the Murphy Ditch and Carey Ditch (fig. D1). Monitoring of the Carey Ditch included a flow station immediately downstream of its diversion from the Boulder River (GWIC 262899). Flow data at this station showed relatively high diversion rates early in the season and low rates later in the season, rather than a mid-summer peak shown in the IWR-based diversion estimates (fig. D2). Flow data at the Murphy Ditch diversion were sparse, but flows in the canal transect area were still useful in evaluating the relative flow rates through the season. The data showed an early season peak as with the Carey Ditch data. The two datasets differed in their seasonal duration; whereas the Carey Ditch ran through the full season (late April–October), the Murphy Ditch began running later (late May) and ended sooner (mid-August), illustrating the variability in canal durations in the study area.

D4.2 River Data

As discussed in Bobst and others (2016), river discharge hydrographs showed the following general pattern:

1. Maximum rates in April through mid-June, a period when snowmelt and rainfall rates are high and diversions begin;
2. sharp declines in late June, as spring snowmelt and rainfall decrease and diversion rates are at their peak;
3. a brief and relatively small increase in mid-July due to haying;
4. minimum flows from late July through the end of the irrigation season in mid-October; and
5. a minor increase at the end of the season (mid-October), followed by relatively steady flow till springtime.

This annual pattern shows the strong influence of irrigation diversions in the study area. A comparison of

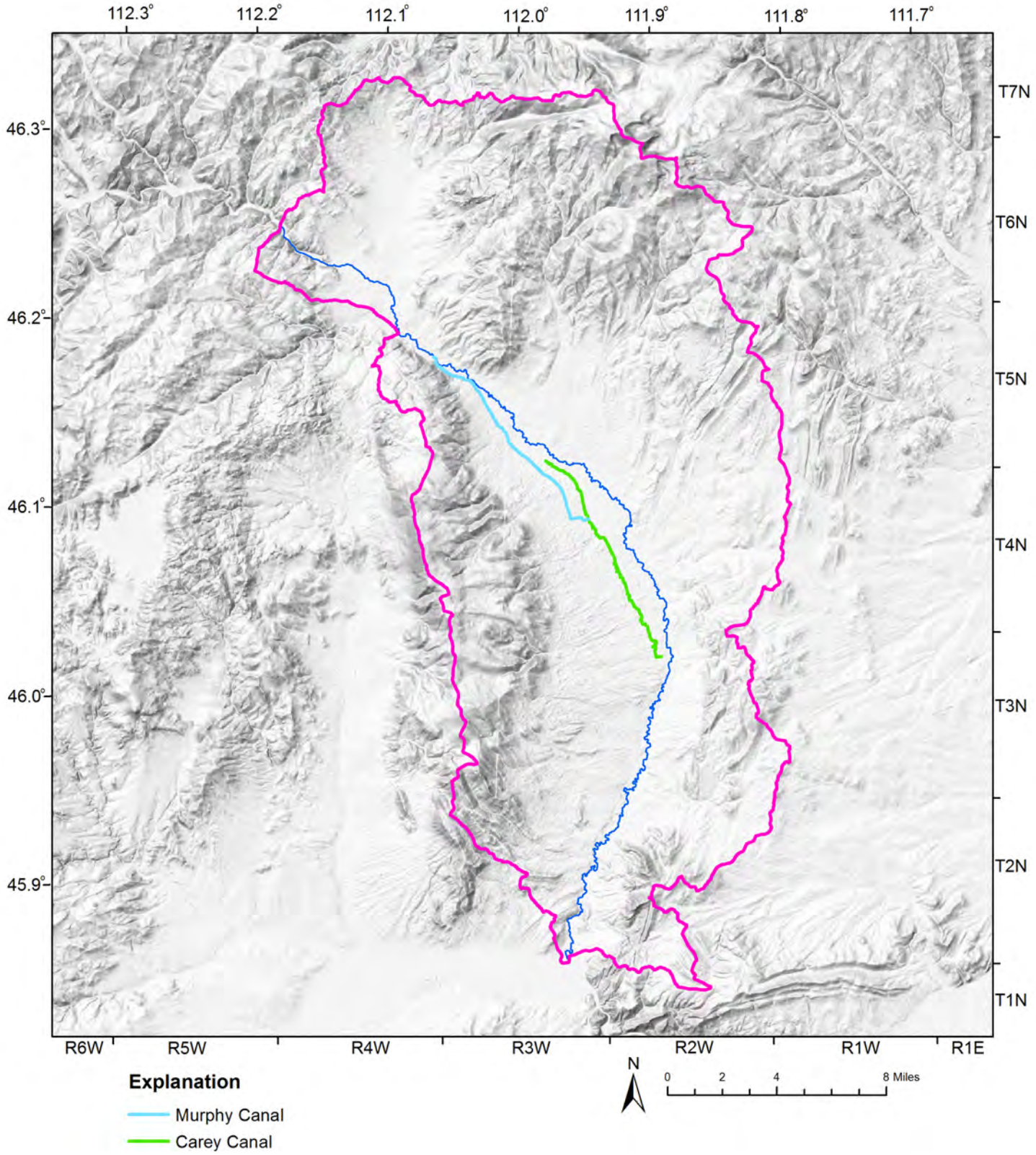

Figure D1. The Murphy Ditch and Carey Ditch were the monitored canals during the study.

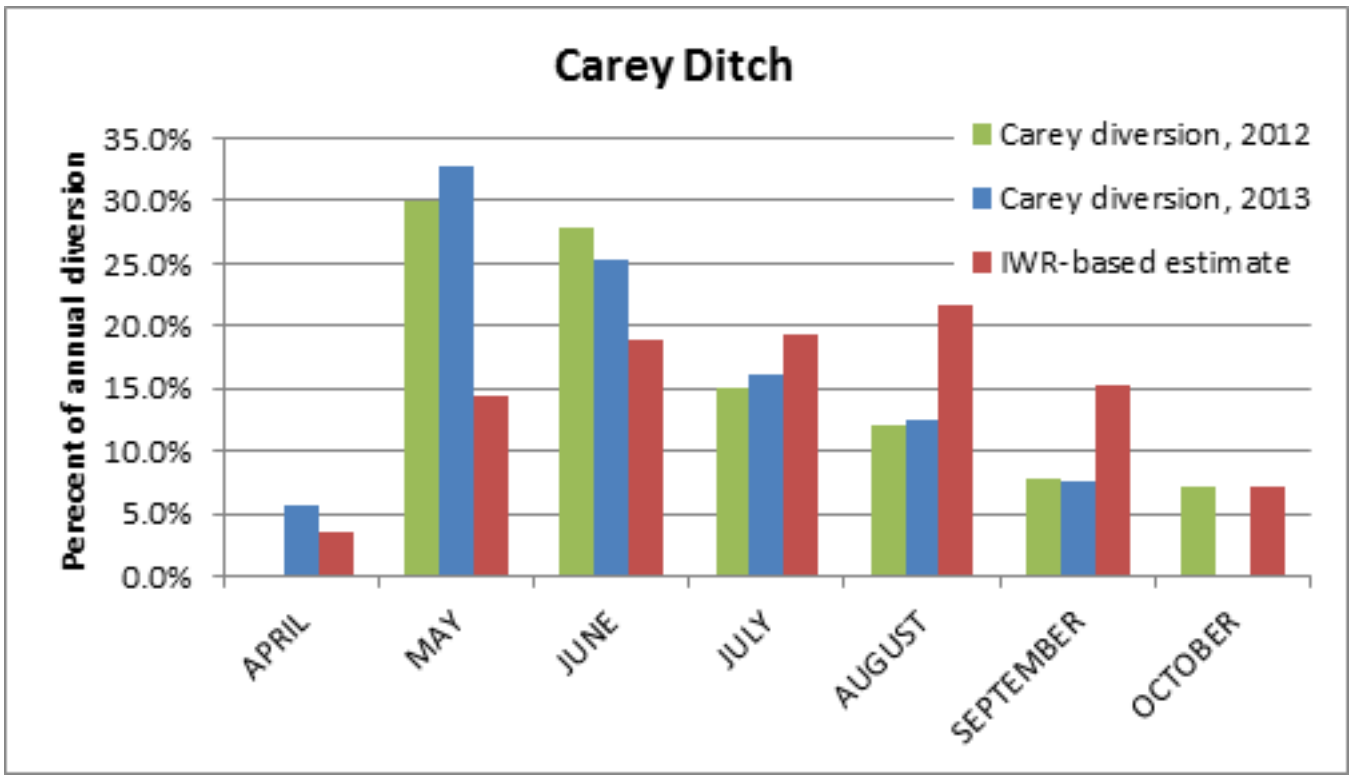

Figure D2. Comparison of IWR-based diversion estimate with observed flow at Carey Ditch diversion during the 2012 and 2013 irrigation seasons. Note that October 2013 flows at the Carey Ditch diversion were unknown because they were not measured.

flow at the six river stations revealed contrasts in water availability, most notably in the central reaches. Flows at Quaintance Lane and Dunn Lane (GWIC 265344 and 265343, respectively) were at or near zero through much of the latter half of the irrigation season and, to a lesser extent, at Boulder Cutoff (GWIC 265348, fig. 9 in text, and appendix G). The timing of these low flows suggests that this portion of the river is heavily diverted in the early season and receives little baseflow or surface-water return flow throughout the season. The lack of baseflow is also supported by groundwater levels in shallow river-side wells in this central valley area; the river stage is consistently above the groundwater level at White Bridge, Quaintance Lane, Dunn Lane, and periodically at Boulder Cutoff during the irrigation season (Bobst and others, 2016).

D4.3 Groundwater-Level Hydrographs

Over 15 hydrographs of groundwater levels strongly influenced by irrigation-derived recharge were reviewed (appendix E). Hydrographs showed strong declines ranging from mid-June to mid-September, with the majority occurring from mid-June to late July. Spatial variability in the peak timing indicated that irrigation from diversions within gaining river reaches tended to run longer through the summer (e.g., GWIC 192299, appendix F), while the diversions from relatively dry reaches ceased in June or early July (e.g., GWIC 262738, appendix F).

D4.4 Landowner Information

Landowner discussions also supported the patterns shown in stage and discharge hydrographs. A longtime rancher in the lower Boulder valley described the timing of canal operations as very variable among different reaches of the river depending on where baseflow and surface-water return flow provide recharge. For instance, diversions between Red Bridge and White Bridge and at the southern end of the valley (below Cold Spring) tend to continue through mid-September; in contrast, diversions between Quaintance and Dunn Lane shut off sometime in July, even in wet years such as 2011 (P. Carey, oral commun., November 8, 2013).

D4.5 Resulting Seasonal Distribution

Collectively, these four lines of evidence were used to estimate the temporal distribution of diversion rates within each of the seven river reaches. Diversions were grouped into three periods: April–October (full season), April–September, and April–July. Each river reach was assigned to one of these periods based on the apparent water availability within it (table D1). The original IWR-based monthly leakage rates were redistributed to be consistent with observed data, namely the Carey diversion and Red Bridge discharge data. Percentages used in this monthly redistribution are provided in table D2 and compared to the original IWR-based percentages in figures D2 and D3.

Section D5: River Loss/Gain by Reach

One approach to estimating stream infiltration and baseflow (i.e., losses and gains) is through comparison of stream stage and groundwater levels in shallow stream-side wells or piezometers. The head difference can be multiplied by the streambed conductance to obtain a point estimate of the loss or gain in the stream:

$$Q_{loss/gain} = C^*(H_s - H_g), \qquad \text{Equation D1}$$

where C is the streambed conductance, H_s is the stream stage elevation, and H_g is the aquifer head elevation. C can be estimated from borehole cuttings or by back-calculating if equation D1 is combined with another $Q_{loss/gain}$ equation, such as equation D2 (below). By performing the $Q_{loss/gain}$ calculation at a pair of flow-measurement sites, an average loss/gain rate can be estimated along the stream reach between the two sites. The flow and head data record should ideally be outside of the irrigation season due to the effects of irrigation diversions and return flows on natural flow conditions.

This approach was used in the water budget analysis for the Managed-Recharge Model (Carlson, 2013). The Managed-Recharge Model encompasses the central portion of the lower Boulder River valley, where the head data indicated consistently losing flow conditions over time. In contrast, conditions were quite variable in both space and time at the scale of the full study area. Analyzing data from all paired well-and-river-flow sites over a number of time intervals (e.g., daily, weekly, biweekly, monthly) revealed that the head data were inconclusive during the brief flow-data record outside of the irrigation season. Head differences at multiple sites (e.g., GWIC 265348 and 262190) changed from positive to negative over the pre-irrigation season (March to mid-April) record that was evaluated; furthermore, riverbank wells were not available at the I-15 and Red Bridge flow stations, so head differences could not be determined upstream of White Bridge.

As an alternative approach, synoptic flow data were used to estimate the net monthly loss or gain per river reach. The procedure was as follows:

1. Segmented the river into seven reaches, each bordered by an upstream and downstream flow-measurement station (table D1)
2. Summed all monthly canal diversions per reach ($Q_{diverted}$)
3. Subtracted the total monthly diversion from the reach's mean monthly upstream discharge ($Q_{upstream}$)
4. Any tributary inputs within the reach were incorporated into $Q_{upstream}$
5. Added ± 5% to $Q_{upstream}$ and $Q_{downstream}$ account for flow-measurement error
6. Subtracted the mean monthly discharge at the downstream end of the reach ($Q_{downstream}$)
7. Evaporative losses were assumed negligible
8. The resulting equation was as follows:

$$Q_{loss/gain} = Q_{upstream} - Q_{diverted} - Q_{downstream} \qquad \text{Equation D2}$$

9. Each monthly $Q_{loss/gain}$ was used to evaluate the seasonal flow conditions per reach if the absolute value exceeded Q_{error}.

The monthly $Q_{loss/gain}$ results per reach are provided in table D3, and the average $Q_{loss/gain}$ over the entire season is provided in table D4. April flow data were disregarded because they were anomalous for all but one reach; the anomalous values were likely due to a combination of high stream flow and runoff rates, as well as a high variability in early season diversion rates.

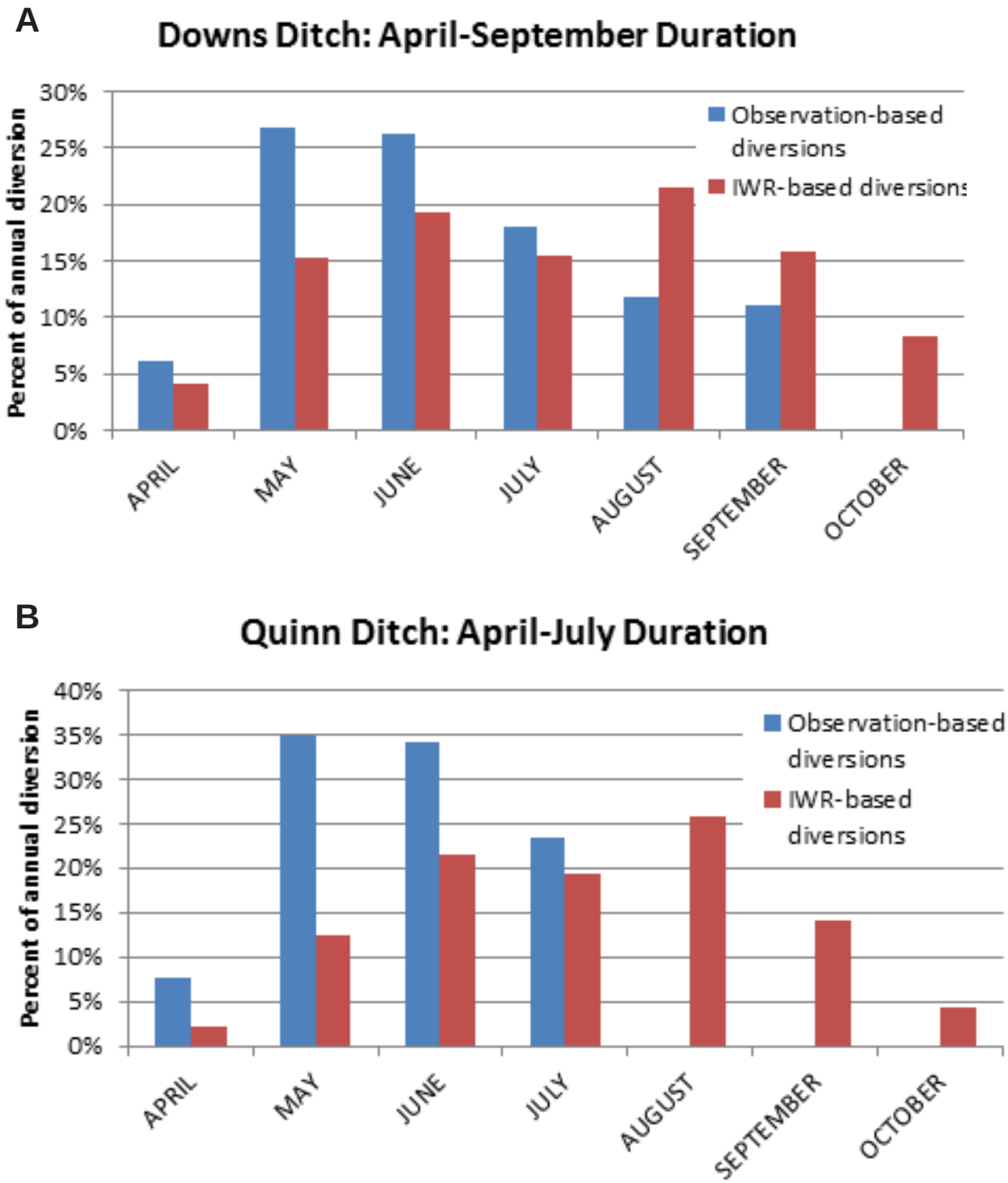

Figure D3. Comparison of IWR-based and data-based diversion estimates through the irrigation season.

Table D3. $Q_{loss/gain}$ per river reach. A monthly $Q_{loss/gain}$ value was used in calculating the seasonal average if it exceeded its corresponding Q_{error} (green values). The April $Q_{loss/gain}$ (gray) values were not used for any reach due to high flows that did not fit well into site rating curves; run off and diversion rates were likely highly variable in April as well.

Reach 1: I-15 to Red Bridge								
		$Q_{upstream}$	± 5%	$Q_{diversion}$	$Q_{downstream}$	± 5%	Resulting $Q_{loss/gain}$	Total Q_{error}
April	8%	365.9	18.3	4.3	222.2	11.1	139.4	29.4
May	35%	435.3	21.8	19.2	420.5	21.0	-4.4	42.8
June	34%	325.1	16.3	19.5	303.5	15.2	2.1	31.4
July	23%	84.8	4.2	12.9	67.6	3.4	4.3	7.6
August	0%	31.2	1.6	0.0	24.0	1.2	7.2	2.8
September	0%	22.8	1.1	0.0	14.8	0.7	8.0	1.9
October	0%	31.6	1.6	0.0	29.8	1.5	1.8	3.1
						Average $Q_{loss/gain}$ for values [$Q_{loss/gain}$ < Q_{error}]:	6.51	cfs
						Average $Q_{loss/gain}$ per mile:	1.34	cfs/mi

Reach 2: Red Bridge to White Bridge								
		$Q_{upstream}$	+/- 5%	$Q_{diversion}$	$Q_{downstream}$	+/- 5%	Resulting $Q_{loss/gain}$	Total Q_{error}
April	6%	268.2	13.4	2.79	487.8	24.4	-222.4	37.8
May	27%	453.4	22.7	11.90	450.6	22.5	-9.1	45.2
June	26%	335.3	16.8	12.09	308.1	15.4	15.1	32.2
July	18%	77.0	3.9	7.97	90.9	4.5	-21.9	8.4
August	12%	26.8	1.3	5.23	35.9	1.8	-14.3	3.1
September	11%	17.1	0.9	5.07	22.5	1.1	-10.5	2.0
October	0%	34.7	1.7	0.00	39.9	2.0	-5.2	3.7
						Average $Q_{loss/gain}$ for values [$Q_{loss/gain}$ < Q_{error}]:	-12.97	cfs
						Average $Q_{loss/gain}$ per mile:	-2.38	cfs/mi

Several sources of uncertainty exist in the river $Q_{loss/gain}$ approach. For instance, in analyzing river flow conditions and assigning diversion periods, the river was segmented into reaches based on flow-measurement locations (fig. 9); however, flow conditions may not have been consistent throughout a given reach, particularly in longer ones such as reaches 3 and 5.

Regarding diversions, a comparison of estimates to monitoring data showed both under- and over-estimates. The estimated total diverted volume to the Murphy Ditch was 19% greater than observed in 2012; this discrepancy could be due to gaining conditions in the low-lying portions of the canal's first 2 mi, as indicated in model results (Boundary Conditions section). In contrast, the estimated total diverted volume to the Carey Ditch was 33% less than observed in 2012, most notably in the early season (May–June); this discrepancy is likely attributable to the fact that early season diversions were in excess of crop needs, and some of the water resulted in runoff and return flow.

As shown in table D3, the margin of error sometimes exceeded $Q_{loss/gain}$ itself; therefore, it was not possible to definitively conclude whether certain reaches are gaining or losing. A related limitation of the $Q_{loss/gain}$ approach is that diversion estimates did not account for any flow that might return to the river; in many of the monthly estimates with a large margin of error, return flows could likely be the source of the discrepancy. The approach also does not account for secondary channels (e.g., sloughs and canals) alongside the river that are lower in elevation, which likely intercept baseflow. Near Quaintance Lane, flow was observed throughout the irrigation season in one such channel while the adjacent riverbed was dry (Carlson, 2013), and others were believed to exist between Quaintance Lane and Dunn Lane based on evaluations of elevation data and NAIP imagery.

Despite the approximate nature of the diversion and river flux estimates, they improved the quantitative understanding of the study area flow system in several respects. For example, they better quantified the temporal and spatial distribution of river gains and losses, especially within reaches showing a strong seasonal shift due to irrigation practices. The estimates also better quantified groundwater recharge derived from irrigation throughout the lower Boulder River valley. Given the scale of the study area and limited availability of diversion records, this approach was a useful means of quantifying surface-water–groundwater interactions. Further insight was also achieved through the model calibration process (Calibration section).

These results match well with the overall estimate from non-irrigation season measurements of about 40 cfs.

Reaches 3, 4, and 5 differ from the estimates based on site-specific water levels and non-irrigation season flows (table D1). This is not unexpected given that more data were used for the table D4 values, and is the reason that this more detailed analysis was undertaken.

Table D4. The modeled average gain/loss per river reach during the irrigation season.

Reach No.	Reach	Loss (+)/ Gain(-) (cfs/mi)
1	I-15 to Red Bridge	1.3
2	Red Bridge to White Bridge	-2.4
3	White Bridge to Quaintance Lane	2.5
4	Quaintance Lane to Dunn Lane	1.9
5	Dunn Lane to Boulder Cutoff	-3.9
6	Boulder Cutoff to Cold Spring	0.3
7	Cold Spring to Cardwell	-3.5

Overall net gain of 42.2 cfs over 44.0 mi; Average gain rate: 0.96 cfs/mi.

APPENDIX E

GROUNDWATER BUDGET METHODOLOGY: PUMPING WELL WITHDRAWALS

This appendix details the methods used to identify locations and estimate rates of pumping wells in the study area. A combination of datasets was used to identify pumping wells (section 1), and withdrawal rates were estimated by well type, including domestic (section 2), stock (section 3), public water supply (PWS; section 4), and irrigation (section 5).

Section E1: Assembling a Pumping-Well Dataset

Initially a point shapefile of GWIC pumping wells was created for the study by clipping the GWIC statewide shapefile to the study area and filtering non-pumping wells. Upon evaluation, however, this dataset was deemed incomplete and some well locations appeared to be in error. Alternatively, the Montana Structures and Addresses Framework (Structures) database (Montana State Library, 2012) was chosen as the primary data source for stock and domestic wells. The GWIC pumping-well dataset served as a supplement as detailed below.

The Structures shapefile was clipped to the study area, and the contained structures were inventoried in several ways. The dataset's attribute table was first evaluated, and structure types unlikely to have wells associated were filtered out of the dataset; altogether, 18 structure types remained. The remaining structures were spatially analyzed by overlaying NAIP imagery (2011), and structures were again eliminated if they were unlikely to have a well associated; for example, those that appeared to be small sheds behind single-family homes were deemed unlikely to require a pumping well. All repeat-address structures were also eliminated from the dataset. Finally, all home and business structures within the downtown Boulder area were eliminated from the dataset based on the assumption that they were on the PWS system. This portion of the eliminated Structures dataset was later used to check the reasonableness of PWS rate estimates (section 4).

The GWIC pumping-well shapefile was then overlain with the Structures shapefile. All well points that did not overlap with those of the Structures dataset were identified and inspected against the 2011 NAIP imagery. Wells with reasonable locations and well-log information were merged with the Structures shapefile. Seven wells were added in this manner and were primarily stock wells. The merged shapefile is referred to here as the Pumping-Well dataset.

Next, the Lower Boulder monitoring-well shapefile was overlain with the new Pumping-Well shapefile. Again, all pumping wells that did not overlap with the Pumping-Well dataset were identified and inspected against the 2011 NAIP imagery. Wells with reasonable locations and well-log information were merged with the Pumping-Well dataset. Ten wells were added in this manner and were primarily stock wells.

Prior to finalizing the dataset, edits were made to domestic wells within a few subdivisions. For instance, in the Boulder View Ranch subdivision, the well density was reduced from one well per household to one per three households, which was based on reports from residents of the subdivision; pumping rates in those wells were tripled accordingly. Similarly, the number of wells in the Lone Tree subdivision and Elkhorn Ghost Town were halved and quartered, respectively, because the grid discretization did not allow for the true well densities. The Lone Tree well rates were doubled accordingly. The Elkhorn Ghost Town domestic pumping rates were not increased based on two field observations; namely, many residents live there only seasonally, and lawn areas were much smaller than those of subdivisions and downtown homes, thus requiring less water use.

Finally, the active City of Boulder PWS wells were added to the dataset based on information provided by the City of Boulder PWS Well Operator (section 4). Determining the quantity and locations of irrigation wells was closely tied to their rate estimation, and so the approach is detailed in section 5.

Section E2: Domestic Well Pumping Rate Estimation

To estimate domestic well pumping rates, those of a previous GWIP study were referenced. Waren and others (2013) estimated domestic well rates from subdivision water-use records over a 15-yr period, and the annual average result was 435 gpd. This rate is within the range of domestic consumptive use estimated by the DNRC Water Resources Division (Montana DNRC, 2011). The monthly distribution of water use (table E1) was also based on the prior GWIP study's estimates.

Table E1. Domestic well monthly consumptive use.

Month	% Use	Rate (gpd)
Jan	0.3%	15
Feb	0.3%	17
Mar	0.4%	21
Apr	0.7%	34
May	10.2%	523
Jun	18.2%	964
Jul	26.2%	1,343
Aug	26.4%	1,353
Sep	14.2%	752
Oct	2.5%	126
Nov	0.5%	26
Dec	0.2%	10

Section E3: Stock Well Pumping Rate Estimation

Cannon and Johnson (2004) served as the primary reference for estimating stock well pumping rates. The study estimated annual stock water use in Montana on a county scale, and estimates were based on the grazing land acreage per county. For this study, grazing land within the Lower Boulder area was measured and calculated as a percent of the total Jefferson County grazing land; the result was 33.5%. The percentage was multiplied by Cannon and Johnson's Jefferson County stock water use estimate. This approach assumes that stock water use is proportional to grazing acreage.

The study area stock water use was then divided by the number of stock wells in the study area (29) to obtain the average annual water use per well. This rate was 92.6 ft^3/day, or 693 gpd. Consumptive use from livestock intake and evaporation from stock tanks was assumed to be 100%. The Montana DNRC Water Resources Division also made this assumption when estimating stock water use requirements (Montana DNRC, 2011). It was also assumed that the average annual pumping rate remained constant throughout the year, because field observations and landowner communications indicated that stock wells do not follow a consistent seasonal pumping schedule; rather, pumping schedules are quite variable due to factors such as livestock distribution.

Section E4: PWS Well Pumping Rate Estimation

To estimate pumping rates for the City of Boulder PWS wells, the city's PWS Well Operator (Operator) was interviewed (D. Wortman, oral commun., April 2013). The Operator provided the locations of the four PWS wells in Boulder. Two of the four were reported to operate on a year-round basis, the third was used occasionally during peak use (late summer) periods, and the fourth was used only for emergency purposes. The Operator also noted that the city's wastewater flows to a lagoon near the southern end of the town, which discharges to the Boulder River.

Water-use records provided by the Operator were limited. Only 2 months of data were available (February and March of 2013) due to data loss from the water treatment plant's SCADA system. Consequently, water-use records from a city of similar size were used to supplement the Boulder data, namely the City of Dillon's 2010 records, which were obtained for a previous GWIP study (Abdo and others, 2013). The City of Dillon's monthly water-use percentages were calculated and assumed to equal those of the City of Boulder. Using those percentages, Boulder's 2-month pumping record was extrapolated to the remaining 10 months of the year. This approach assumes that the February and March water use in 2013 was typical of most years in Boulder. Because the City of Boulder's PWS was reportedly supplied primarily by two wells, the pumping-rate estimate for each month was divided in half to obtain a per-well pumping rate (table E2). Consumptive use was set at 100% because wastewater is discharged from lagoons to the Boulder River. This approach assumes that groundwater recharge from the lagoons and household lawns is negligible.

Table E2. PWS monthly consumptive use per PWS well.

Month	% Use	Rate (gpd)
Jan	5%	181,913
Feb	5%	186,690
Mar	5%	196,952
Apr	6%	225,261
May	7%	247,161
Jun	9%	335,673
Jul	17%	621,369
Aug	16%	572,613
Sep	11%	394,714
Oct	9%	307,945
Nov	6%	210,337
Dec	5%	194,851

Section E5: Irrigation Well Pumping Rate Estimation

Estimating irrigation well withdrawals involved the use of several data sources, including GWIC, the DNRC Water Rights Query System (Montana DNRC, 2013), Montana Cadastral (Montana State Library,

2013), the Montana Final Land Unit (FLU) classifications (Montana DOR, 2012), NAIP imagery, and the NRCS IWR Program (NRCS, 2012a).

First, all study area wells with an irrigation-use designation were extracted from GWIC. Well locations were verified by matching well ownership to the land ownership reported in Cadastral, and by inspecting NAIP imagery to see if the well was on or near an irrigated parcel.

Second, the DNRC Water-Rights Query System was searched. Groundwater-rights records in the study area were screened for data that matched any of the wells previously found in GWIC, such as the location, landowner, total depth, casing diameter, and installation date. In addition, the reported irrigation method and maximum acreage were compared to FLU data at each site. Water-rights records that did not report irrigation as the primary water use were filtered out of the search results.

Pairs of GWIC and water-rights records were matched using this approach. Certain details within a given pair that did not match were flagged. A single conflicting attribute (e.g., well depth) did not necessarily rule out a match between a GWIC well and a water right; however, if multiple attributes did not match, it was concluded that GWIC was missing the well associated with the given water right. This approach resulted in a total of five irrigation wells.

Based on the reported maximum acreage and irrigation method for a given parcel, the gross irrigation water requirement (gross IWR) was calculated per parcel. Gross IWR estimation is described in appendices C and D, and table E3 presents the monthly results; flood irrigation values are not included because none of the irrigation wells were matched with flood-irrigated parcels. The per-acre gross IWR was multiplied by the reported maximum acreage to obtain a volumetric water use, which was termed the "calculated volume." The calculated volume was then compared to the maximum volume assigned to the water right, and the lesser of the two was used in the remaining water-use calculations.

Some groundwater-rights records were reported as overlapping with surface-water rights. In such cases, the area of overlap was measured and multiplied by the appropriate gross IWR value to obtain an "overlap volume." Where applicable, this overlap volume was subtracted from the original calculated volume, and the difference was assumed to be the annual groundwater withdrawal.

Table E3. Gross IWR estimates for irrigation wells per irrigation method (in).

	Sprinkler	Pivot
	Average (Alfalfa + Grass Hay) Gross IWR	Average (Alfalfa + Grass Hay) Gross IWR
April	0.06	0.08
May	2.10	2.06
June	5.98	5.32
July	8.66	7.41
Aug	7.54	6.44
Sept	2.87	2.54
October	0.19	0.20
Annual	27.40	24.05

APPENDIX F

GROUNDWATER HYDROGRAPHS FROM 3-YR TRANSIENT SIMULATION

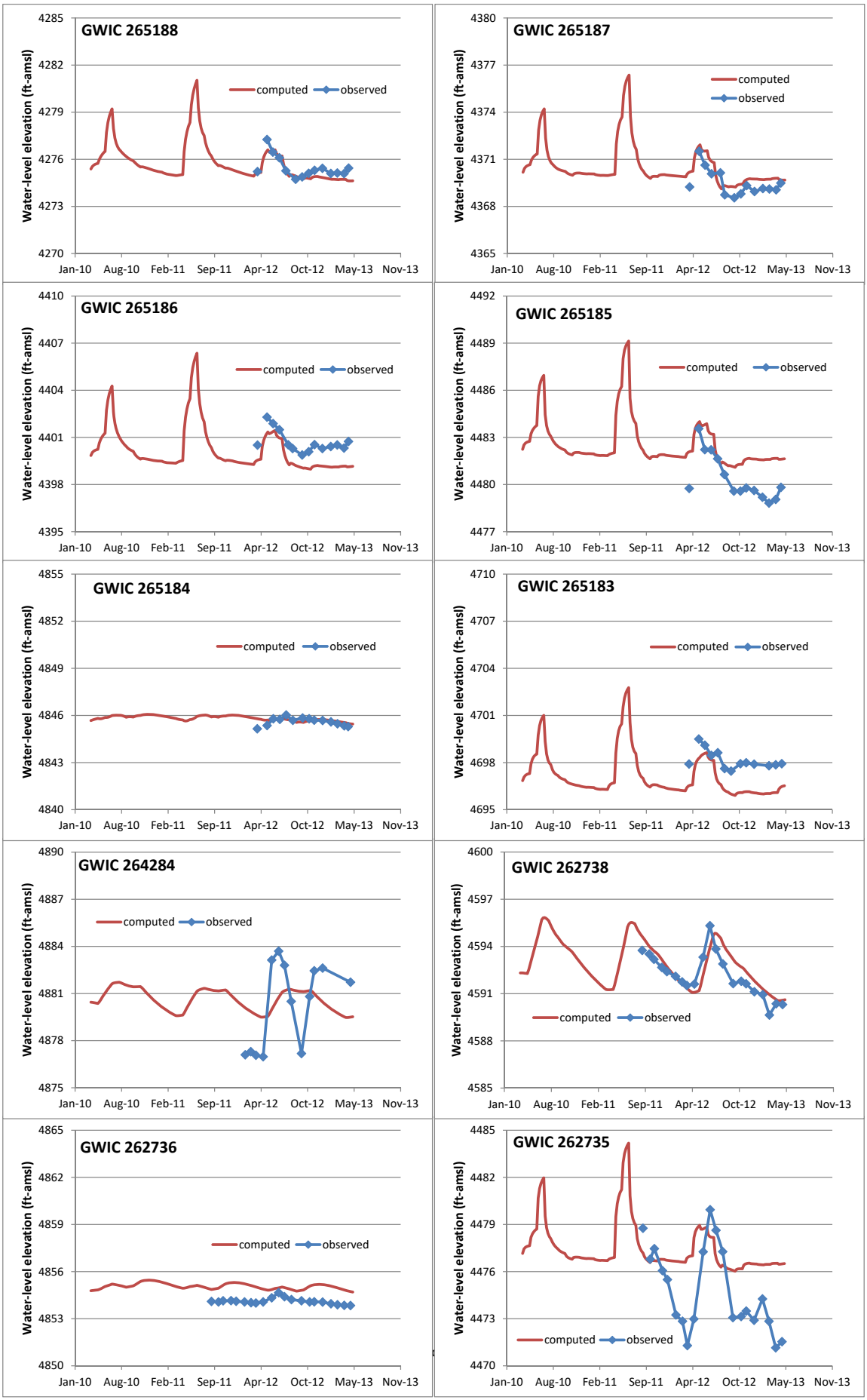

Groundwater hydrographs for the transient model compared to observed values–Floodplain and Pedimont, page 1.

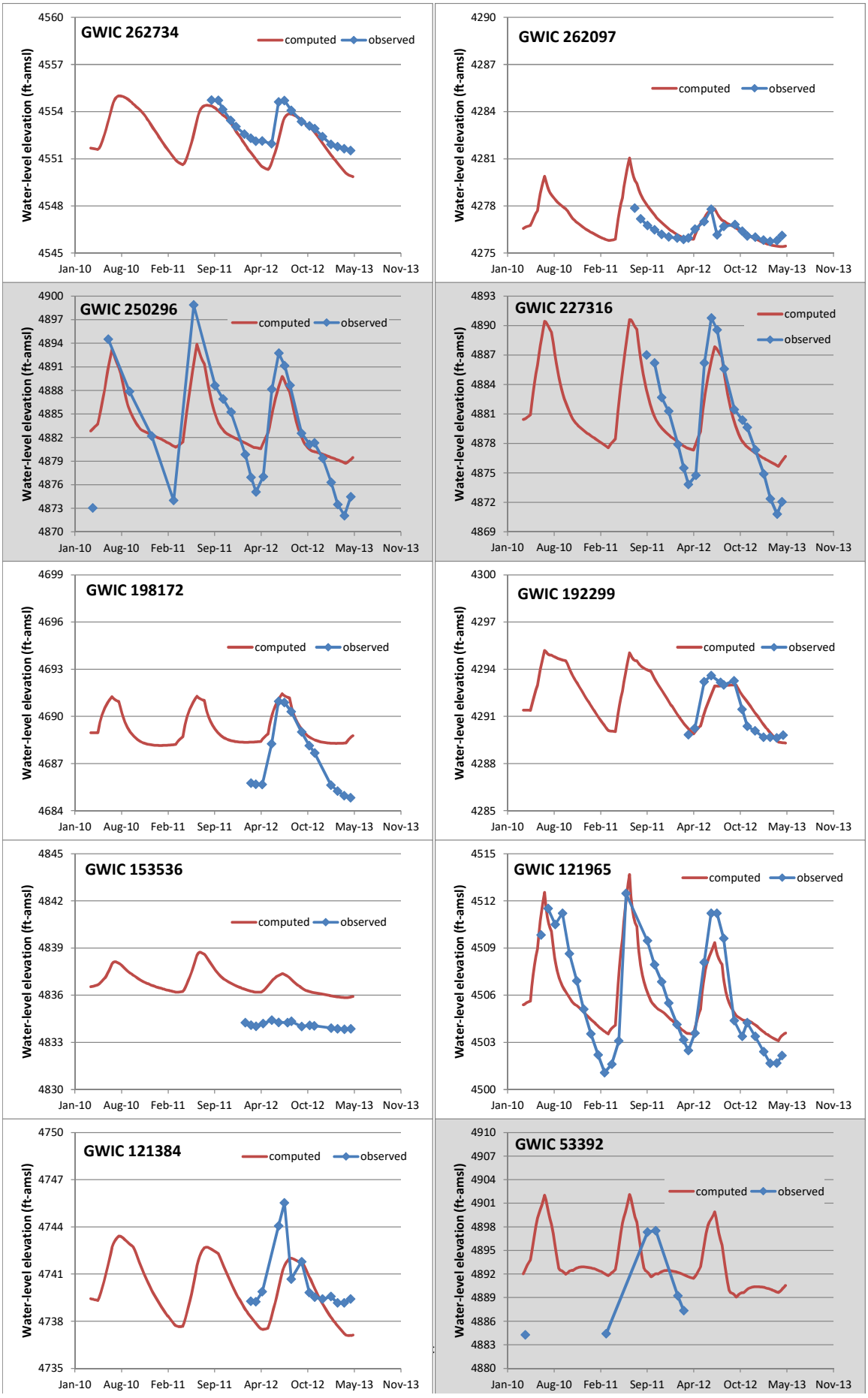

Groundwater hydrographs for the transient model compared to observed values–Floodplain and Pedimont, page 2. Note: gray graphs have a different scale on the Y-axis.

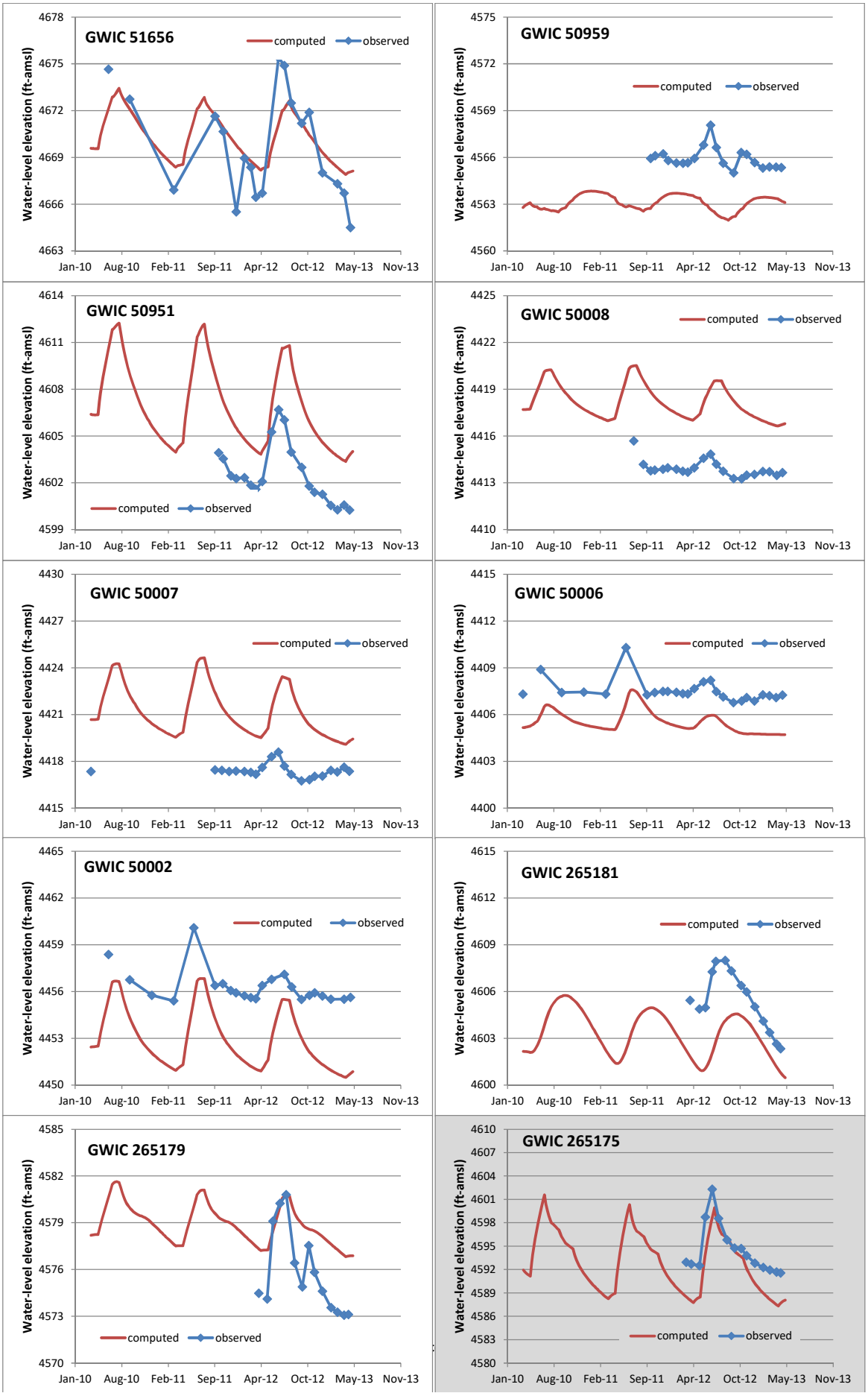

Groundwater hydrographs for the transient model compared to observed values–Floodplain and Pedimont, page 3. Note: gray graphs have a different scale on the Y-axis.

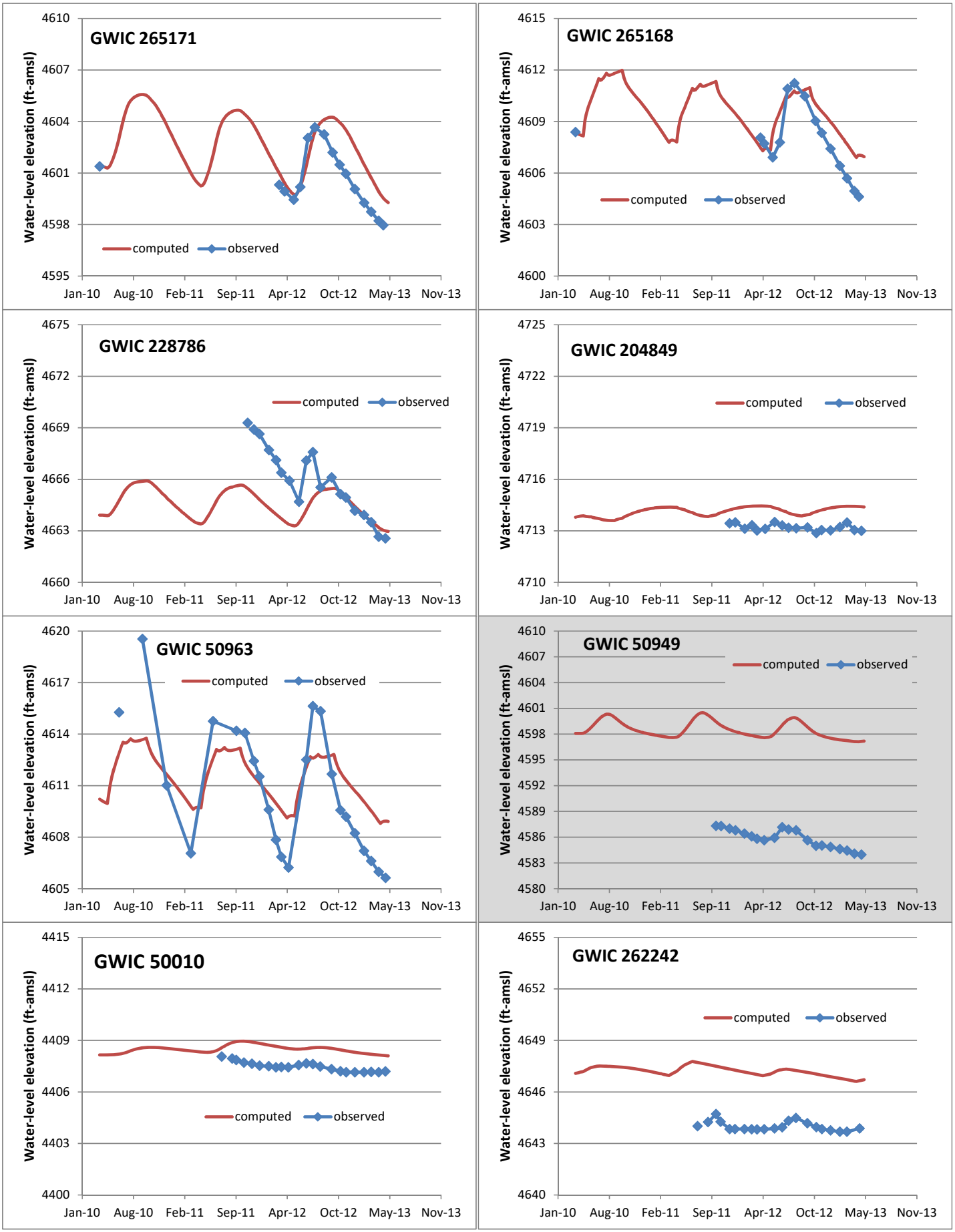

Groundwater hydrographs for the transient model compared to observed values–Floodplain and Pedimont, page 4. Note: gray graphs have a different scale on the Y-axis.

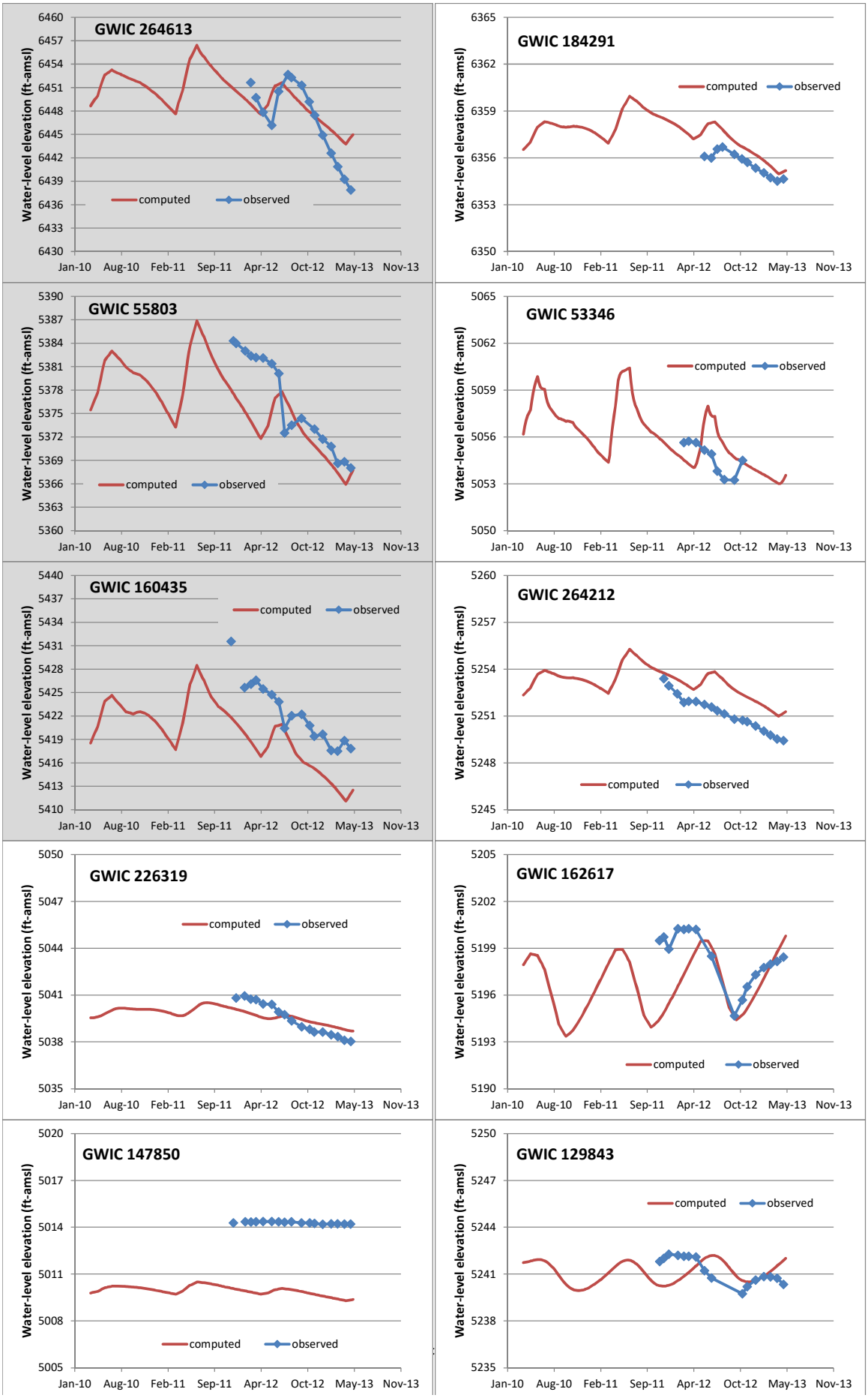

Groundwater hydrographs for the transient model compared to observed values–Upland, page 1.
Note: Gray graphs have a different scale on the Y-axis.

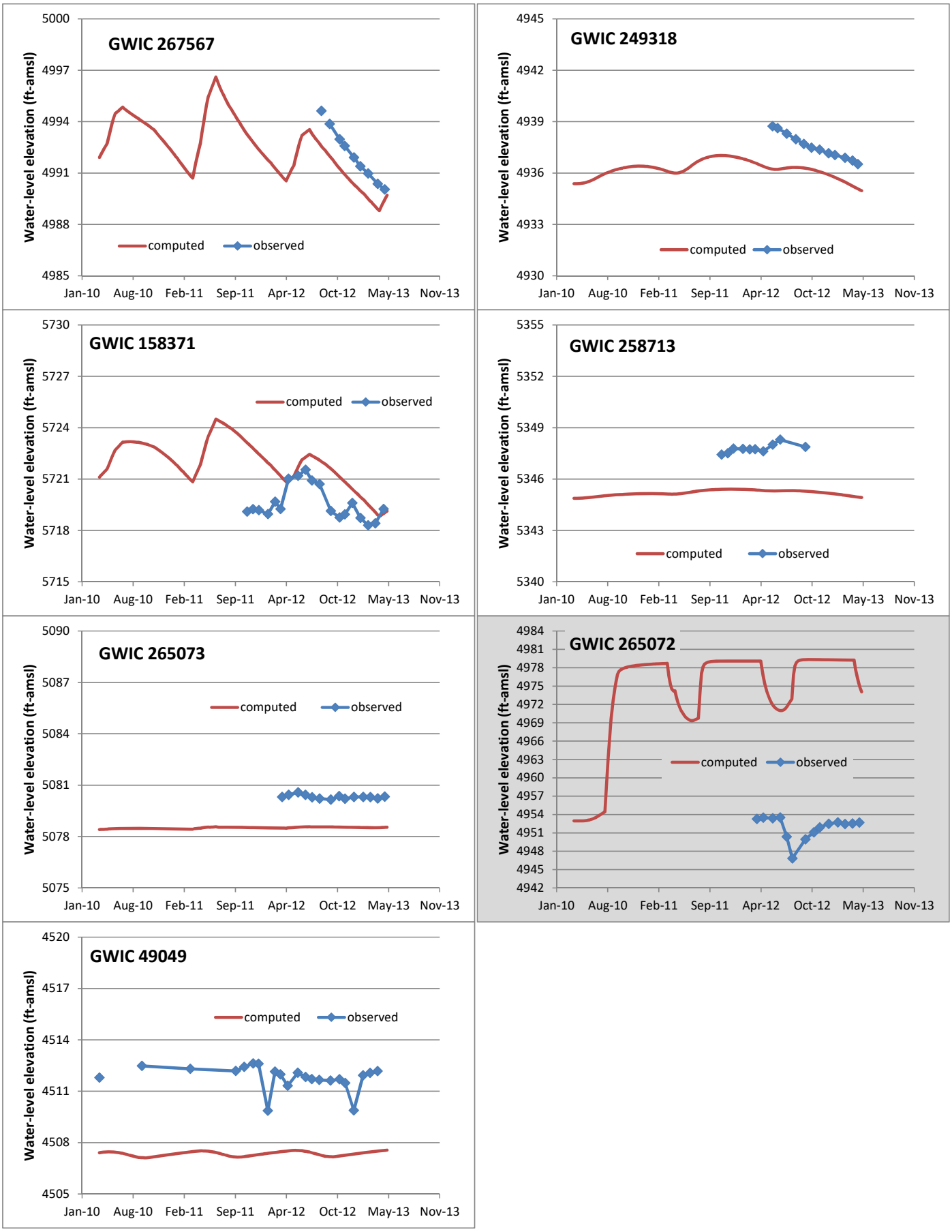

Groundwater hydrographs for the transient model compared to observed values–Upland, page 2.
Note: Gray graphs have a different scale on the Y-axis.

APPENDIX G

STREAM FLOW HYDROGRAPHS FROM 3-YR TRANSIENT SIMULATION

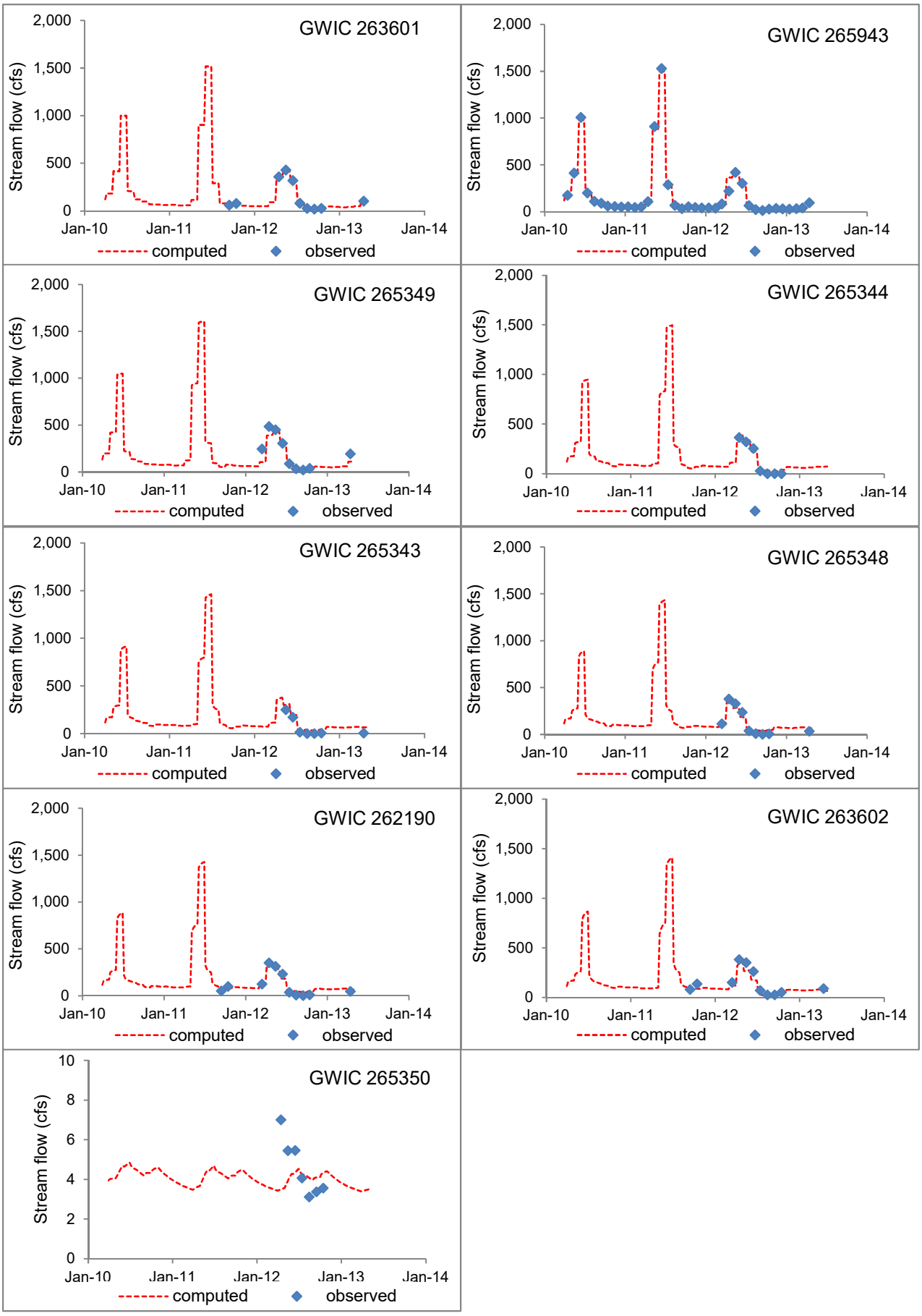

Surface-water hydrographs for the transient model compared to observed values.